PLANETARY SEISMOLOGY

Philippe Lognonné
Institut de Physique du Globe de Paris,
UMR7154, Equipe Planétologie et Etudes Spatiales,
4 Avenue de Neptune, 94100 Saint Maur des Fossés
France

And

Catherine Johnson
Earth and Ocean Sciences,
University of British Columbia, Vancouver
Canada

Abstract:

In-situ extra-terrestrial seismic measurements have, to date, been limited to data collected during the lunar Apollo missions. These data have provided significant contributions to our understanding of the interior structure of the Moon, and by inference, permissible thermal and mineralogical models. In addition, the seismic activity recorded by the Apollo stations provides information on both internal (moonquakes) and external (meteoroid) sources.

The seismic activity of other bodies, notably Mars and Venus, has never been measured. It can however be estimated, subject to approximations regarding the thermal structure of the lithospheres of these bodies, strain rates, and plausible present-day tectonic activity. For both Mars and Venus, events detectable by surface seismometers are likely: Martian estimates are 50(10) quakes annually with moment magnitude M_w greater than 3.8(4.5). In addition, impacts large enough for seismology may occur at a rate comparable to the Moon. Venusian estimates are 100(25) quakes annually with M_w greater than 5(6). Such seismic activities, much larger than the lunar ones, justify the deployment of seismic monitoring systems on these planets.

In the foreseeable future, Mars is the new body most likely to be explored through surface landers: current understanding of the interior structure, seismic noise levels and scattering on this body indicate that body wave and regional surface wave investigations could yield enormous insight into the structure and evolution of this planet. Other targets, like asteroids, Europa will also benefit similarly from passive seismic experiments, as well as a return to the Moon with more sensitive seismometers.

The deployment of surface landers might be much more difficult on Venus, due to the high surface temperature. Acoustic coupling of a planet's atmosphere with its internal body provides however opportunities for seismic investigations, and can be used either on Venus, a planet with a dense atmosphere, or on Giant planets. On Venus, signals at a given height in the atmosphere for a given quake magnitude can have amplitudes 600x their terrestrial counterparts for a given quake seismic moment. The possibility of detection of Venusian quakes from orbit exists through a combination of the near-source thermal and albedo signatures and ionospheric perturbations associated to Rayleigh waves. Detection of atmospheric normal modes of the giant planets can on the other hand be forseen with ground or space-based techniques and may provides opportunities for future exploration of the interiors of these bodies.

Outlines

Keywords

Moon, Mars, Venus, Jupiter, Seismology, Network, Core, crust, mantle, planetary interior, Normal modes, Ionosphere

1. Introduction

120 years after the first detection of a remote seismic event by Von Rebeur-Paschwitz (1889) and 60 years after the elaboration of complete mean seismic models of the Earth from body waves travel times (Bullen 1947), seismology is generally accepted as the best geophysical tool for the determination of the internal structure of a planet. Seismology has led to a revolution in Earth science, especially since the advent of three-dimensional tomographic models of the Earth's mantle (e.g. Dziewonski *et al.* 1977; Woodhouse and Dziewonski 1984) that depict the shape of major discontinuities and reflect convection patterns and/or lateral variations in temperature or mineralogy in Earth's mantle. For a complete and extensive describtion of seismology applied to Earth, see the volume 1 of Treatise On Geophysics: Seismology and Structure of the Earth.

We are a long way from such level of detail in planetary seismology and the seismic identification of the Earth's core, realized by R.D. Oldham one century ago (Oldham 1906), remains the only example of the detection of seismic waves refracted by a planetary core. The same is true for the detection of the normal modes of a planet, the first successful detection on Earth following the great Chilean Earthquake in 1960 (e.g. Bennioff *et al.* 1961). As a consequence (see the other chapters of this Treatrise), we have today no precise measurement of the core radius of the Moon and Mars, no direct informations on the Martian mantle structure, including on the discontinuities, no direct measurements on the Martian seismic activity, no direct measurement of the mean crustal thickness of Mars, etc...

The use of seismometers in planetary exploration was proposed early in the history of space missions (e.g., Press *et al.* 1960). Almost 45 years after the launch of the first seismometer to a telluric body (Ranger 3, in 1962), success in planetary and small body seismology has been limited to Earth's Moon. The Apollo program deployed a network of 4 seismic stations (Latham *et al.* 1969, 1970a, 1970b, 1971) and the short-lived Apollo 11 seismometer for passive monitoring; three active seismic experiments were also conducted on Apollo 14-16 and 17 (Watkins and Kovach 1972; Kovach and Watkins 1973a). The thirteen other extra-terrestrial seismometer experiments that launched successfully never recorded any quakes (see Table 1 for a complete list). For the Moon, this includes the seismometers (Press *et al.* 1960; Lehner *et al.* 1962) onboard the 3 Ranger Lunar probes, that were lost with their missions in the early 1960s, the seismometer lost with the cancellation of the Moon landing of Apollo 13 and the gravimeter onboard the last Apollo 17 mission, which failed to operate and had been expected to extend the previous Apollo instruments with long period seismic data. Several attempts have been made to conduct seismic experiments on Mars. Two seismometers were deployed by the Viking mission ; however, one was never unlocked and the other provided no convincing event detection after 19 months of nearly continuous operation (Anderson et al. 1977a, 1977b). Both the Optimism seismometers (Lognonné *et al.* 1998a) onboard the Small Surface Stations (Linkin *et al.* 1998), and the Kamerton short period seismometers (Kravroshkin and Tsyplakov 1996) onboard the two penetrators were lost with the Mars 96 mission, after launch. Finally, for small bodies, the two short period seismometers onboard the Phobos landers (Surkov 1990) never reached Phobos. The SESAME/CASSE (Kochan *et al.* 2000) acoustic experiment, onboard the Rosetta lander en route toward comet 67P/Churyumov-Gerasimenko, is therefore today the only experiment which might gather some seismic signals on another solid body than Earth.

The seismometers developed for early missions used pioneering techniques as compared with then-state-of-the-art Earth instruments. The Ranger seismometer, proposed by Press *et al.* (1960) and designed by the California Institute of Technology (Lehner et al. 1962) for the first missions to land on the Moon, was designed to survive up to a 3000 g shock (1 g = 9.81 m s^{-1}). This was a vertical axis seismometer with a free frequency of 1 Hz and a mass of 3 kg, and was one of the first digital instruments. Although the three Ranger probes failed, the technology was re-used for operating one of the first terrestrial digital seismometers used at Caltech (Miller 1963). A new experiment was proposed for the Surveyor mission, including a 3-axis long period seismometer and a short period vertical axis seismometer, built at the Lamont Doherty Geological Observatory (Sutton and Latham 1964), with a total mass of 11.5 kg. This was later descoped to a single short period vertical axis seismometer (Sutton and Steinbacher 1967), and then canceled in the Surveyor program. Although this effor had to await the Apollo missions for flight to the Moon, it was re-used in terrestrial

seismology, notably in the first ocean-bottom seismometers deployed in the 1970s. The deployment of seismometers was also planned for the Soviet Lunakhod, using a 1 Hz vertical fused quartz seismometer. This experiment was cancelled (Osika and Daragan, personal communication, 1990).

The installation of the first operational seismometer on a planetary body other than the Earth was achieved in July 1969, during the Apollo 11 mission. The Passive Seismic Experiment (PSE), consisted of a tri-axis Long Period (LP) seismometer, with a resonance period of 15 s, and one vertical Short Period (SP) seismometer, with a resonance period of 1 s. The total mass of both instruments plus the electronic and thermal control module was 11.5 kg and the consumption power was between 4.3 and 7.4 Watt (Latham *et al.* 1969, 1970a, 1970b). These seismometers were extremely sensitive, capable of detecting a displacement of 3 10^{-10} m at frequencies of 0.1 Hz to 1 Hz, for the LP in flat mode; 0.5 10^{-10} m at 0.45 Hz for the LP in peaked mode; and 0.5 10^{-10} m for the SP seismometer at 8 Hz**.** The corresponding nominal acceleration response curves are shown in Figure 1, as well as the noise recorded on the Moon. Practically, these instruments were unable to detect the continuous micro-seismic noise of the Moon, and detected only a significant background noise around the sunrise and sunset, associated with thermal effects located in the shallow subsurface. The Moon noise recorded on the vertical component seismometer is as low as 10^{-10} ms^{-2} $Hz^{-1/2}$ at frequencies in the range 0.1 to 1 Hz (Earth's micro-seismic peak). This allowed the detection of about 12,500 seismic signals between July 1969 and September 1977 (a mean of 4 quakes per day); many more unreported events were seen on the SP instruments. The most recent LP event catalogue is available on line at the University of Texas, at ftp://ftp.ig.utexas.edu/pub/PSE/catsrepts/levent.0104 (Nakamura 2004).

The first PSE experiment was operated by solar panels, and survived the first lunar night but failed, due to high temperatures, during the second lunar day (Latham *et al.* 1969; Latham *et al.* 1970a, 1970b). Subsequent seismometers used a radio thermal generator allowing continuous day and night operation. A seismic network of 4 stations (Figure 2) was installed by Apollo 12, 14, 15, 16. This network has been of critical importance in understanding the internal structure of the Moon, as has been discussed in several other lunar and seismological reviews (e.g. Hood 1986; Hood and Zuber 2000; Lognonné 2005). Due to its low seismic noise, the Moon has been also proposed as a right place for the detection of astrophysical gravitational waves (e.g. Gusev and Kurlachev 1976; Tobias 1978) and a gravimeter designed with that respect was onboard Apollo 17. It was however never completely deployed and failed to operate. More recently, the possibility for strange quark matter detecetion (Banerdt *et al.* 2006) has been proposed, reinitiating the possible interest for using on the Moon seismic or gravity sensors for astrophysics purposes.

In this chapter, we summarize the experiment and seismological data in section 2. We devote some attention to 1-D seismic velocity models for the Moon's crust and mantle, and discuss differences among current models, especially their likely causes and implications. We explore what has been learned about the mineralogical structure of the Moon, as a consequence of the integration of the Apollo seismic data with other geophysical and petrological constraints. In section 3 we discuss the seismic activity of the Moon in the context of other terrestrial planets.

We address the field of atmospheric seismology in section 4. The basic theory for coupling of solid body modes to the atmosphere and ionosphere is presented. We discuss the giant planets, especially Jupiter, for which the atmospheric signals associated with continuously excited global oscillations have been monitored from Earth for about 20 years (Lognonné and Mosser 1993; Mosser 1995). We develop a comparative study of the atmosphere/interior seismic coupling for Mars and Venus and discuss the prospect of remotely sensed seismology

The seismic exploration of Mars has been much less successful than that of the Moon, starting with the deployment in 1976 of the Viking seismometers (Anderson *et al.* 1977a, 1977b). Only the seismometer on board Viking 2 worked, the seismometer on Viking 1 lander failed to unlock. The sensitivity of the Viking 2 seismometer was one order of magnitude less than the SP Apollo seismometer for periods shorter than 1 s, and 5 orders less than the LP seismometer, for periods longer than 10s (see Figure 1). No convincing event detection was made during the 19 months of nearly continuous operation of the Viking Lander 2 seismometer. As shown by Goins and Lazarewicz (1979), this was probably related to the inadequate sensitivity of the seismometer in the frequency bandwidth of teleseismic body waves, as well as high sensitivity to wind noise (Nakamura and Anderson 1979). In 1996, the Mars 96 mission was launched. Each of the 2 small stations (Linkin *et*

al. 1998) carried the OPTIMISM seismometer in their payload (Lognonné *et al*. 1998). The sensitivity of the OPTIMISM seismometer was improved by about 2 orders of magnitude relative to the Viking seismometers at frequencies of 0.5 Hz, and thus better adapted to teleseismic body wave detection. The Mars 96 mission was, however, lost shortly after its launch and the seismic exploration of Mars remains an outstanding avenue of investigation in solar system science. We return to the discussion of Mars seismology in section 5, as it leads the way in potential future surface-based exploration of other bodies. We discuss current understanding of the martian interior along with noise levels and other issues relevant to marsquake detection.

MISSION	Launch	Major mission events	Instrument description	Seismometer deployment	Reference
Ranger 3	1962-01-26	Failure due to the booster. Moon missed	Vertical axis seismometer, with a free frequency of 1 Hz. (Mass: 3.36 kg)	Seismometer in a lunar capsule designed for a 130-160 km h^{-1} landing. Batteries powered for 30 days of operations	Lehner *et al.* (1962)
Ranger 4	1962-04-23	Failure of spacecraft central processor. Moon crash.			
Ranger 5	1962-10-18	Failure in the spacecraft power system. Moon missed.			
Surveyor	1966-1968	The seismometer was finally deselected from the payload of the Surveyor missions	Single short period vertical axis seismometer (mass: 3.8 kg, power: 0.75 W)	Fixed to the lander.	Sutton and Steinbacher (1967).
Apollo 11	1969-7-16	Successful installation. Powered by solar panel, worked during the first lunation and stopped after 21 days	Passive seismic experiment (PSE). Triaxis Long Period seismometer (LP) and one vertical Short Period (SP) seismometer, with resonance periods of 15 sec and 1 s respectively. (mass: 11.5 kg , power: 4.3 -7.4 W)	Installation performed by crew. Seismometers were manually leveled and oriented with bubble level and sun compass. A sun protection/thermal shroud was covering the instruments. Power was delivered by a Plutonium thermal generator for A12-14-15-16	Latham *et al.* (1969, 1970a, 1970b).
Apollo 12 **Apollo 14** **Apollo 15** **Apollo 16**	1969-11-14 1971-01-31 1971-07-26 1972-04-16	Successful installation of a network of 4 stations. For all but the Apollo 12 SP seismometer and Apollo 14 vertical LP seismometer operated until the end of September 1977, when all were turned off after command from the Earth. 26.18 active station years of data collected.			
Apollo 13	1970-4-11	Moon landing aborted. No installation of the PSE experiment but lunar crash of the Apollo 13 Saturn-IV upper stage recorded by the A12 PSE.			
Apollo 14 **Apollo 16** **Apollo 17**	1971-01-31 1972-04-16 1972-12-07	Successful installation and operation of the active seismic experiments. Seismic sources were thumper devices containing 21 small explosive sources and a rocket grenade launcher with 4 sources exploding up to 1500 m on A-14 and A-16. 8 sources were used containing up to 2722 g of explosive and deployed at 3500 m by astronauts	String of 3 geophones on A-14 and A16 and on 4 geophones on A-17. Frequency was 3Hz-250 Hz.	Geophones were anchored into the surface by short spikes as they were unreeled from the thumper/geophone assembly.	Watkins and Kovach (1972) Kovach and Watkins (1973a)
Apollo 17	1972-12-07	Deployment of the Lunar Surface Gravimeter. The gravimeter was unable to operate properly due to an error in the design of the proof mass.	Gravimeter designed for gravity waves detection. Additionnal long period vertical seismic output (10^{-11} lunar g resolution) for free oscillation detection, with a 16 Hz sampling.	Installation performed by crew.	Weber (1971)
Viking Lander 1	1975-08-20	Successful landing but instrument failure.	Short period instrument, with an undamped natural period of 0.25 s, a mass of 2.2 kg, a size of 12x15x12 cm and a nominal power consumption of 3.5 W.	The seismometer was installed on the Lander platform. No recentering was necessary since the 3 axis seismometer had been designed to function even when tilted to up to 23 degrees.	Anderson *et al.* (1977a, 1977b)
Viking Lander 2	1975-09-09	Successful landing and 19 months of nearly continuous operation. Too high wind sensitivity associated to the elastic recovery of the Viking landing legs to the loading of the station by pressure fluctuations induced by the wind.			
Phobos 1-2	1988-07-07 1988-07-12	Respecivelly:Lost during transfer to Mars and Phobos ; Contact lost just before the final phase of lander deployment, after Mars orbit insertion		Instrument onboard the long-service lander.	Surkov (1990)
Mars 96-Small surface stations	1996-11-16	Failure of the Block-D propulsion system in parking orbit. Earth re-entry. 2 small stations and 2 penetrators lost.	Long period vertical axis seismometer (0.1-4Hz, 0,405kg for the sensor) combined to a magnetometer. 55 mW of power	Seismometer in the small surface station. Semi-hard landing (200g-20 ms). Nominal operations of one Martian year with 90th first days of nearly continuous mode with internal batteries	Lognonné *et al.* (1998a)
Mars 96 Penetrators			High frequency seismometer (10-100Hz, 0.3kg, 20 mW)	Seismometer in the penetrator. Hard landing. Nominal operations of one Martian year.	Kravroshkin and Tsyplakov (1996)
Rosetta	2004-03-04	Landing on the comet 67P/Churyumov-Gerasimenko planned a few months after rendez-vous, expected on 22-05-2014	CASSE/SESAME experiment: High frequency accelerometer covering the frequency bandwidth ~10 Hz-20 kHz.	Instrument mounted on the lander	(Kochan *et al.* 2000)

Table 1: Summary and History of Planetary seismology experiments. Successfull experiment, leading to detection and interpretation of data in terms of quakes are indicated by their name in bold, in the Mission column. Bold and italic names are for successfull deployment, but without clear event detection or interpretation.

2. Lunar Results

2.1 The Apollo Passive Seismic Experiment Data

The lunar passive seismic experiment data, recorded by the Apollo Lunar Surface Experiment Package (ALSEP) from 1969 to 1977, provide a unique and valuable resource for constraining the interior structure of the Moon. The Apollo seismic "network" comprised four stations at Apollo sites 12, 14, 15, and 16. Stations 12 and 14 were about 180 km apart, and formed one corner of an approximately equilateral triangle, with stations 15 and 16 at the other corners, each about 1100 km away (Figure 2). The lunar event catalogue (Nakamura *et al.* 1981) documents 12,558 events. Recorded events exhibit different signal characteristics, from four types of sources, which were originally classified as: artificial impacts (9), meteoroid impacts (~1700), shallow moonquakes (28), deep moonquakes (~1360) and unclassified events. Many of the originally unclassified events have since been classified as deep moonquakes, with a total of 7245 deep moonquakes proposed by Nakamura (2003).

Compared with terrestrial quakes, moonquakes are small seismic moment events and generated small signals, most of the time with amplitudes smaller than the Earth micro-seismic noise, even in the best seismic vaults on Earth. Event identification was originally made by eye, using hard copy print-outs and overlays of the seismograms recorded at Apollo stations 12, 14, 15, 16. Criteria used to identify and classify seismic sources were: the time interval from the start of a signal to its maximum amplitude (rise time), the dominance of low frequency versus high frequency content in the records, and the presence of compressional (P) and/or shear (S) waves (see review in Lammlein 1977 and details in Lammlein 1973 and Lammlein *et al.* 1974). Shallow events are also referred to in the literature as High Frequency Teleseismic (HFT) events, due to their unusually high frequency content and poor depth location (Nakamura *et al*. 1974; Nakamura 1977; Nakamura *et al*. 1980). Analyses of data early during the ALSEP suggested that deep moonquakes have two important characteristics that were subsequently used to help identify additional such events: similar waveforms, and the presence of tidal periodicities in moonquake occurrence times (Ewing et al., 1971; Lammlein 1977). The main properties of the seismic sources, in term of seismic moment, stress drop, rupture times will be given in section 3. Examples of waveforms recorded at the Apollo stations from each of the four sources are shown in Figure 3. Events are, in general, apparent only after filtering of the seismic data; the raw waveform data are dominated by large amplitude signals at each station due to expansion and contraction of the thermal Mylar shroud at sunrise and sunset (Duennebier and Sutton 1974, see Figure 3 of Bulow *et al.* 2005).

During the Apollo era, digital data were extracted from the complete continuous passive seismic experiment records in time windows encompassing identified events, and were stored as the "event" waveform data set. This derived data set and the original continuous records are now available, with documentation, from the IRIS Data Management Center (www.iris.edu). Recent work (Nakamura 2003) has classified a significant fraction of identified, but unclassified, events (Nakamura *et al.* 1981) and has led to almost a factor of five increase in the number of catalogued deep moonquakes. Additionally, work by Bulow *et al.* (2005) shows that the waveform repeatability of deep moonquakes can be exploited to search for additional, previously unidentified events, associated with known deep source regions. Implementation of this algorithm has led to an approximately 35% increase in the number of events at the 9 most seismically active (at the detection level of the Apollo seismometers) source regions (Bulow *et al.* 2005, 2006a, 2006b). Despite the seemingly large number of lunar seismic events, the poor signal-to-noise ratio for emergent arrivals on most of the records mean that it is possible to measure arrival times and accurately locate events only for a subset of data in the lunar catalogue (Figure 4). Small event magnitudes and restricted receiver locations mean that events for which travel times can be clearly identified mainly occur on the near-side.

The Apollo passive seismic data set has contributed enormously to our understanding of the internal structure of the Moon. The temporal and spatial distributions of lunar seismicity provide

constraints on subsurface structure. Of particular importance is the evidence for brittle failure at depths of 700-1200 km, and likely concentrated in the 800-1000 km depth interval. Unfortunately, the small magnitude of these events, combined with the limited number and geographical distribution of receivers, means that it has not been possible to unambiguously establish a focal mechanism for any of the deep moonquakes, although this has been attempted (Koyama and Nakamura 1980). Seismic velocity models for the crust and mantle (see section 2.2) constrain the physical properties of the lunar interior (including temperature) and provide indirect constraints on mineralogy and the thermal evolution of the Moon. Studies of seismic attenuation indicate a dry lunar mantle (Nakamura and Koyama 1982). Scattering of seismic energy, manifested as long coda in the observed waveforms, has been used to investigate shallow (upper crust and regolith) fracturing (e.g. Nakamura 1977). Attempts have been made to investigate lunar normal modes (Khan and Mosegaard 2001) to constrain the core size and state. However these have been largely unsuccessful because of the limited bandwidth of the Apollo seismometers (Figure 1). In the following section, we discuss attempts to establish seismic velocity profiles for the lunar crust and mantle. Because of their potential to provide significant insights concerning the lunar interior, these seismic velocity models have been used for many seismological, mineralogical and thermal studies of the Moon.

2.2 Seismic Velocity Structure: Crust and Mantle

Due to scattering in the lunar seismograms, as well as the limited computational resources of the 1970s, most investigations of the lunar interior have used arrival times of body-wave phases to investigate plausible 1-D models for seismic velocity structure. This approach has been used with great success in terrestrial seismology, in a series of efforts leading to the long-standing Preliminary Reference Earth Model (PREM) for Earth's interior structure (Dziewonski and Anderson 1981). Lunar studies use arrival times of direct P and S waves, picked from seismograms for as many channels and stations as possible. Individual seismograms are used for impacts and shallow moonquakes. For deep moonquake sources, all records of a specific source region are stacked to improve the signal-to-noise ratio (Nakamura 1983, Lognonné *et al*. 2003). Source-to-receiver P and S wave travel times depend on receiver location (known), source location (generally unknown, though natural impacts occur on the surface, and artificial impact locations are known), source time (unknown, except for artificial impacts), and interior velocity structure (unknown). The standard seismological approach is to simultaneously solve for source locations and times, along with interior velocity structure (e.g. Shearer 1999).

P- and S-wave arrival times measured from the lunar seismograms have been either inverted or forward-modeled to estimate lunar seismic velocity profiles (e.g., Nakamura *et al*. 1976; Goins *et al*. 1981b; Nakamura 1983; Khan *et al*. 2000; Khan and Mosegaard 2002; Lognonné *et al*. 2003, Gagnepain-Beyneix *et al*. 2006). As the construction of lunar seismic velocity models has been reviewed elsewhere (Lognonné 2005), we do not repeat this overview here. Instead we restrict our discussion to four 1-D models for P and S wave velocities that illuminate the main unresolved questions concerning lunar interior structure (Figure 5).

Figure 5 shows the P and S velocity models of Goins *et al*. (2001b), Nakamura (1983), Khan and Mosegaard (2002), (see also Khan *et al*. 2000) and Gagnepain-Beyneix *et al*. 2006. We choose these studies since they exemplify state-of-the-art calculations immediately following the publication of the complete lunar event catalog (Goins *et al*. 1981b; Nakamura 1983), alternative modern probabilistic techniques applied to the early travel time data set (Khan *et al*. 2000), and recent revised travel time picks and derived velocity models (Lognonné *et al*. 2003; Gagnepain-Beyneix *et al*. 2006). The models of Nakamura (1983), Khan *et al*. (2000), and Khan and Mosegaard (2002) have been used in mineralogical modeling of the Moon (see later), and Gagnepain-Beyneix *et al*. (2006) specifically discuss the thermal and mineralogical implications of their model.

The model of Nakamura (1983) (hereafter referred to as N83) uses travel times from a total of 81 events. A layered model was specified with 4 crustal layers and mantle interfaces at 270 and 500 km

depth. The model minimized the root-mean-square misfit of the predicted and observed travel times; linearizing about the starting model. Nakamura (1983) stressed that the choice of interface depths and the specification of constant velocity layers was arbitrary. Khan *et al*. (2000) and Khan and Mosegaard (2002) used a Monte Carlo simulation approach to find, with a bayesian probability view, families of models compatible with the Nakamura's (1983) travel time data set. We refer to Khan *et al*. (2000) and Khan and Mosegaard (2002) hereafter as KM02 collectively, as the approach and broad conclusions of these two studies are in agreement. Models were computed by perturbing an initial 56-shell model in which seismic velocity varied monotonically within each shell. Bayesian probabilistic tests were conducted to distinguish between two different depth ranges of the crust-mantle boundary. P- and S-wave travel times were repicked for 59 events by Lognonné *et al*. (2003), and used in models by Lognonné *et al*. (2003), and Gagnepain-Beyneix *et al*. (2006) (hereafter L03 and GB06 respectively) that specify 3-4 mantle layers and 4-6 crustal layers.

Crustal structure is primarily controlled by impacts. Seismic ray theory predicts that near-receiver impacts (mostly the artificial impacts) will have rays that turn within the crust. In addition, distant impacts produce seismic energy that travels through the crust near the source location, and again near the receiver location. Thus, in theory, travel times of P- and S- waves should constrain crustal thickness and velocity structure within the crust, in particular near the longest-lived Apollo stations (12 and 14). Additional data that can be used to investigate crustal structure come from observations of S-to-P converted phases (Vinnik *et al*. 2001); these have been studied at stations A12 and A16 (at A14 and A15, data were either missing or too noisy). Converted phases were detected only at the Apollo 12 station and originate at a seismic velocity discontinuity interpreted as the crust-mantle boundary. These types of studies are referred to as receiver function studies in the terrestrial seismological literature. The combination of differential travel time and relative amplitude of the primary and converted phases provide information on the depth to, and the impedance contrast across, the discontinuity. However, the lunar data set is less than ideal. Recent studies (L03, GB06) use 103 travel times from 7 artificial and 19 natural impacts. The latter require estimates of 3 (latitude, longitude and source time) source parameters, reducing the number of degrees of freedom to 46. Travel times and relative amplitudes for converted phases from only one receiver location are sufficiently reliable for incorporation into velocity profile modeling (L03, GB06).

Figure 5 shows significant variability among crustal velocity models, in particular in estimates of crustal thickness. By analogy with Earth, the lunar seismological crust-mantle interface is defined by a velocity discontinuity or steep gradient (>0.1 km s^{-1} km^{-1}), below which the P-wave velocity should attain a value of at least 7.6 km s^{-1}. Specifically, crustal thickness estimates are 58 km (N83, and see earlier work by Toksöz, 1974), 45 km (KM02) and 30 km (GB06) (Figure 5). The model of GB06 requires a 10km brecciated zone beneath the crust. Velocity structure at depths of 30 – 60 km is quite sensitive to a few travel time data (see discussion in GB06). Figure 6 shows sampling of the lunar interior by ray paths for the event and receiver locations in Figure 4. Ray path coverage is uneven with depth. Coverage of very shallow depths (< 60km) is hard to see in Figure 6, but is poor. While uncertainties in crustal thickness remain, four main conclusions can be drawn from the seismological data. First, although the profiles shown in Figure 5 are 1-D velocity profiles, the source-receiver geometries and seismic ray theory indicate that the averaged crustal thickness reflects primarily crustal structure at the Apollo 12 and 14 sites. Second, several recent tests indicate that a 30-45 km thick crust at the Apollo 12/14 sites (KM02, L03, GB06) is preferred over previous estimates of ~60 km (N83). Third, these more recent crustal thickness estimates are consistent with estimates based on analyses of gravity and topography data (Wieczorek *et al*. 2006 and references therein). Fourth, although not discussed here, an attempt has been made to investigate geographical variations in crustal thickness using the Apollo seismic data (Chenet *et al*. 2006). While only a few estimates are possible, they are in good agreement with relative crustal variations deduced from gravity and topography data (Chenet *et al*. 2006).

Within the crust, estimates of seismic velocity structure are variable (Figure 5). While some discussion has been given to this in the literature, the variability among models reflects mainly the

limited data set. Perhaps the most satisfactory summary of the seismic data is that it is broadly consistent with a crustal structure in which there are two major compositional layers - an upper anorthositic and lower noritic crust – consistent with inferences from gravity and topography data (Wieczorek *et al*. 2006). Seismologically, higher velocities are associated with the noritic lower crust. Some suggestions of a mid-crustal reflector have been made (e.g., the 20km discontinuity of KM02). Furthermore, a near-surface regolith and fractured layer likely results in scattering of seismic energy and significantly reduced seismic velocities in the upper ~1 km (GB06 and see review in Wieczorek *et al*. 2006). Finally, a gradual increase of velocity with depth, may reflect the closing of microfractures with increasing lithostatic pressure.

Despite the variability in shallow structure, upper mantle (< 300 km) velocity estimates are generally in agreement, around 7.7 km s^{-1} for P-waves and 4.5 km s^{-1} for S-waves (L03, N83, GB06). Mean upper mantle P-wave (S-wave) velocity estimates by KM02 are systematically higher (lower), although estimates from all the studies shown in Figure 5 agree within the uncertainties, typically ranging from 100 to 250 m s^{-1} for P velocities and up to about 100 m s^{-1} for S velocities (see Table 1 of Lognonné 2005). Velocity estimates in the 270 – 1000 km region are constrained primarily by travel time picks from deep events. A mid-mantle (300–500 km depth) low velocity zone or negative velocity gradient was suggested by (N83); this is permitted, although not required (Figures 5 – 7 and following discussion). In particular, the crustal structure of N83 results in very poor ray coverage of the depth region 300 – 500 km (Figure 6); the trade-off is that improved coverage of this region can be obtained (e.g., with thinner crustal thicknesses), at the expense of poor coverage at 500 - 800 km depth (Figure 6, and see the discussion in GB06). Mid-mantle velocities from all three models shown in Figure 5 agree within uncertainties, although differences among models affect velocity estimates below 500km. In the depth range 500 – 1000km, there is considerable difference among the models shown here – in particular estimates by KM02 are consistently higher than those of N83, L03, and GB06. Seismic velocities below ~1000 km are essentially unconstrained (Figure 6). However, we note the absence of moonquakes below this depth may be consistent with possible high shear wave attenuation, the latter having been proposed to explain the lack of far side deep moonquakes detection (Nakamura 2005). Inversions of the seismic data for a lunar temperature profile (Gagnepain-Beyneix *et al*. 2006) suggest temperatures of about 1200°C at this depth. All these observations argue for a warmer, more ductile lower mantle.

The effect on seismic velocity model resolution of raypath coverage is also illustrated by a sensitivity analysis of the model of GB06. We examine the sensitivity of the travel time data set to perturbations to GB06. Weighted RMS misfits are calculated for velocity models in which the velocity is as specified in GB06, except in one depth interval. In this depth interval the velocity is either increased (red line, Figure 7) or decreased (blue line, Figure 7) by 10% relative to the published value. Depth intervals are 100km thick intervals, except where the published model comprises a thinner layer, in which case the published layer thickness is used. The root mean square (RMS) misfit of the travel times predicted by the GB06 model (Figure 5) to the measured travel times is ~ 5.9 seconds, comparable to the rms of the errors assigned to the data (~ 6.2 seconds). We instead show a weighted RMS misfit, (Figure 7) where each travel time residual (observed minus predicted) is divided by the uncertainty in the travel time pick (1s, 3s, or 10 s, see Lognonné *et al*. 2003), and the total RMS further normalized such that model GB06 fits the data to a weighted RMS of 1.0.

We investigate perturbations to the P-wave and S-wave velocity models, calculating the RMS misfit using only the P or S arrival times respectively (Figures 7b and 7c). In each of these cases the Vp/Vs ratio can vary compared with that specified in GB06. The travel time data are more sensitive to perturbations in Vs, than Vp with the corresponding RMS misfits showing greater variation (Figure 7c). Models with a lower Vp/Vs ratio than GB06 (higher Vs, Figure 7c, or lower Vp, Figure 7b) compared with GB06 are not only acceptable, but in fact can result in improved misfit to the data set. (The xecpetion is the depth interval 1000-1100km, the source depths of some deep moonquakes). This may seem surprising at first, however it should be remembered that the analysis of GB06 is an inverse approach with a priori constraints applied, ie, the best fit model according to some a priori

criteria is determined; such a priori are not applied here. Models with higher Vp/Vs ratios (ie increased Vp or decreased Vs) have larger rms misfits than GB06, and with the exception of the perturbations to Vp in the depth range 500-800km, these models result in more than a 10% RMS misfit increase, and as high as 50% for -10% perturbations to Vs in the depth range 100-200km.

Somewhat different results are obtained if Vs and Vp are both allowed to vary, holding the Vp/Vs ratio constant. At depths shallower than 200 km, the travel time observations are able to discriminate among plausible models. In particular, decreases in seismic velocity at depths less than 200km generate increases in misfit levels of more than 30%. At depths of 300 – 500km, there is some sensitivity to seismic structure, models with 10% increases or decreases in velocity provide poorer fits to the data. Sensitivity at depths of 5000 – 800 km is more limited, in particular higher velocities can be tolerated with little difference in RMS misfit. Sensitivity in the region of deep moonquakes again increases; in particular lower velocities result in a poorer fit to the data.

In summary, lunar seismic events recorded by the Apollo network have resulted in travel time data sets (Nakamura 1983, Lognonné *et al*. 2003) that enabled 1-D seismic velocity profiles to be inferred to depths of about 1200km. Recent work indicates a revision of previous crustal thickness estimates of ~60 km (Nakamura 1983) (an average value, probably most representative of the Apollo station 12 and 14 region) to less than 45km (Khan *et al*. 2000): about 38 km for Khan and Mosegaard (2002) and possibly as low as 30km (Lognonné *et al*. 2003; Gagnepain-Beyneix *et al*. 2006). While both models are compatible with the receiver function arrival times (Vinnik *et al*. 2001), modeling of receiver function amplitudes favors a thin crust with low seismic velocities. Upper mantle seismic velocity estimates are generally in agreement. Sensitivity to seismic velocity in the mid-mantle (300km to as deep as 700km) is limited, and depends critically on the crustal structure; a range of models including those with small amplitude negative seismic velocity discontinuities/gradients at ~300km depth, and those with sharp positive discontinuities at ~500km depth are permitted (Figures 6 and 7). Seismic velocity estimates in the deep moonquake zone differ; P-wave velocities as high as 10 kms^{-1} are obtained by some of the travel time data inversions (Khan *et al*. 2000; Khan and Mosegaard 2002), and all models show higher velocities than in the upper mantle. In section 2.4 we summarize the constraints on lunar thermal and mineralogical structure that the seismic models provide. It is likely that much of the remaining disagreement among existing 1-D velocity models results from errors in the arrival time determinations, lack of resolution, differences in the inversion techniques used, and averaging of 3-D structure. The low resolution of the Apollo seismometers and their limited bandwidth may lead to a misinterpretation of the P and S arrival time, if the true first arrivals are too small to be detected. Differences exist among the inversion procedures used in KM02, GB06 and N83, especially in the relocalisation procedure performed after each iteration. Finally, the combined effect of real 3-D structure (geographical variations in crustal thickness; spatial variations in mantle seismic velocities due to thermal and compositional heterogeneities) and poor seismic sampling of the lunar interior due to the limited source-receiver geometries means that new data provided by future networks with very broadband seismometers are required to resolve existing questions to afford major new advances.

2.3 Very deep interior and joint seismic/gravity inversions

The geometry of the lunar network, in particular the lack of any antipodal stations, means that few, if any ray paths propagating deep in the Moon (>1200 km depth) have been recorded (Figure 6; and see Nakamura et al. (1974) for an impact on the far side). An alternative approach for investigating core structure, involves investigations of a planet's normal modes (e.g. Lognonné and Clévédé 2002). A search for free oscillations in the Apollo data has been performed by a few authors, as low angular order normal modes are sensitive to core structure. After an unsuccessful attempt by Loudin and Alexander (1978), Khan and Mosegaard (2001) claimed detection of free oscillations from flat mode LP Apollo signals generated by meteorite impacts. However, Lognonné (2005) and Gagnepain-Beyneix *et al.* (2006) have shown that the signal-to-noise ratio of these events was probably too small to result in detectable long period signatures. Hence, seismic constraints on the

lunar core are indirect. Nakamura (2005) has suggested the presence of about 30 possible deep moonquake source regions on the lunar farside: however no events were detected within 40° of the antipode of the mean sub-Earth point, suggesting that this region is either aseismic or strongly attenuates or deflects seismic energy (Nakamura *et al.* 1982; Nakamura 2005).

Many geophysical studies indicate that the Moon has a core (see for a review Hood and Zuber 2000), either based on magnetic induction signatures (Hood *et al.* 1999), or the existence of remanent magnetism (Hood 1995; review in Cisowski *et al.* 1983; Fuller *et al.* 1987). Geochemical analyses of mare basalt samples indicate a depletion of highly siderophile elements (e.g. Righter 2002), relative to that expected from any lunar core formation scenario (Canup and Asphaug 2001). Impact simulations (see for a review Cameron 2000) suggest that a low fraction of iron from the proto-earth and proto-Moon was put into orbit after the giant impact. These mass fraction estimates are typically 1% or less, and reach 3% in only a few extreme cases. Further iron can, however, be added during late-stage accretion.

The only methods that have directly investigated the lunar core are magnetic sounding and geodesy. Magnetic sounding (Hood 1999) is based on the induced magnetic dipole moment produced by the motion of the Moon through the Earth's geomagnetic tail. A core radius of 340±90 km is inferred, under the assumption that electric currents in the core can be approximated by a current "sheet" localized on the core surface. The second approach, measurement of the moment of inertia ratio (0.3932±0.0002, Konopliv *et al.* 1998), indicates a higher density toward the center of the Moon than inside the lunar mantle. Moreover, analyses of lunar rotation (Bois *et al.* 1996; Williams *et al.* 2001) have shown that the rotation of the Moon is influenced by a dissipation source, which has been interpreted as the signature of a liquid core.

More precise interior structure models can be obtained from joint inversion of the density, moment of inertia, Love number (k_2), and induction signature, with or without the additional constraints provided by the seismic data. Bills and Rubincam (1995) used the mean density and the inertia factor only, and estimated a core size between 400km and 600km for densities of 8000 kg m^{-3} and 6000 kg m^{-3} respectively. Khan *et al.* (2004) used these constraints, along with the Love number, and performed a Monte Carlo inversion assuming a 5-shell model. A core with a radius of about 350 km, with a density of 7200 kg m^{-3} was inferred.

As several tradeoffs exist between the size and density of these layers, the independant constraints from seismology can be added in order to limit the space of acceptable models. Interior structure inversions based on a priori seismic models were first performed by Bills and Ferrari (1977), using a preliminary seismic model, and later by Kuskov and Kronrod (1998) and Kuskov *et al.* (2002), using Nakamura's (1983) seismic model. Either a pure γ-Fe core with density of 8100 kg m^{-3} and a radius of 350 km, or a core with smaller densities and larger radius, including the largest troilite FeS core with a radius of 530 km and a density of 4700 kg m^{-3} were proposed. Khan *et al.* (2006) performed another study using seismic information, the inertia factor and the mean density and found a core with a density of about 5500 kg m^{-3}. Figure 8 shows the results of our inversion, where the k_2 Love number is used together with the density, inertia factor and an a priori seismic model. The inverted parameters are the density of the middle and lower mantle, the shear velocity of the lower mantle and the density and radius of the core. Both the seismic models of Nakamura (1983) and of Gagnepain-Beyneix *et al.* (2006) are used. The results show that a wide range of acceptable core models comprising 1%-2% of the lunar mass fit the data. For a given mass fraction, higher S waves velocities are necessary in the lower mantle for the Gagnepain-Beyneix *et al.* (2006) seismic model than for Nakamura (1983) model. Densities are generally less than 6000 kg/m^3, suggesting a core containing some light element(s). This is consistent with estimates of the temperature at the core-mantle boundary, which are compatible with a liquid core only if the latter contains light elements (Gagnepain-Beyneix *et al.* 2006; Lognonné *et al.* 2003; Khan *et al.* 2006). A core with little or no light elements, corresponding to the high densities found by Khan *et al.* (2004), will likely be solid at those temperatures and can be excluded.

Finally, we note that the depths of deep moonquakes provide another important constraint on deep lunar structure. As shown above, the inversion of seismic models and gravity data allow calculation of acceptable interior models. Density and elastic moduli from these models can then be used to explore tidal stresses as a function of depth (Figure 9c) and/or time (Bulow *et al.* 2006). Understanding tidal stresses as a function of time and position is critical to understanding how and why deep moonquakes occur, because the seismic data distribution and quality prohibit the inference of focal mechanisms for these events.

2.4 Mineralogical and Thermal Interpretation of Lunar Seismic Models

Considerable effort has been expended in interpreting the depth dependence of lunar seismic velocity in terms of mineralogical and thermal structure. An excellent review of this topic has been given recently by Wieczorek *et al.* (2006), and so we focus here on only the major results and outstanding issues from these studies. Two general approaches have been used: investigations of a limited suite of compositional/mantle mineral assemblages (e.g. Hood and Jones 1987; Mueller *et al.* 1988; Lognonné *et al.* 2003; Gagnepain-Beyneix *et al.* 2006), and a more complete thermodynamic treatment (series of papers by Kuskov and coworkers e.g., Kuskov 1995, 1997; Kuskov and Kronrod 1998; Kuskov *et al.* 2002 and recent work by Johnson *et al.* 2005; Khan *et al.* 2006). In the latter approach, a bulk composition is specified as a function of depth and, the equilibrium mineralogical assemblage is calculated for a given selenotherm (lunar temperature profile), from which the elastic moduli and resulting seismic velocities can be predicted. Seismic velocity models predicted from mineralogy can then be compared with those inferred from travel time data. Alternatively, travel times can be calculated using the predicted seismic velocity models and compared directly with the observations (Johnson *et al.* 2005; Khan *et al.* 2006). Of particular interest for the Moon, have been (i) the bounds that crustal thickness (through the concentration of heat producing elements in the crust) and mantle seismic velocities place on temperature, (ii) whether mantle seismic velocities can discriminate among broad classes of interior differentiation models, and (iii) whether phase changes are identifiable in the seismic velocity structure.

Studies to date (Hood and Jones 1987; Mueller 1988; Khan *et al.* 2006) show that no single compositional model predicts seismic velocities that match both the upper and lower mantle 1-D profiles, even when temperature and pressure effects are accounted for. In general, models that assume differentiation of the upper mantle and that are more aluminous in bulk composition than the terrestrial mantle are favored. As most mineralogical studies compared their predicted seismic velocities with the Nakamura (1983) model, a focal point was the presence or absence in the predictions of a velocity discontinuity at 500km; both phase changes (Hood and Jones 1987; Mueller 1988) and compositional boundaries (Mueller 1988, Kuskov 1997) at this depth were inferred. Compositional boundaries were of interest as they may reflect initial compositional zoning of the Moon, the base of and early lunar magma ocean or its resulting crystallization sequence, and/or the maximum depth of melting of the mare basalt region (see discussion in Wieczorek *et al.* 2006). The discussion in section 2.2 indicates limited sensitivity of the arrival times to velocity structure in the region 300km – 500km, and as deep as 800km, and cautions against over-interpretation of mantle structure in this region. Overall, however, the increase in seismic velocity from the uppermost mantle (0-300km) to the region of deep moonquakes (700-1200km) is consistent with a change in bulk composition from a dominantly orthopyroxene upper mantle (with lesser amounts of olivine, clinopyroxene, plagioclase and garnet) to a dominantly olivine lower mantle (with smaller amounts of garnet and clinopyroxene) (Wieczorek *et al.* 2006). Associated with such a compositional change is an increase in magnesium number with depth. The recent studies by Lognonné *et al.* (2003), Gagnepain-Beyneix *et al.* (2006), and Khan *et al.* (2006) demonstrate the broad range of acceptable models, given current seismic constraints.

Crustal thickness plays an important role in determining the thermal profile of the lunar interior due to the preferential sequestration of heat producing elements into the crust. Again a large range of thermal profiles and resulting mineralogical assemblages are compatible with the seismic data (Khan *et al.*

2006); recent studies indicate that "cold" thermal profiles are preferred (Lognonné *et al.* 2003; Gagnepain-Beyneix *et al.* 2006), with temperatures of 1073K (equivalent to the base of the terrestrial elastic lithosphere) and 1473K (base of terrestrial thermal lithosphere) at depths of 340km, and 740km respectively. Such depths are comparable to the depth found in thermal evolution models of the Moon (e.g. Spohn *et al*. 2001). Bulk lunar abundances of the heat producing elements uranium and thorium in these models are similar to terrestrial values, with an enriched crust and a depleted mantle. For example, mantle abundances of about 8.2 ppb of U and 30 ppb of Th are suggested by Gagnepain-Beyneix *et al.* (2006) in order to fit the temperature dependence of seismic velocity. These values are close to those proposed by Waenke *et al.* (1977) and Taylor (1982).

Taken together, mineralogical and thermal studies of the lunar interior that use seismic data show that a broad range of interior models are compatible with the data. Limitations of existing models include the details of the thermodynamic parametrization, and the absence of titanium (and sometimes sodium) from calculations. Furthermore, the likelihood of 3-D structure in the Moon is great, and the broad range of acceptable mineralogical and thermal models may simply reflect 3-D structure in the seismic data that has been (necessarily, given the data set) mapped into 1-D structure.

3. Seismic activity of the Moon and terrestrial planets

3.1 Internal seismic activity

So far, no conclusive indication of present-day plate tectonic activity has been observed on a planet other than Earth. Moreover, only the seismic activity of the Moon is constrained by seismic data and from a practical perspective, only the activity of Mars and Venus can be estimated. During the seven years of the Apollo seismic network operation, about 12,500 seismic signals were detected on the LP instruments and catalogued, and many more events seen on the SP instruments remain uncatalogued. Figure 10 shows the statistics of detection on the horizontal component of Apollo 14 station per year, based on Nakamura's catalog. We focus first on the internal activity of the Moon, then address the internal activity of other planets, followed by a discussion of impact seismology.

Assuming that the largest deep moonquakes have a seismic moment of 5 10^{13} N m and associated stress drops of about 10 kPa (Goins *et al.* 1981a), quakes with seismic moment 30 times smaller were detected. These smallest reported moonquakes correspond to terrestrial events with body-wave magnitudes as low as 1.6 and are detectable due to the low seismic noise level on the Moon (Figure 1). Note however that the definition of the body waves magnitude or surface wave magnitudes are generaly defined for the Earth. We will therefore use later, unless specified differently, moment magnitudes, directly related to the seismic moment by $M_w = \frac{2}{3}(\log_{10}(\frac{M_0}{Nm}) - 9.1)$, where M_w is the moment magnitude and M_0 the seismic moment in N m (Hanks and Kanamori 1979).
Deep moonquakes originate from regions that appear to undergo repeated failure, giving rise to sets of moonquakes with similar waveforms and periodic occurrence times (Lammlein *et al.* 1974). The number of known source regions for deep moonquakes is currently estimated as ~250 (Nakamura 2003, 2005), and source depths are 700-1200 km. Figure 11a shows the variation in the number of moonquakes recorded per week, for the duration of the Apollo seismic experiment. The installation dates of the stations are provided in Table 1. The activity at all known moonquake nests (reported in Nakamura *et al.* 2004) is shown in red, and the activity recorded at 9 clusters that dominate the catalog is shown in blue. Figure 11a illustrates that activity at these 9 well-studied clusters closely resembles the behavior of the larger deep moonquakes population. Individual peaks in the time series occur at approximately 2-week and 4-week intervals. More obvious over the duration of the experiment is the modulation of moonquake activity at the 206-day period, and possibly at a period close to the duration of the experiment (6 years). Figure 11b shows the power spectrum of moonquake activity. The number of moonquakes per 24-hour day was calculated, and the power spectrum computed using the minimum-bias multi-taper method of Riedel and Sidorenko (1995). A multi-taper method was chosen because tidal effects with periods of 206 days and 6 years are suggested by the time series in Figure

11a. The 6-year period in particular, requires the full length of the time series (8 years) to be analyzed. Various choices of number of tapers were explored; Figure 11b shows the power spectrum computed using 6 tapers. This number allows frequency resolution at the expense of noisy spectral estimates, as is evident at high frequencies. Spectral peaks are seen at 13-14 days and 27-28 days, with some structure seen in the monthly peak. A broad peak in the power spectrum is seen close to the previously-noted 206-day period, and the increase in power at the longest periods likely reflects the 6-year modulation of moonquake occurrence times (Lammlein *et al.* 1974; Lammlein 1977)(Energy from this period is spread over the 5 lowest frequency spectral estaimtes which occur at periods of 2916, 1458, 972, 729, and 583 days). Increased smoothing using more tapers or the fully adaptive multi-taper approach results in spectra with broader peaks at the monthly and fortnightly periods, and the loss of any resolution at around 200 days. Thus, this spectral approach, which is typically used in investigating tidal periodicities in terrestrial quakes (e.g., Tolstoy *et al.* 2002), provides only crude insight into the lunar data.

In addition to the deep quakes, 28 other events were detected at much shallower depths. These events may be analogous to terrestrial earthquakes. They show no obvious correlation with tidal activity, nor with surface features on the Moon. No events in the south-east quadrant of the nearside of the Moon were detected, and focal depths are below the crust, but above 200 km depth The largest shallow events have a seismic moment of about 3 10^{14} N m for Goins *et al.* (1981a) or 1.6 10^{15} N m for Oberst (1987). On Earth, events with such moments will have body waves magnitudes ranging from 4.8 to 5.5. Their depths have been estimated to be less than 200 km, and they are interpreted as resulting from the release of tectonic stresses (Nakamura *et al.* 1982). Flat displacement spectra were recorded even on the SP seismometers, indicating a corner frequency higher than 10 Hz in most the cases (Goins *et al.* 1981a). This implies very high stress drops - less than 40 MPa for Goins et al. (1981a) but up to 210 MPa for Oberst (1987) - perhaps due to the cold, volatile-poor (and hence rigid) lunar lithosphere. Interestingly, these events are similar to Earth's intraplate earthquakes, which also exhibit much higher stress drops (for a given seismic moment) than plate tectonic earthquakes (Scholz 1990). (Intraplate earthquakes have been used a reference for all estimates of the seismic activity of telluric planets.)

We now examine how quakes can be released by the thermoelastic cooling of the lithosphere. We apply the theory to the Moon, in order to possibly understand the shallow lunar events, and to Mars, in order to predict a possible background seismic activity. The cumulative seismic moment, over a time Δt, is given by

$$M_{cum} = \eta \dot{\varepsilon} V \mu \Delta t \,, \tag{2}$$

where V is the seismogenic volume, η is the seismic efficiency and μ is the mean shear modulus of the seismogenic layer (Phillips 1991; Bratt *et al.* 1985). Following Phillips (1991), the strain rate $\dot{\varepsilon}$ is given as

$$\dot{\varepsilon} = \frac{1}{H\left(a - \frac{H}{2}\right)^2} \int_{a-H}^{a} \alpha \dot{T} r^2 dr \,, \tag{3}$$

where H is the thickness of the seismogenic layer, α is the thermal expansion coefficient, $\dot{T}$ is the cooling rate, and a is the planetary radius. If we assume that the thermal gradient in the seismogenic layer is linear and give by $T = T_0 + \frac{a-r}{H}\Delta T$, and that H thickens with time at a rate, $\dot{H}$ (both $\dot{T}$ and $\dot{H}$ are counted positively), we then have

$$M_{cum} = 2\pi\alpha\eta\mu a^2 H \Delta T \left(\frac{\Delta \dot{T}}{\Delta T} + \frac{\dot{H}}{H}\right)\beta \Delta t, \tag{4}$$

where is the constrast of temperature between the bottom of the seismogenic layer and the surface and where

$$\beta = \left(1 - \frac{H}{a} + \frac{1}{3}\frac{H^2}{a^2}\right)\frac{1 - \frac{4}{3}\frac{H}{a} + \frac{1}{2}\frac{H^2}{a^2}}{1 - \frac{H}{a} + \frac{1}{4}\frac{H^2}{a^2}}, \quad (5)$$

is a geometrical factor correcting the thin shell approximation. It is more than 0.95 for Mars, the Earth or Venus and 0.72 for the Moon.

For the Moon, we have assumed H = 400km, an estimate of the depth of the 1073K isotherm (Spohn *et al*. 2001a). The isotherm corresponding to the base of the lunar seismogenic layer is unknown. Abercombie and Ekström (2001) take a 873K for the limit of brittle failure in oceanic crust, which is reached at about 250 km – 300 km on the Moon, using the thermal models of Spohn *et al*. (2001a) and Gagnepain-Beyneix *et al*. (2006), respectively. None of the shallow moonquakes occurred at depths greater than 200km however. On the other hand, the lucar crust might be rich in anorthite and in that case, the pressure and temperature at that depth might be those of the transition of feldspath from brittle to plastic, found between 20-30 km in the Earth's continental crust (Scholz 1990). Deep moonquakes occur at much larger depth, up to 1100-1200 km, where the temperature seems high (1600-1700K) for all published models. This remains a paradox, either related to our models of the lunar interior, lunar mineralogy or to our current understanding of fault rupture under these conditions. However, as noted above, the deep moonquakes release limited energy compared with the shallow quakes.

For Mars, Phillips (1991) has assumed a constant cooling rate of $\dot{T}$ equal to 1.1 x 10^{-7} K/year, and using a thermal evolution model Knapmeyer *et al*. (2006) have set the $\dot{T}$ value to 0.5 x 10^{-7} K yr^{-1}. Taking the 873K lower bound on the isotherm at the base of the seismogenic layer, and the thermal evolution models of Spohn *et al*. (2001b), we estimate $\dot{H}$ in the range 3.15x10^{-8} to 4x10^{-8} km yr^{-1} (For comparison, this is 10-20 times smaller than the rate of thickening of 100Ma oceanic lithosphere). Using α=2x$10^{-5}K^{-1}$, μ =66 GPa (obtained for V_s=4.5 km s^{-1} and ρ=3300 kg m^{-3}) and 3.5x10^{-8} km yr^{-1} for $\dot{H}$, $M_{cum/year} = \alpha\mu\Delta t 2\pi a^2 \dot{H}\Delta T \approx$ 5.5x10^{17} Nm yr^{-1}, a value to be compared with the annual release of the shallow quakes (7.3x 10^{14} Nm yr^{-1}). Such a rate is comparable to the one obtained if a constant $\dot{T}$ = 0.5x10^{-7} K yr^{-1} is taken for a 200 km seismogenic layer. The ratio between observation and model is about 1.3x10^{-3}, 20 times smaller than the lowest seismic efficiency parameters η reported for Earth (e.g. Ward 1998). The shallow seismic energy release of the Moon, is then, an outstanding puzzle: calculations of the type above, modeled on the approach of Phillips (1991) are either inappropriate or require extreme choice of parameters relative to our current understanding. Lunar seismic efficiency may be lower than on Earth, possibly due to a cold, volatile- less seismogenic layer able to support large initial stress without rupture. On the other hand, if these calculations are correct, we cannot exclude much larger shallow moonquakes, with a recurent time however larger than the 7 years of operation of the Lunar Network.

The activity of Mars is unknown and can be estimated only by a comparative approach with respect to the Moon, as shown on Figure 12. Only one event has been tentatively proposed as a quake, during the 19 months of nearly continuous operation of the Viking Lander 2 seismometer (Anderson *et al.* 1977a, 1977b). During most of the experiment, the seismometer signal was correlated with the wind-related vibrations and lift of the lander. (See Lognonné and Mosser (1993) for a detailed explanation, and Nakamura and Anderson (1979) for an application of the seismometer as wind sensor.) As the proposed event was detected at a time when no meteorological wind data were recorded, this single detection is far from conclusive! Moreover, Goins and Lazarewicz (1979) have shown that the 4 Hz frequency of the seismometer, due to the Martian a priori mantle attenuation, was

not optimised for the detection of remote events and that a seismic activity of Mars comparable or lower than the terrestrial intraplate activity was still compatible with this lack of detection.

An activity lower than the Earth's one is indeed found by all the available theoretical predictions. Golombek *et al.* (1992) use surface fault observations, and Phillips (1991) use a lithospheric thermo-elastic cooling model to propose an activity 100 times greater than the shallow moonquake activity detected by the Apollo seismometers. The greater activity results from the effect of surface area (a factor of about 4), a seismogenic efficiency closer to Earth values (a factor of at least 20), and a possibly greater cooling rate (a factor of about 2). However, amplitudes of the largest Mars seismic signals are still expected to be about 4 orders of magnitude lower than those of the largest earthquakes at long periods, i.e., at frequencies below the source cutoff. Figure 13 shows that Martian seismicity might result in about 50 quakes with a seismic moment of 10^{15} Nm per year, with an increase/decrease of the quake frequency by a factor of 5 for a decrease/increase of the seismic moment by a factor of 10. This represents a cumulative seismic energy release of 10^{18}-10^{19} Nm per year (purple curve, Figure 13). These early estimates have been updated by Knapmeyer *et al.* (2006), with seismic activity ranging from a high seismic moment budget distributed over many events, to a low seismic moment budget distributed over a few events (Figure 13).

Other sources of seismicity, not modeled here, are possible. Volcanic activity, in the form of volcanic tremors or magma chamber retreat and associated faulting, (e.g., as observed on Alba Patera by Cailleau *et al.* 2003) could lead to quakes, but although surface evidence for activity in the last 10 My has been proposed (Neukum *et al.* 2004), no evidence for present activity exists. The cooling of these most recent volcanoes along with stresses associated with known gravity anomalies (e.g. at Argyre or Isidis (Zuber *et al.* 2000)) can supplement thermo-elastic stresses. Landslides can also be associated with locally increased seismic activity. The distribution of potential tectonic quakes was studied by Knapmeyer *et al.* (2006) using the MOLA altimetry data. A total of about 7,000 faults with a cumulative length of 600,000 km were found, half of them thrust faults and the other half normal, with no obvious correlation between fault density and ages. Figure 14 shows the results of a MonteCarlo simulation of seismic activity on these faults, and shows that activity in the Tharsis region is very likely (Knapmeyer *et al.* 2006).

We mention briefly seismicity estimates for two other planets that might be targeted for seismic missions in the coming decades: Venus and the jovian satellite Europa. Estimation of the seismic potential activity of Venus, performed as part of the NASA Venus Internal Structure Mission study (Stofan *et al.* 1993), suggested a seismically active planet. Assuming a seismogenic layer of 30 km, more than 100 quakes of M_w greater than 5 could be released by an intra-plate activity with a strain rate of 10^{-19} sec^{-1} (Grimm and Hess 1997). Quakes with M_w greater than 6 might be 5 times less frequent. A suggested rise in surface temperature on Venus, over the period for which we have a geological record, generates compressive thermo-elastic stresses in the crust (Solomon *et al.* 1999; Dragoni and Piombo 2003). Such stresses might either generate reverse faults, or act on pre-existing reverse faults, and, by analogy with Earth, might lead to quakes of maximum moment magnitude 6.5. A complicating issue on Venus is that of rheology; the absence of volatiles means that crustal rocks are much stronger than their terrestrial counterparts (Mackwell *et al*. 1998). Finally, as we note in our concluding remarks, there are severe technical challenges to surface-based seismological experiments on Venus.

The seismic activity of the Jovian satellites is of course also unknown, although Io could be the most active of all known satellites in the Solar System (Kuskov *et al*. 2000) and a perfect target for a seismological mission. The possible activity of Europa has been reviewed by Panning *et al*. (2006), following studies of Kovach and Chyba (2001) and Lee *et al.* (2003) on the possibility of seismic experiments on this satellite of Jupiter. Putative seismic sources are the opening of tensile cracks due to the Jovian tides; these might lead to quakes ranging from 2 to 4 in moment magnitude. Nimmo and Schenk (2005) have also identified regions of normal faults from an analysis of Galileo data, indicating potential quakes up to possibly M_w =5.3 magnitude. The frequency of such proposed events remains unknown.

3.2 External seismic activity : artifical and natural impacts

Impacts constitute about one fifth of the detected events (1742 of the 9315 identified and classified events) on the Apollo seismic network, and the strongest ones have amplitudes comparable to the largest moonquakes. As discussed in section 2, these surface seismic sources permit more detailed studies of crustal seismic structure, including lateral variations in thickness (Chenet *et al.* 2006). A meteorite impact can be modeled as a point force seismic source, with an amplitude equal to the momentum of the impactor (i.e. mass times impact velocity, in kg m s^{-1} or Ns). During the Apollo seismic experiment, controlled impacts of the Saturn V upper stages and the Lunar Modules were performed, and it may be possible to use these to calibrate the energy flux from natural impacts. Signals from the impact of the Apollo 17 upper stage are shown in Figure 15. The momentum of this impact was about 37,000 kg km s^{-1} (14,487 kg at 2.55 km s^{-1}), and knowledge of its position and occurrence time, provides unique seismic data with well-constrained P- and S-wave arrival times.

Even if the locations of natural impactors are not known, they are still useful seismic sources. In the case of the Moon and Earth, the frequency and size of impactors can be obtained using statistical properties of the Earth-crossing asteroids (ECAs, e.g. Poveda *et al.* 1999) and of the collision rates (e.g., Shoemaker *et al.* 1990). Figure 16 shows the frequency distribution of impactors as a function of seismic impulse, for the lunar cross section. Even when uncorrected for geometrical spreading of seismic waves, the frequency of the detected impacts with respect to the amplitude of the seismic signal (extracted from Figure 1), matches the distribution of impactors fairly well for the largest impacts (note that only the distribution in impactor diameter is taken into account). The amplitude of the largest impacts was estimated by Gagnepain-Beyneix *et al.* (2006) and typically releases a seismic momentum of about 3×10^8 Ns. This is a factor of 10 larger than the Apollo Saturn 5 upper stage impact, and a factor 100 larger than the Lunar Module impact. We have used this value to anchor the observed impact curve on Figure 16.

On planets with an atmosphere, both the velocity and the mass of the impactors are reduced during atmospheric entry. This effect can be assessed by integrating the impactor equation in the atmosphere (Chyba 1993; Poveda *et al.* 1999):

$$m\frac{dv}{dt} = \frac{1}{2}C_D \rho v^2 A - mg$$
$$\frac{dm}{dt} = \frac{1}{2}\frac{C_H}{Q}\rho v^3 A \qquad (6)$$

where m is the mass of the meteoroid, v its velocity, ρ its density, g the gravity, C_D the drag coefficient (here taken as 1.7, the cylinder value), C_H the heat transfer coefficient (taken as 0.1), Q the heat of ablation of the meteoroid (taken as 10^7 J kg^{-1}), A its cross section, and t is time. Figure 16 gives the effect of the Mars and Earth atmospheres on the ECAs or Moon-impacting meteoroids, for an asteroid density of 2400 kg m^{-3}, an entry velocity of 20 km s^{-1} and standard atmospheric models (US standard atmosphere 1976) of the planets. We see that in contrast to on Earth, the atmospheric shielding effect on Mars is small. Shoemaker (1990) and Davis (1993) have proposed that the entry flux of meteorites entering the atmosphere of Mars is 2.6 times that on Earth due to the proximity of the asteroid belt. Based on these data, the number of impacts per year detected by a seismic station on Mars is comparable to that on the Moon (Davis 1993), assuming an instrument detection level similar to that of the Apollo seismometers.

Lastly, we consider small bodies. Currently the experiment SESAME/CASSE is onboard the Rosetta mission to comet 67P/Churyumov-Gerasimenko (Kochan *et al.* 2000), for a landing expected in 2014. This experiment aims to investigate the outermost surface of the comet by means of active and passive acoustic-wave monitoring in a frequency range from a few hundred to several kilohertz, and may re-open the study of small bodies seismology after the failure of acoustic sensors onboard the

Phobos 1 and 2 landers (Surkov 1990). Both internal (related to degassing events) and external sources might generate seismic signals on comets, in contrary to asteroids, for which only impacts are expected. Future missions may be targeted toward asteroids, either to study the interior or as a deflection strategy in asteroid mitigation (Ball *et al.* 2004). Both active seismology (using explosives or impactors) or passive seismology (with natural impacts) have been already proposed (e.g. Walker and Huebner 2004), Due to their limited size, these bodies have low gravity. As a consequence, minor impacts on asteroids produce ground accelerations higher than the local gravity and seismic reverberation may have a major effect on the morphology of the asteroid regolith, including in the shape and density of small craters (Richardson *et al.* 2004). The amplitudes of the body P and S seismic waves generated by impacts can be estimated with simple models. Scattering processes will affect body-wave amplitudes; and the irregular asteroid surface will strongly affect the amplitudes of surface waves.

For large impacts, such as the artificial impacts made in the Deep Impact mission (3.8×10^6 Ns by the impact of 370 kg at 10.2 km s^{-1})(A'Hearn *et al.* 2005) or those expected in the Don Quichotte mission (4×10^6 Ns by 400 kg at 10 km s^{-1})(e.g. Ball *et al.* 2004), the displacement amplitude of body waves can be roughly expressed by:

$$a_{\mathrm{p}} = \frac{F\left(t - \frac{r}{c_{\mathrm{p}}}\right)}{4\pi\rho c_{\mathrm{p}}^2 r} \quad \text{and} \quad a_{\mathrm{s}} = \frac{F\left(t - \frac{r}{c_{\mathrm{s}}}\right)}{4\pi\rho c_{\mathrm{s}}^2 r} \quad , \qquad (7)$$

where c_p and c_s are P and S velocities, ρ is bulk density, and r is radial distance (Aki and Richards 1980) and F are the point force source functions (in N). By scaling the impact probability of Figure 16 by the ratio of the surface body areas, we see that these impacts, on a 5 km radius asteroid, will occur naturally at a rate of about one event every 1000-1500 years for an ECA flux, and will generate accelerations in the range of 0.01-1 ms^{-2} depending on frequency (Figure 17). As the frequency of impacts is typically a function of the diameter with a power of -5/2 (e.g. Poveda *et al.* 1999), and therefore of the mass with a power of -5/6, accelerations 10^6 times smaller (in the range of 1-100 ng) will occur at a rate of 10^5 events a year at 1 AU, and possibly higher at larger distances from the Sun. This translates into rates of hundreds of events per year that could possibly be recorded by space qualified short period seismometers with ng sensitivities. Such natural impacts might provide excellent seismic sources for tomography studies of asteroids.

4. Atmospheric seismology

4.1 Theoretical background

Over the last decade, many observations in terrestrial seismology have shown that the coupling between the atmosphere and the solid part of the Earth leads to an exchange of seismic energy between the two sub-systems. A first example of atmospheric-solid body coupling is the detection in the ionosphere of seismic signals. As shown by Lognonné *et al.* (1998), a small fraction of the seismic energy escapes indeed into the atmosphere at frequencies higher than 3.7-4.4 mHz. Near the seismic source, the acoustic generated waves propagate as a plume, which can reach the high atmosphere after being amplified by the exponential decay of the atmospheric density (Kelley *et al.* 1985). At greater distances, acoustic waves are primarily generated by the Rayleigh surface waves and lead to ionospheric oscillations. These were first detected in the 1960s following very large quakes (e.g. Yuen *et al.* 1969; Weaver *et al.* 1970; Leonard and Barnes 1965; Davis and Baker 1965), and are now more commonly observed for quakes with magnitudes greater than 7-7.5, using GPS (Calais and Minster 1995; Ducic *et al.* 2003; Garcia *et al.* 2005) or Doppler sounders (Artru *et al.* 2001, 2005).

The excitation of seismic waves by volcanic eruptions (e.g. Kanamori *et al.* 1984, Zürn *et al.* 1986) or the continuous excitation of normal modes (Suda *et al.* 1998; Kobayashi and Nishida 1998; Tanimoto *et al.* 1998), called Earth's hum, has been proposed as second examples of such coupling, that time with transfert from the atmosphere to the solid Earth.

In the Hum case, the amplitudes of the signal are small – in the range of 0.3-0.5 nanogal between 2 and 7 mHz, but strong enough for identifying the resonance peaks of the fundamental normal modes. Early studies proposed that the turbulences in atmospheric boundary layers (Nishida *et al*. 2000; Tanimoto 1999) were strong enough to generate the observed signal. Recent studies show however that the source is located over the oceans (Tanimoto 2005; Rhie and Romanowicz 2004, 2006) and that infragravity waves over the continental shelves are much more efficient seismic sources (Webbs 2007). In summary the Hum on the Earth seems therefore to result from several coupling effects where energy from the atmosphere is first transfered to the oceanic infragravity waves and finaly to the Earth's interior. If such a transfer is more efficient than the direct exitation of the normal modes by the atmosphere, what will be the case for a planet without ocean?

This question is adressed to Earth's two nearest neighbors, for which the energy transfered in the atmosphere by the Sun is comparable to the Earth case. The solar flux driving the atmospheric fluid layer circulations is proportional to $(1\text{-}A)/D^2$, where D is the distance to the Sun and A the bound albedo (de Pater and Lissauer 2001). The relative ratio of this flux for Venus and Mars compared with the Earth is 0.67 and 0.51 respectively and demonstrates the need to quantify the efficiency of seismic conversion of this energy for planets without oceans.

As we will see later, all these topics might offer tremendous prospectives for new seismological discoveries. For Mars, continuous excitation of free oscillations, if strong enough, could enable the determination of fundamental mode frequencies, even if no large quake is directly detected. For Venus, a remote detection in the atmosphere might provide the opportunity to perform seismic measurements, avoiding the major challenges associated with a long-lived lander able to withstand the 500°C surface temperature. More generally, any planetary body with an atmosphere will exhibit acoustic/seismic coupling between the atmospheric and interior parts of the planet: other bodies of particular interest include Titan and the giant planets, for which no discontinuity exists between the interior and the atmosphere. In this section we explore therefore atmospheric coupling on Mars and Venus, focusing on the expected amplitude of signals. We then provide a short review on the status of giant planet seismology, for which the first seismic observations also remain to be performed.

Let us start by reviewing the main properties related to surface-atmosphere seismic coupling. Density and sound speed for the lower 150 km of the atmospheres of Earth, Venus and Mars are given in Table 2 and Figure 18. The theory of interior/atmospheric coupling must first take into account the fact that a fraction of the seismic wave energy is transmitted in the atmosphere when the seismic wave reaches the surface of the solid (or for the Earth, liquid) planet. For a vertically incident acoustic wave, the amplitudes of transmission (t) and reflection (r) coefficients from the interior to the atmosphere are given by:

$$t = \frac{2\rho_{\text{int}} c_{\text{int}}}{\rho_{air} c_{air} + \rho_{\text{int}} c_{\text{int}}} \approx 2$$
$$r = \frac{\rho_{\text{int}} c_{\text{int}} - \rho_{air} c_{air}}{\rho_{\text{int}} c_{\text{int}} + \rho_{air} c_{air}} \approx 1 \qquad (8)$$

while the energy transmission (T) and reflection (R) coefficients are

$$T = \frac{\rho_{air} c_{air}}{\rho_{\text{int}} c_{\text{int}}} t^2,$$
$$R = r^2 \qquad (9)$$

and R+T=1. The initial amplitude of the waves in the atmosphere is therefore twice the vertical amplitude of the waves (or the amplitude of the ground, due to continuity), while the relative energy transmitted is 4 times the acoustic impedance ratio. Surface waves of angular order ℓ have a horizontal wavelength of $\lambda = 2\pi a / (\ell + 1/2)$ and will bounce on the surface once per cycle, with amplitude decreasing each time by $e^{-\pi/Q}$ due to attenuation in the solid part, where Q is the quality coefficient of the mode. During these successive bounces, the portion of energy transmitted to the

atmosphere will therefore be $E = e\frac{2Q}{\pi}\rho_{air}c_{air}\Big/\rho_{\text{int}}c_{\text{int}}$, where e is the partition ratio between the energy in vertical displacement and the total energy, the latter being typically of the order of 0.5. Such energy transmission, given in Table 2, is approximately found in the high ℓ limit of Figure 19.

	Crust	Earth	Mars	Venus
Surface Sound speed (m s^{-1})	5800	340	214	426
Surface density (kg m^{-3})	2600	1.225	0.0175	65
Acoustic impedance ratio/crust	1	2,76e-5	2.48e-7	1.83e-3
Energy transfer ($E = \frac{Q}{\pi}\rho_{air}c_{air}\Big/\rho_{\text{int}}c_{\text{int}}$) (Q=100)		8.8e-4	7,9e-7	5.8e-2
High Q Atmospheric resonances mHz		3.7	2.05	3.10; 4.15

Table 2: Atmospheric coupling parameters for Venus, Earth and Mars. The atmospheric model used for the Earth is the US Reference Atmospheric model. For Mars, it is the mean model from a GCM run of Forget *et al*. (1999).

In the atmosphere, in the non-viscous case, the seismic wave equation is given by:

$$\begin{aligned}
&\rho_0 \frac{\partial \vec{v}}{\partial t} = -\vec{\nabla} p + \rho_1 \vec{g}_0 + \rho_0 \vec{g}_1 \\
&\frac{\partial \rho_1}{\partial t} + div(\rho_0 \vec{v}) = 0 \\
&div(\vec{g}_1) = -4\pi G \rho_1 \\
&\frac{\partial p}{\partial t} = -\gamma p_0 div(\vec{v}) - \rho_0 \vec{g}_0 . \vec{v}
\end{aligned} \quad . \qquad (10)$$

where ρ_0, ρ_1, p are the equilibrium density, perturbation in density, pressure and where $\vec{v}, \vec{g}_0, \vec{g}_1$ are the velocity, equilibrium gravity and perturbation in gravity associated to the mass redistribution. p_0, γ and G are the equilibrium pressure, the adiabatic index and the gravity constant. The upward propagation of the waves is modeled by renormalizing the amplitudes in order to account for the exponential decay of the density. Quasi-analytical expressions can be obtained when the atmospheric structure has a vertical scale much larger than the wavelength of the wave and when pure upward propagation is assumed. Gough (1986) shows that under these conditions equations (10) lead to

$$(\frac{\partial^2}{\partial t^2} + \omega_c^2)\frac{\partial^2 \psi}{\partial t^2} - c^2 \frac{\partial^2}{\partial t^2}\nabla^2 \psi = 0, \qquad (11)$$

where the cutoff frequency is given in first approximation by $\omega_c = \frac{c}{2H_\rho}$ and where $\psi = c^2\sqrt{\rho_0}\,div(\vec{v})$ is related to the square root of the acoustic energy $c\gamma_0 p_0 div^2(\vec{v})$, where $c^2 = \frac{\gamma_0 p_0}{\rho_0}$ is the squared speed of sound. Here, H_ρ is the density height scale given by $H_\rho = -\left(\frac{dLn\rho}{dr}\right)^{-1}$. The plane wave solution to equation (11) obeys the dispersion equation:

$$\omega^2 = \omega_c^2 + k^2 c^2. \qquad (12)$$

Waves with frequency lower than the cutoff frequency have negative k^2 and exponentially decaying energy in the atmosphere; waves with frequency higher than the cutoff frequency can propagate upward. This energy is not trapped and the waves progressively lose energy during their upward propagation through viscous and non-linear processes. Note that other parametrizations are possible, leading to slightly different expressions for the dispersion equation and cutoff frequencies (Beer 1974;

Mosser 1995). The trapping of free oscillations, which can be used to model the waves with summation techniques, can be modeled when the full system (i.e., the solid and atmospheric parts of a planet) is considered, and when a radiating boundary condition (Lognonné *et al*. 1998) is assumed at the top of the atmosphere. We give here the results of forward modeling based on this theory for the Earth, Mars, Venus and Jupiter.

For planets with solid parts, the normal modes of the system can be computed for all modes: spheroidal solid modes, atmospheric acoustic modes and atmospheric gravity modes. The summation of these normal modes then allows the computation of either seismograms for the solid surface and for the atmospheric perturbations, or barograms for the atmosphere as a function of altitude. More details and the theoretical background can be found in Lognonné *et al*. (1998b) and Lognonné and Clévédé (2001). An extension to the viscous case is given by Artru *et al*. (2001). Figure 19 illustrates the efficiency of coupling for Venus, Mars and the Earth, and shows the fraction of energy of the fundamental Rayleigh modes in the atmosphere when the latter are computed with the atmospheric coupling. Resonance effects appear with a peak in the atmospheric energy; they are observed at frequencies associated with the fundamental and overtones of the atmospheric waves guide and are dependent upon the atmospheric model used.

At these frequencies, a much larger fraction of the seismic waves is transferred to the atmosphere. On the Earth, such resonance frequencies between the atmosphere and interior exist near 3.7 mHz and 4.44 mHz and are preferential windows for studying the atmospheric/interior coupling. Large atmospheric eruptions, such as those of El Chichon in 1982 and Pinatubo in 1991, led to selective excitation of Rayleigh surface waves at these frequencies (Kanamori and Mori 1992; Widmer and Zurn 1992; Zürn and Widmer 1996). The fundamental resonance frequency on Mars is found at about 2.05 mHz while the fundamental and the three first harmonics on Venus are found at 3.10, 4.15, 4.75 and 5.15 mHz. On Venus, the two first overtones are strongly trapped while only the fundamental branch is trapped on the Earth and Mars.

Figure 20 shows the Rayleigh Normal modes for angular orders smaller than 50. Below the atmospheric fundamental frequency, amplitudes decay with altitude and full trapping of the modes is observed. At higher frequencies, oscillations appear, as a consequence of the upward propagation associated with energy leakage, and the normal modes also have significant imaginary amplitudes in the atmosphere. Due to its smaller size and to a low resonance frequency (associated with the cold atmospheric temperature), this transition for Mars is found for order ℓ=8, while it is observed for ℓ=28 and ℓ=22 for the Earth and Venus respectively. The amplitudes are also proportional to the ratio of acoustic impedance between the ground and atmosphere.

4.2 Mars hum and Martian atmospheric sources

We now address the possibility of continuous excitation of normal modes by the Martian atmosphere. Kobayashi and Nishida (1998) originally proposed amplitudes on Mars to be a factor of 2-3 smaller than on Earth, while amplitudes on Venus were expected to be comparable to Earth. These early studies however considered primarily excitation by turbulence in the boundary layer. See more on the theory and assumptions in Tanimoto (1999, 2001). This theory has been later however critized by Webb (2007), who shows that an overestimation by several orders of magnitude is done on the normal modes amplitudes.

Can we still imagine that normal modes might be excited with potentialy observable amplitudes? Instead of turbulences, let us consider the non-turbulent large scale winds and atmospheric circulation. As they generate wind Reynolds stresses, they act as a potential seismic source. As shown by Lognonné *et al*. (1996), the density of pressure glut can then be expressed as

$$m_{ij} = (p + \kappa \nabla . \vec{u})\delta_{ij} + \rho v_i v_{j,} \qquad \textbf{(13)}$$

where p is the atmospheric pressure, v_i the i^{th} wind velocity component, ρ the density, κ the bulk modulus of the atmosphere and $\vec{u}$ the displacement field of the normal modes in the atmosphere. In

the isotropic case, when wind is neglected, the pressure is much greater than the Hook pressure of normal modes, and we have $m_{ij}=pd_{ij}$. The amplitude of a normal mode with angular order ℓ and eigenfrequency ω_ℓ can then be expressed as

$$a_\ell^m(t) = \int_{-\infty}^{t} d\tau\ e^{i\omega_\ell(t-\tau)} \int\int d\Sigma\ \bar{Y}_\ell^m(\theta,\phi) \int_0^{+\infty} dz\ A_\ell(z)\ \frac{Mp(z,\theta,\phi,t)}{R\rho_0(z)} \qquad (14)$$

where z, θ, ϕ are the altitude, latitude and longitude, $a_\ell^m(t)$ is the acceleration of a given normal mode at a time t, $A_\ell(z)$ an excitation term depending on the atmospheric-solid planet coupling, related to divergence of the normal mode eigenfunction times the amplitude of the mode on the recording direction, $\bar{Y}_\ell^m$ the complex conjugate of spherical harmonic of degree ℓ and order m, p the atmospheric pressure, R the thermodynamical constant, ρ_0 the atmospheric density and M the mean atmospheric molar mass (Note that $Mp/R\rho_0$ has the dimension of temperature). Values of the excitation terms, $A_\ell(z)$ at the surface of the planets are shown in Figure 21 for the fundamental normal modes in the Earth and Mars cases. On the Earth, up to an angular order of 28-29, acoustic energy is trapped and therefore not radiated. This transition on Mars is achieved at angular order below 10, for all realistic atmospheric models of Mars, leading to a dynamic coupling of the normal modes with the atmospheric circulation of Mars quite efficient for the low order angular modes. The coupling coefficient is comparable to that on Earth, at angular orders of about 10 and typically a factor 10 smaller for angular orders greater than 20, as a consequence of the smaller atmospheric density. However, temperature fluctuations and winds are significantly larger.

Global circulation models (Forget *et al*. 1999) can be used to obtain more precise estimates of the continuous excitation of normal modes, through a computation of the pressure glut. Lognonné and Forget (2001) have performed such study. Figure 22 shows the right hand side of equation (14), corresponding to the excitation term related to the pressure field at a given local time and for a classical GCM model just before time integration and multiplication by $e^{i\omega_\ell(t-\tau)}$. Large excitations are observed, including along atmospheric fronts in the south hemisphere. After integration, such models provide the acceleration amplitudes of the modes (Figure 23). As mentioned above, these estimates are probably a minimum value, because GCMs do not model short scale circulations in the atmospheric boundary layer. The results show however that a small excitation is achieved by atmospheric global circulation. Moreover the global circulation is more coherent than on Earth from one day to the next. So if long duration measurements become available, an increase of the signal by stacking methods can be envisaged. Even though the search for continuous excitations will be challenging, due to the extremely low amplitudes and the high noise associated with the surface installation of seismometers on Mars, it can open exciting opportunities for the detection of low angular order normal modes and will benefit from long lived seismic monitoring, enabling such stacks.

Let us now briefly consider the effect of the atmosphere at shorter periods. The atmospheric wind-induced turbulences are known to be a source of short period seismic noise in the frequency range 0.1-10 Hz (e.g. Steeples *et al*. 1997). Recent studies in terrestrial seismology using cross-correlation techniques have shown that the shallow and middle crust can be imaged by extracting the Rayleigh wave Green's Function from long sequences of ambient seismic noise generated by atmospheric sources. The same technique has been used on the Moon at much shorter periods, by using thermal generated noise, for the investigation of near subsurface (Larose *et al*. 2005). Such a technique was applied in California on short period (6-20 second) surface waves (Shapiro and Campillo 2004; Shapiro *et al*. 2005) and this can also be applied to shorter wavelength surface waves, sensitive to the uppermost few kilometers of the crust. Martian atmospheric turbulence, especially localized dust devils, can probably generate comparable surface waves. Such a method may be an alternative to future active seismic experiments for studying the Martian subsurface and the associated water reservoirs. This would obviate the technological and safety challenge of carrying explosive seismic sources to Mars, as was done on the Moon for the Apollo seismic experiments.

4.3 Venus atmospheric seismology

As noted earlier, ionospheric disturbances associated with acoustic waves generated by the Rayleigh surface waves have been observed on Earth in the far field of very large (M_w >7) quakes (e.g. Ducic *et al*. 2003; Artru *et al*. 2004; Garcia *et al*. 2005) but also in the near-field of smaller quakes. Calais and Minster (1995) reported ionospheric perturbations on GPS data following the Northridge M_w=6.7 earthquake, and observations have been made for magnitudes as low as 5.9, with reported thermospheric perturbations of about 300 K between 300 and 400 km of altitude (Kelley *et al*. 1985). For a short review on the ionospheric post-seismic perturbation, see Lognonné *et al*. (2006). The detection of atmospheric signals associated with quakes might therefore be an interesting alternative to observation performed by seismometers, especially if measurements can be performed by orbiting spacecraft or Earth-based telescopes. However, Venus is the only planet where possibly weaker seismic activity is counterbalanced by a better atmospheric coupling, enabling seismic studies by such an alternative strategy.

We estimate approximately the amplitude of the expected atmospheric signals on Venus associated with large quakes. The amplitudes of seismic waves in the venusian atmosphere are related first to the acoustic jump at the surface and associated transmission coefficient, and then to the amplification with altitude. At the surface, the pressure is about 90 bars, density about 65 kg m^{-3}, acoustic velocities are slightly higher (425 m s^{-1}) than on Earth and ground coupling (ρc) is about 60 times greater than on Earth. At an altitude of 50 km in Venus' atmosphere, the pressure is comparable to that at the surface of the Earth, but the density is already almost two orders of magnitude lower than that at the Venusian surface. These two effects mean that signals are expected to be about 600 times greater at the same altitude on Venus compared with Earth for the same quake moment magnitude. Good prospects for detection are therefore possible.

The first possibly detectable signal might be the atmospheric and ionospheric perturbation in the vicinity of a Venusian quake. Such signal will consist of a plume, generating both temperature, possibly brightness-albedo as well as atmospheric/ionospheric oscillations. The characteristics of the acoustic plume generated near the source were first studied by Garcia *et al*. (2005), who showed that either adiabatic oscillations corresponding to the acoustic waves or non-adiabatic deposition could be generated. For M_w=6, adiabatic temperature oscillations of about 100K and post-seismic temperature heating of about 10K are found (Figure 24). These perturbations, however, take place very near the source, within a distance comparable to the event depth. Their observation will therefore require a global, high resolution survey, which might be achieved only by spacecraft near Venus. The detection of such signal will be attempted with the Virtis experiment (Drossart *et al*. 2004), which is onboard the ESA's Venus Express spacecraft, in orbit around Venus.

In addition to these signals in the vicinity of the quakes, infrasounds and surface waves generated by the quake will also produce atmospheric signals, which can be detected at larger distances. These waves can be computed more precisely following the theory developed by Lognonné *et al*. (1996), and the difference in the atmospheric coupling can be analyzed by taking, for both the Earth and Venus interior case, the spherical model PREM (Dziewonski and Anderson 1981), the latter being corrected with respect to pressure for Venus.

A first and impressive effect of the coupling is the strong perturbation of the quality factor of the fundamental normal modes of the interior (Figure 25). The presence of the atmosphere is indeed decreasing the attenuation coefficient of Rayleigh modes Q, due to the escape of energy. For the Earth, this effect is comparable or smaller than the error in the Q determination. The Earth normal mode ${}_0S_{98}$, for example, close to 10 mHz, has a Q of 115 with the atmosphere and a Q of 118 without the atmosphere, a decrease of only 2.5%. On Venus, we get a Q of 108 for the mode ${}_0S_{93}$ with the atmosphere, and a Q of 121 without, corresponding to a decrease of more than 10%. This means that about 10% of the energy of the Rayleigh waves is dissipated in the Venus atmosphere and confirms the importance of the coupling.

Comparison of synthetic seismograms for the two planets allows further examination of the coupling effects. Figure 26 shows the atmospheric oscillations at 150 km, for the same epicentral distance and seismic source. We find amplitudes about 100 times larger on Venus than on Earth, reaching 0.3 m s^{-1} at these periods, corresponding to wavelengths larger than 300 km. Amplitudes will be about one order of magnitude larger at 20 sec but are much less, of course, for the low order angular modes. Figure 27 shows the amplitude of the latter, for the fundamental Rayleigh mode as well as for the fundamental and two first overtones of the atmospheric waveguide. For a quake releasing a moment of 10^{18} Nm, we get individual mode amplitudes of a few cm s^{-1} at 150 km for angular orders greater than 30. At 120 km, however, amplitudes do not reach 1 mm s^{-1}. The detection of oscillations in the neutral atmosphere (below 120 km) seems therefore not to be feasible, due to the limited length of the Q-cycle of these modes, which is expected to be around a half-day at 5 mHz, for a Q of 200. The existing tools used in Jovian seismology have indeed a typical detection threshold in the range of 0.5-1 m s^{-1}. Amplitudes at higher altitudes might be however detectable with ionospheric sounders. The Venus ionospheric structure is indeed thinner and the maximum ionization is found at about 150 km. A sounding from the top is therefore possible at such an altitude, contrary to Earth where the maximum of ionization, at about 300-350, prevent the access from the top of the 150-200 altitude layers. With electron density ranging from $5x10^3$ cm^{-3} to $15x10^3$ cm^{-3} during the night and from $5x10^5$ cm^{-3} to $5x10^5$ cm^{-3} during the day, this gives electron plasma frequencies ranging from 0.5-1.5MHz during the night and 3 MHz-7MHz during the day. A Doppler sounder, with performances below 1 cm s^{-1} in Doppler measurement (Artru *et al.* 2004), might offer exciting perspectives for remote sensing seismology on Venus and has to be considered for a future, high altitude, Venus orbiter.

4.4 Giant planets seismology

As for the telluric planets, the internal structure of the giant planets is weakly constrained by geophysical data and seismology could provide important new data. For a review on the giant planets' internal structure, see Guillot (2005).

We review briefly the main seismological properties of giant planets and followed by the state-of-the-art in observations. For a more complete review, including early observations, see Lognonné and Mosser (1993) and Mosser (1997). In contrast to telluric planets, the mantle and possibly even the rocky core are fluid (Guillot 2005), meaning that only acoustic and gravity waves can be detected. Moreover, the waves are not trapped by a solid-atmospheric discontinuity but only by the effect of the atmospheric density decay. Thus, only waves with frequencies lower than the atmospheric cutoff frequency are reflected back into the interior.

Figure 28 shows the sound speed and density structure for two typical Jovian interior models, with and without a plasma phase transition (PPT). At this transition, molecular hydrogen is dissociated into metallic or plasma hydrogen (e.g. Saumon and Chabrier 1989; Saumon *et al*. 1992). For Jupiter, the cutoff frequency, also shown on Figure 28, reaches a maximum of about 4.5 mHz 50 km above the one bar level and then decreases to about 3.3 mHz, a stable value between 100 and 200 km of altitude. Low attenuation normal modes can therefore be found only below 3.3 mHz, while leaky modes can exist between 3.3mHz and 4.5 mHz. No surface waves exist at frequencies higher than the maximum value of the cutoff frequency; a detailed description of the propagation of seismic waves in the Jovian troposphere and stratosphere can be found in Mosser (1995).

The theoretical spectrum of free oscillation of Jupiter was computed for theoretical models of Jupiter in the late 1970s (Vorontsov *et al*. 1976; Vorontsov and Zharkov 1981). As for the Earth and other planets, these theoretical studies, as well as more recent ones (Gudkova and Zharkov 1997, 1999), have shown that the free oscillation frequencies were very sensitive to the internal structure. As noted earlier, free oscillations with frequencies higher than about 3 mHz are not trapped. We show in Figure 29 the spectrum of free oscillations for the model without PPT shown in Figure 28. Only a bulk Q of 10^6 was considered and the viscosity was neglected. As a result, the low Q values found for

frequencies higher than 3 mHz are due mainly to the non-trapping of the waves. Note that the fundamental mode is in fact a gravity mode and that the first acoustic mode is for n=1 (Lognonné *et al*. 1994). Figure 30 shows the amplitudes of the modes, scaled by the square root of the density. Note the trapping of the modes below the cutoff frequency again and the oscillating characters of the acoustic n=1 mode for frequencies higher than the cutoff frequency.

The search for the free oscillations of Jupiter started in the late 1980s, with infrared observations (Deming *et al*. 1989), Doppler spectrometry observations (Schmider *et al*. 1991; Mosser *et al*. 1991; Cacciani *et al*. 2001) and Fourier transform interferometry (Mosser *et al*. 1993, 2000). The main difficulties are:

- the limited angular resolution, enabling first only full disk measurement and observation of very low angular orders modes ($\ell \leq 0-3$) and, since 2000, resolution up to $\ell \leq 20-25$.
- The effects associated to the rotation of Jupiter. The normal modes are indeed observed in a non-rotating frame (corresponding to the Earth view for ground observations) and only disk imaging with reprocessing can restore signals associated with a given spherical harmonic Y_ℓ^m
- The windowing effects associated with the duration of observations, which has motivated the development of Observatory networks, enabling continuous observation of Jupiter (e.g. Schmider *et al*. 2003).

The observations performed were not able to detect any free oscillations and an upper limit on the global oscillation of 1 m s^{-1} has been proposed. However, an excess of signal in the frequency band (0.5-1.8 mHz) was detected (Schmider *et al*. 1991; Mosser *et al*. 1993). If albedo variations of Jupiter (Cacciani *et al*. 2001) might be responsible for contamination in the lower part of the spectrum, below 0.7 mHz (Lederer *et al*. 1995), the upper part might be associated to global excitations. Future observations might be able to reduce the detection threshold. In contrary to telluric planets, global low frequency oscillations of Jupiter have indeed very high-Q and the phase coherency of the oscillation is practically limited by the excitation processes, as for the Sun, for which oscillations with phase-coherent amplitudes up to 1 year have been observed (e.g. Libbrecht and Woodhard 1991) (p-modes have, however, much shorter phase coherency times of a few days). Continuous future observation might therefore be able to reduce the detection threshold by an order of magnitude after one month of continuous observation, putting the limit to about 10 cm s^{-1}. The improvment of performances will also open prospects for the other giant planets, especially Saturn, for which no observations have been reported. Only works on theoretical estimates (e.g. Gudkova *et al*. 1995) or on the possible impact of the oscillations on the ring structures (Marley *et al*. 1993) have been therefore sofar published.

As noted earlier, body waves cannot be trapped in the atmosphere but can in principle be excited by a localized source. The impact of the Shoemaker-Levy 9 comet, due to the high energy of the impact, was such an event. The amplitudes of signals were theoretically predicted for different masses of impactors (Marley 1994; Kanamori 1993; Lognonné *et al*. 1994). For an impact with an energy greater than 10^{21}J, peak-to-peak temperature fluctuations greater than ~0.01 K were expected for 10 mHz frequency P waves, while surface waves below 3 mHz were expected to generate fluctuations in excess of 0.01 K for impacts greater than 2 10^{21}J (Lognonné *et al*. 1994). No observations were reported by Mosser et al (1996) for impacts A and H nor by Walter *et al*. (1996) for impact R, putting upper limits on the impact energy of 1-2 10^{21} J. Though the impact did not generated detectable body waves, it did produce a ring-like pattern in the Jovian atmosphere, with two rings propagating at 210 m s^{-1} and 450 m s^{-1} (Hammel *et al*. 1995). If such a wave is neither an acoustic body wave nor a surface wave, it is probably a gravity wave, propagating either in the stratosphere (Walterscheid *et al*. 2000) or in a deeper layer. In the later case, an enhancement by a factor 10 of the water content at the 10 bar depth is necessary for explaining the wave speed (Ingersol *et al*. 1994; Ingersoll and Kanamori 1995). See Kanamori (2004) for a detailed discussion of this wave.

5. THE FUTURE: Mars Seismology

We now return to the inner solar system, specifically to discuss in detail Martian seismology. In the previous section, we showed that indirect seismological exploration of Mars may be possible (but very challenging and still subject to further theroretical discussions) through studies of continuous excitation of normal modes by the Martian atmosphere global circulation. Here we revisit traditional, quake-based seismology. Though several seismic network missions has been studied in the last 15 years, as described in detail in Lognonné (2005) none of these projects has so far led to launch of a seismic experiment. Such a network would, contribute enormously to our understanding of Mars as a planet, and in our opinion should be one of the highest priorities for imminent exploration of Mars.

The lack of detection of quakes on Mars by the Viking landers (Anderson *et al.* 1977a, 1977b), along with the failure of the Mars96 mission, including the two small seismometer-equipped autonomous stations and two penetrators, means that no past missions have returned seismic information on the martian interior. Consequently, the internal structure of Mars is very poorly known. We briefly review the existing constraints on models of the internal structure. We then describe the typical variations of the seismological parameters (e.g. seismic velocities, attenuation), which can be expected from current knowledge of Mars. We finaly discuss issues related to the design of a passive seismic experiment that could provide observations of body waves, surface waves and normal modes. We focus on considerations relevant to a network with a relatively small number (e.g., 1-5) of seismic stations.

5.1 Interior structure of Mars

Seismic and density models of Mars have been proposed by several authors since the Viking mission. The two main types of constraints used in such studies are geophysical and geochemical. Geophysical constraints include the mean density of the planet, obtained from the planetary mass (M) and the planetary radius (a) the mean moment of inertia factor (I) or the moment of intertia with respect to the rotation axis (C), and the k_2 Love number, associated to the gravity signal generated to the Sun tide. Okal and Anderson (1978) proposed a model based on the preliminary earth model (PREM), with a core size adjusted to fit only the mean density. In this model (and similarly for other models) the pressure range in the entire Martian mantle corresponds to that in Earth's upper mantle.

A second set of constraints is provided by geochemical inferences of the bulk composition, based on analyses of the composition of Martian meteorites. One of the most-used models, proposed by Dreibus and Wänke (1985) assumes that the bulk silicate Mars composition is a mixture of C1 material and volatile-depleted C1 material, with a Mars crustal composition constrained by the SNCs. Other model mixtures have been proposed, in order to match the $\delta^{17}O/\delta^{18}O$ ratio: a 55% ordinary chondrite H and 45% enstatite chondrite EH (Sanloup *et al.* 1999), or a 85% H chondrite, 11% CV chondrite and 4% C1 chondrite (Lodders and Fegley, 1997; Lodders, 2000). One of the important features of these models is the enrichment in iron in the mantle (around twice the Earth's value). As illustrated by Mocquet et al. (1996), the presence and depth of seismic discontinuities in the mantle of Mars will be related to the iron content if the mantle is olivine rich (about 60% in volume). A pyroxene-rich mantle (e.g. Sanloup et al., 1999) should display different discontinuities with smaller amplitudes of the seismic jumps (Verhooven et al. 2005).

Several models have proposed revised estimates of the inertia factor, as compared with that in Sohl and Spohn (1997) and Zharkov and Gudkova (2000), who used a value of $C=0.365\ Ma^2$, corrected for the non-hydrostatic contribution of the Tharsis bulge (Kaula 1979). This value is close to that obtained later from the measurement of the precession rate of the planet by the Pathfinder mission ($C=(0.3662 \pm 0.0017)Ma^2$, Folkner *et al.* 1997). More recent estimates that include data from the Mars Global Surveyor (MGS) mission are slighly lower ($C=(0.3650\pm0.0012)MR_e^2$ where R_e is the equatorial radius, Yoder *et al.* 2003). This gives a value of $C=(0.3660 \pm 0.0012)Ma^2$ when the mean planetary radius is used. All these values should be corrected from the gravitational oblateness J_2 (Munk and MacDonald 1975) and from the J_{22} term (Sohl *et al.* 2005) in order to get the mean moment of inertia:

$$I = C - \frac{2}{3} J_2 Ma^2 - \frac{8}{3} J_{22} Ma^2 \quad (15)$$

These corrections reduce the C value by 1.30e-3 and 1.68e-4 respectivelly (Sohl *et al.* 2005) leading to C=(0.3645 ±0.0012)Ma^2 for the Yoder *et al.* (2003) value The other geophysical datum measured to date is the Love number k_2, obtained from gravity analysis of orbiting spacecraft. This value is, however, poorly known. If, following Yoder *et al*. (2003) and Bills *et al.* (2005), the value of k_2 is about 0.15 or larger, then only models with large core radius will be possible, as shown by van Hoolst *et al.* (2003). However, lower values for k_2 in the range of 0.10-0.13, have been determined by other authors (Smith *et al.* 2003; Balmino *et al.* 2005). In general, as shown in Figure 31, these data support iron cores with some light element(s). Light elements that have been proposed in addition to sulfur (e.g. Dreibus and Wänke 1985), include hydrogen (Gudkova and Zharkov 2004), silicon (Stevenson 2001; Sanloup *et al.* 2002) and carbon (Kuramoto 1997), while oxygen, another light element possibly present in the Earth's core is less likely on Mars (Rubie *et al.* 2004). A relatively low density core with high H content, as suggested by Gudkova and Zharkov (2004), seems less supported by the new reduced values of the moment of inertia. A detailed analysis of the models proposed by these authors shows that the core's size variations are about ±150km (Figure 31). This is large enough for major differences in term of planetary evolution. As an example, the presence of a perovskite-bearing lower mantle becomes impossible, due to insufficient pressures in the mantle. An endothermic phase transition from spinel to perovskite has been suggested to be required in mantle convective models for the early formation of Tharsis (Harder and Christensen 1996; van Thienen *et al.* 2006). The size and state of the core are also critical to understanding the cessation of an early Martian dynamo (Acuna *et al.* 1999; Stevenson 2001; Breuer and Spohn 2006). Thus, the determination of the core size is a key objective for seismology, not just for the knowledge of present-day interior structure, but in order to constrain models for the geodynamical evolution of Mars.

Two other deep interior parameters that affect seismic wave propagation and therefore the design of future seismic experiments on Mars are the physical state of the core (liquid or solid) and mantle attenuation. A liquid (outer) core may result in a seismic shadow zone, as observed on the Earth, and a highly attenuating mantle (due to volatiles, and perhaps locally warm temperatures) can strongly reduce the amplitudes of the short period body waves, as may be the case on the Moon (Nakamura 2005). A liquid core is likely and is supported by Phobos tidal acceleration value (Bills et al. 2005) and by the large k_2 value. As noted by Lognonné and Mosser (1993) and by Zharkov and Gudkova (1997), the low value of the martian Q at the Phobos tidal period would imply an unrealistically low intrinsic Q of the planet if the core is solid. In contrast, a Q corresponding to silicate material is found for a liquid core (Lognonné and Mosser 1993). The extrapolation from the tidal Q to the seismic Q can be performed using the frequency dependence proposed by Anderson and Given (1982). Assuming that Phobos' frequency is in the seismic bandwidth, we obtain a shear Q of about 200 at 100 seconds (using a power law of 0.15, Lognonné and Mosser 1993; Zharkov and Gudkova 1996), as compared to a Q of 85 at the 5h32min Phobos period. This is between the lower mantle PREM (Dziewonski and Anderson 1981) shear Q (about 310) and the upper mantle one (about 140). Moreover, we can assume that higher Q might be found in the upper mantle, depending on the actual temperature profile.

Other details of mantle structure remain largely unknown. A key parameter, in terms of seismological inferences, will be the iron content of the mantle. Mocquet *et al*. (1996) have studied the effect of increasing iron content from 10% to 40% and many other models have Fe ranging from 20 to 30% (Dreibus and Wänke 1985; Sanloup *et al*. 1999; Gudkova and Zharkov 2004). The main effect of an increase in iron is to smooth the seismic discontinuities associated with α-olivine to β-spinel and β-spinel to γ-spinel, as seen in Figure 32 for both the density and acoustic velocity v_k ($v_k^2 = v_p^2 - 4/3\ v_s^2$). For an iron content of 20%, the width of the transition zone is seen to be between 50km and 100km. This is in contrast to the Earth, for which both the reduced iron content and the higher pressure gradient result in sharp discontinuities, with a typical width of less than 10 km (e.g., Tibi and Wiens 2005). Reflections from mantle discontinuities on Mars might be expected to be less impulsive than on

Earth and observable only at long periods, when the seismic wavelength is much greater than the width of the discontinuity, i.e. below frequencies of 0.05-0.1 Hz. Consequently, these phases might be observed only for the largest quakes. In summary, we can expect that, as for the Moon, most of the mantle information will be obtained from direct P and S waves and from phases reflected at the core and the surface (PKP, PcP, ScS, PP, etc).

5.2 Martian seismic noise

One of the main reasons for the lack of seismic activity detected by the Viking seismic experiment was the wind sensitivity of the seismometer. This wind noise was primarily the consequence of the seismometer location. The seismometer was deployed on the platform of the lander; coupling with the ground was provided by the elastic legs of the lander and the seismometer detected the vibrations of the lander due to noise. We can expect better success from a future mission with installation of the seismometer directly on the ground. A rather simple wind-shield covering the seismometer can strongly reduce wind effects. Field tests have demonstrated performance on the Earth at a noise level almost comparable to the Low Noise model at periods of a few 10s of seconds (Lognonné *et al*. 1996) and we can therefore expect noise levels as low as 10^{-9} ms^{-2} $Hz^{-1/2}$ in the bandwidth 1Hz-0.05 Hz, dominated on Earth by the micro seismic peaks.

As Mars has neither an ocean (the major source of terrestrial noise between 0.07 Hz and 0.14 Hz) nor human activity, we can expect low seismic noise compared with Earth. Wind-generated noise has been estimated by Lognonné and Mosser (1993), and temperature-generated noise by van Hoolst *et al.* (2003). Ground accelerations produced by the direct deformation of the Martian surface by the wind pressure fluctuation could have peak-to-peak amplitudes on the order of 10^{-9} m s^{-2} in the range of 0.1 to 0.01 Hz, during relatively calm conditions with wind speeds of ~4 m s^{-1} (Lognonné and Mosser 1993). Moreover, Lognonné *et al.* (1996) have shown that even on Earth, prototype Martian seismometers can reach such noise levels at a quiet site when protected by a light windshield. In contrast to the Viking mission, temperature variations may be the major source of noise for surface-installed VBB (very broad band) seismometers. However, as shown by van Hoolst *et al.* (2003), most of the temperature variations on Mars are associated with the daily cycle and can be approximated by a Fourier series with the fundamental mode (of 24h 56min) and its harmonics. Moreover, thermal insulation of space-qualified seismometers can reach time constants larger than 2 hours (D. Mimoun, personnal communication). This will reduce temperature variations experienced by the sensor by a factor of ~7 at 1 mHz, and ~700 at 0.1 Hz, leading to temperature fluctuations smaller than a fraction of a degree in the seismic band. An installation with a noise level comparable to the terrestrial low noise model (e.g. about 10^{-9} m s^{-2} $Hz^{-1/2}$ in the seismic bandwidth, see Pederson 1993) is therefore a realistic challenge, and could be further improved with an environmental correction performed using pressure and temperature data (e.g. Beauduin *et al.* 1996).

5.3 Body wave detection

Due to the lower event magnitudes as compared with Earth (see Figure 13 in Section 3), the best signal-to-noise data will probably be found in the bandwidth of body waves and regional surface waves. The main limitations for body wave detection will be attenuation and diffraction. The importance of attenuation on Mars was originally pointed out by Goins and Lazarewicz (1979), who showed that the Viking seismometer, operating with a free frequency of 4 Hz, was unable to detect remote events due to attenuation. For a Q of 325, obtained as explained in section 5.1, and a velocity of 5 km s^{-1}, amplitudes of S waves are reduced by a factor of 10 after 1200 km of propagation at 1 Hz. Amplitudes at 4 Hz are reduced by the same amount only after 300 km of propagation. The amplitudes of body waves are plotted in more detail in Figures 33a and 33b after Mocquet (1999). The amplitudes are computed for two frequency bands (0.1-1 Hz, 0.5-2.5 Hz), for an isotropic surface source (quake) with a seismic moment of 10^{15} Nm. Transmission across a crust-mantle boundary is taken into account, as well as geometrical spreading and attenuation, for a Mars model compatible with the present a priori knowledge and a shear Q provided by $Q_\mu=325-\log_{10}T$, where T is the period.

At frequencies higher than 0.5 Hz (0.5-2.5 Hz), the amplitudes of the body waves decrease rapidly with epicentral distance (Figure 33). Amplitude is relatively independent of epicentral distance only for P waves in the frequency band 0.1-1 Hz. Consequently, this frequency band, with a 1 ng resolution, was chosen for the Optimism seismometer (Lognonné *et al.* 1998a). At higher frequencies (0.5-2.5 Hz bandwidth), however, amplitudes decrease rapidly with source-receiver distance and are less than S wave amplitudes at the longest periods (Figure 33a). For an instrument with noise characteristics of 1 ng $Hz^{1/2}$, noise levels of ~2.5 ng rms will be expected in the 0.5 – 2.5 Hz frequency bandwidth, limiting the detection of S waves at large epicentral distance to quakes with a moment larger than 10^{15} Nm.

Short period body waves are also sensitive to scattering. This has been demonstrated on the Moon and is due to the intense fracturing of the crust, from meteoritic impacts as well as tectonic structure (e.g. Dainty and Toksöz 1977; Nakamura 1977). On the Earth, scattering is also very strong in volcanic regions. These combined effects suggest that significant scattering may occur in volcanic areas on Mars, particularly in the Tharsis region. For body waves, scattering reduces the peak-to-peak amplitudes by producing conversions (mainly P to SV, P to SH), and spreads this energy in time. This leads to energy transfer from P to S waves up to an equipartition given by $E_p = \frac{v_s^3}{v_p^3}\frac{E_s}{2}$, where E_p, E_s are the energy of P and S waves and v_p , v_s are the velocities of P and S waves respectively (e.g. Aki 1992; Papanicolaou 1996).

This scattering mainly affects P waves. For shallow quakes it will reduce the amplitude of the P waves near the source and the receiver: first during the downward propagation from the crust to the mantle, near the source, and again during the upward propagation from the mantle to the surface, near the receiver. The effect can be a reduction by a factor of 10 of the P wave energy, with larger amplitude reduction due to the length of the coda.

The potential efficiency of a future network configuration can be investigated using these results, as shown by Mocquet (1999). Figure 34a details such a study for a possible network configuration, assuming total detection for signals with accelerations greater than 10^{-8} m s^{-2} peak-to-peak. They show that a rate of 60% can be achieved for the detection of quakes with seismic moment greater than 10^{14} Nm, i.e., corresponding to Earth moment magnitude greater than 3.2. As shown on Figure 13, depending on the seismic activity, between 40 and 400 quakes with at least this seismic moment are expected to occur during one Martian year. Note that the 4-station network configuration, in contrary to the lunar seismic network, will allow a much better characterisation of the core, with antipodal stations near Hellas Planitia. Figure 34b shows the increase in coverage for a network configuration with an additional station, which would also provide redundancy. Source localisation errors will affect the determination of the seismic velocities and might be large for network with only a few stations. These have been discussed by Gagnepain-Beyneix *et al.* (2006), for the lunar case.

5.4 Normal mode excitation and tidal observations

While the extraction of internal structure information from the direct body waves will need precise event localization, and hence at least 3 stations for travel time analysis (6 travel time data enabling the determination of the 4 source parameters and two mean mantle velocities), surface wave and normal mode analyses have the potential to provide useful information on the interior with fewer stations. As noted above, a cumulative activity of 10^{18}-10^{19} Nm per year means it may be possible to record quakes with moments as large as 10^{18} Nm if the station is operated for one Martian year or more. The excitation of normal modes by marsquakes was studied by Lognonné *et al.* (1996) and later by Gudkova and Zharkov (2004). Both studies concluded that the observation of normal modes between 5 mHz and 20 mHz with a noise level of 10^{-9} ms^{-2} $Hz^{-1/2}$ will be possible from stacked records of quakes with a cumulative 10^{18} Nm moment or from single record analysis of the greatest quakes (Figure 35). Normal modes will peak, with a signal to noise ratio of about 10, within Q-cycle windows

for such quakes, which correspond to moment magnitudes of 5.5 (Lognonné *et al*. 1996). Due to the size of the planet however, the frequencies of the modes, for a given angular order, are typically twice those on Earth (Figure 36). The observation of normal modes below 5 mHz, which are the most sensitive to the core size, will be more challenging with such quakes: modes like ${}_0S_2$ might remain below the instrument or station noise, especially because of temperature fluctuations due to operation of the first Mars seismometers at the surface.

As noted by Lognonné and Mosser (1993) and van Hoolst *et al.* (2003), an alternative core structure constraint will be a measure of the solid tide amplitude, and therefore of the associated Love numbers, by a surface sensor. A successful measurement will be mainly determined by the temperature noise and will require a stack of year-long time series. Van Hoolst *et al*. (2003) have shown that a noise level of about 0.5 K rms in a frequency bandwidth of 1 mHz around the Phobos tide is expected, based on the Viking temperature data. Both temperature decorrelation and thermal protection can reduce this signal by a factor of 100-250 after data processing, leading to a final noise level of 2.5-1 ng rms after one Martian year of stacking and an error in the core determination equal to 60 km for 1 ng rms of noise.

5.6 Surface waves

Though no surface waves were recorded on the Moon by the Apollo seismometers, the better performance at long period expected of the seismometers bound for Mars and the larger magnitude of marsquakes suggest the possibility of such detections on Mars. By sampling the crust, lithosphere and upper mantle, surface waves will be an important source of information. Their group velocities for example are very sensitive to the crustal thickness, with 10% typical variations for crustal variations of 20 km (Figure 10). The sensitivity to the upper mantle will also be important, and the group velocity of surface waves (or the differential group velocity between the fundamental and the overtones) varies by 5-10% for the models of Mocquet *et al.* (1996) with different iron content (Figure 10).

The practical difficulties in data analyses will be related to quake localization errors and to the effect of lateral variations in the surface waves. These errors will be the most critical if only a limited number of stations are deployed and may produce errors in the determination of spherically symmetric models of the mantle. In the band 5 mHz-50 mHz, surface wave analysis could be performed by two stations equipped with 3 axis seismometers, enabling the determination of the back-azimuth of surface waves. Figure 38 shows that errors in the relative epicentral distance of less than 2.5% can be achieved over a wide equatorial band of the planet (± 20° latitude), for two typical landing sites around the Tharsis Buldge, when back-azimuth errors of 15° are assumed. Such measurements could resolve the major differences among currently-proposed mantle models (Figure 32). However, limitations due to the sensitivity of surface wave azimuth to lateral variation in crsutal thickness means that it will not be possible to detect smaller differences, such as those related to the FeO content in the mantle (Mocquet *et al.* 1996). On the Earth, such aziumthal variations can reach typically 10° and it is possible that lateral variations in crustal structure on Mars will lead to larger effects (Larmat *et al.* 2006). However, as observed on the Earth, much of the lateral variations of surface waves can be modeled with a priori on the lithosphere and upper mantle (Nataf and Ricard 1996). With the recent improvements in crustal thickness estimates (Zuber 2001), lithospheric thickness (Belleguic *et al.* 2004) and crustal heating, we can expect future developments in the modeling of the effect of the crustal and lithospheric lateral variations on surface waves and associated corrections.

6 CONCLUDING REMARKS

Planetary seismology began almost concurrently with planetary exploration, with seismometers onboard the Ranger probes in the early 60s. The success of the Apollo seismic network has shown that a planet much less active than the Earth might nevertheless, due to the very low noise level, allow the

detection of several events per day. Both meteorite impacts and moonquakes were recorded on the Moon over a period of more than 7 years. Deep moonquakes remain enigmatic: repeated brittle failure at specific source locations is inferred on the basis of waveform similarity and tidal periodicities. Major questions remain however – tidally generated stresses are small relative to those expected to result in failure, and why brittle failure occurs at depths of 800-1000km is not well understood. Large uncertainties in many source region locations exist; to date it has not been possible to determine focal mechanisms for these events, although the prominence of shear wave arrivals in the seismograms suggests that shear failure is occurring.

Meteorites and moonquakes, together with known artificial impacts have allowed first order investigations of the variation of seismic velocity with depth. Crustal thickness estimates made shortly after the Apollo missions were suggested to be on the order of 60km, more recent studies have revised these estimates to 30-45km. Seismic velocity estimates to depths of ~1000km are possible; source receiver geometries prohibit direct seismic investigation of lowermost mantle and core structure. Differences among current model estimates for mantle seismic velocities reflect a combination of network geometry, instrument limitations, and likely three-dimensional structure. Thus the seismic exploration of the Moon is far from complete. Large uncertainties remain in the internal structure and major discontinuities (core/mantle, lower/upper mantle, mantle crust) are still not well constrained. Moreover, currently umnapped geographical variations in crustal and mantle stucture are a critical key to understanding early lunar evolution.

The work reviewed in this chapter demonstrates that the technology exists to perform ground-based seismic experiments on the Moon and on Mars. The installation of a seismic network on Mars has been recommended repeatedly (NRC, 2006); understanding the global internal structure is crucial complementary information to the extensive satellite and rover-based imaging currently underway. Characterization of local, regional, and global seismicity is essential to understanding the present day tectonic, volcanic and climatic environment of the planet.

Exciting possibilities also exist for remote(satellite)-based detection of seismicity and seismic waves, via atmospheric sounding. This could prove fruitful in future studies of Venus, for which long-lived ground-based observations are severely challenging due to surface conditions. In addition it could allow investigations of the giant planets.

Planetary seismology is therefore a virgin territory for future planetary investigation. The deployment of planetary seismic networks will be mandatory for determining the internal structure of telluric planets – critical not only for understanding these bodies, but for comparison with and increased understanding of Eart. Satellite-based observations may afford new opportunities in the seismic exploration of solar system bodies with atmospheres, providing otherwise unavailable avenues for investigating Venus and several outer solar system planets and satellites.

7. ACKNOWLEDGMENTS

CLJ acknowledges support from NASA grants NASA NNG05GK34G, and NAG5-11563, and from IPGP. PL acknowledges support from CNES, PNP and INSU/CNRS for a continuous support in the last 10 years. We thank B.Romanowicz, A.Mocquet, Y.Nakamura and M.Knapmeyer for their constructive reviews. We thank several colleagues who contributed to this chapter through discussions, figures and ideas including A. Mocquet, H.Chenet, J.Gagnepain-Beyneix, B.Banerdt, T.Spohn, M.Knapmeyer, D.Giardini, R. Bulow, M. Wieczorek, P. S. Mohit and M. Jellinek. A special thank to all engineers, technicians and staff members, who have realised the instruments of the various projects described in this paper. This is IPGP contribution xxxx.

8. FIGURE

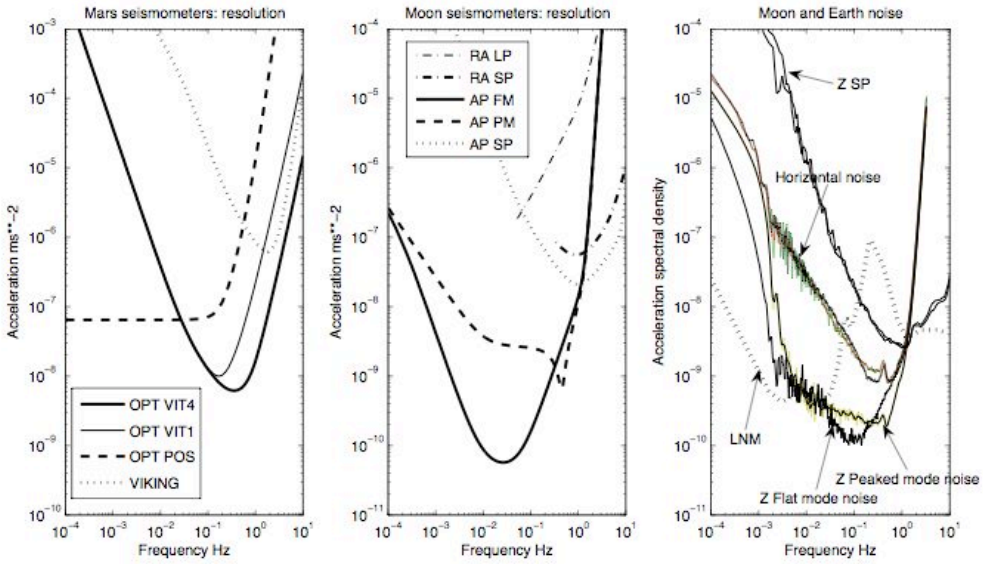

Figure 1: Response curves of the past (a, left) Mars and (b, middle) Moon seismometers. Figure (a) shows the resolution of the Viking seismometer, the Optimism seismometer, in the long period position mode (POS), in the velocity mode OPTVIT1 at 1 sample per second (sps), and at 4 sps (OPT VIT4). Figure (b) shows the Moon case, with the long (RA LP) and short (RA SP) period analog outputs of the Ranger seismometer, the Flat (AP FM) and peaked (AP PM) mode of the Apollo LP seismometer and the short period seismometer (AP SP). The noise levels, recorded on the Moon by the different channels of the Apollo seismometers are compared with the earth-based Low Noise model of Peterson (1993). Noise levels are from the Apollo 12 instrument for the long period (LP) component and from Apollo 14 instrument for the short period (SP) component. These noise levels are likely an upper estimate of the Moon noise and may be related to the instruments.

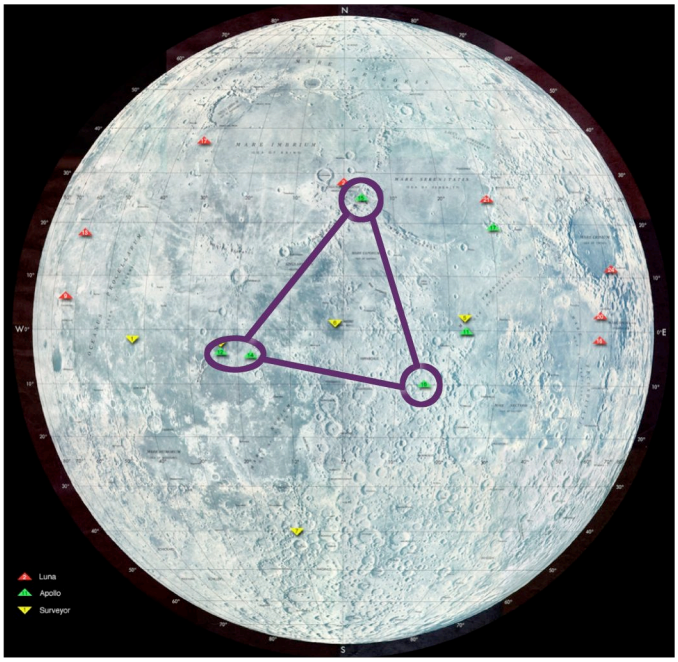

Figure 2: Configuration of the Apollo Seismic Network, A12 is in the Oceanus Procellarum area at 3.01 S, 23.42 W, A14 is located near the crater Fra Mauro at 3.64 S, 17.47 W, A15 is at the foot of the Apennine mountain range at 26.13 N, 3.63 E and A16 is just north of the crater Dolland at 8.97 S, 15.50 E. Note that all stations were on the near side, leading core seismic studies almost impossible. Base map credit NASA.

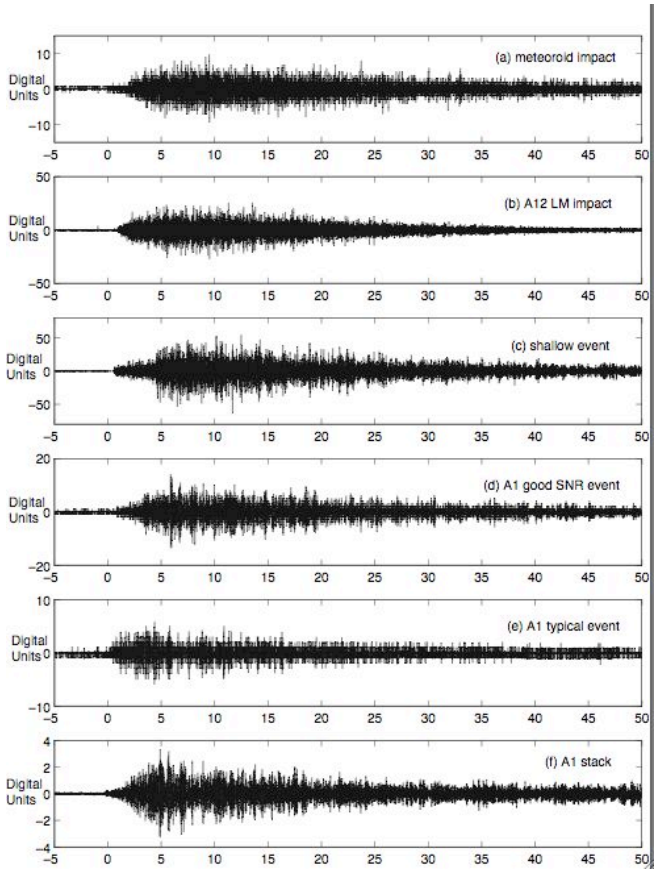

Figure 3: From top to bottom, examples of waveforms for natural and artificial impacts (a-b), shallow event (c), and for the three bottom ones (d-f), from deep moonquakes recorded on long period channels by the Apollo Passive Seismic Network. All records span 55 minutes – x-axis time is in minutes, y axis is in digital units. The following characteristics aided the identification of different seismic sources in the Apollo data: (1) the rise time (defined as event onset to maximum signal amplitude) of moonquakes is typically less than that of meteoroids – see the approximately 5 minute rise time in (c), (d), and (e) above versus the more emergent arrival (perhaps 10 minute rise time) in (a); (2) the large amplitude of the artificial impacts compared with natural events – see the scale for (b) versus (d) and (e) above. (Note that in our example we have chosen one of the largest magnitude shallow events, and this does have comparable amplitude to the chosen artificial impact. (3) Low amplitude and poor data quality of typical deep moonquakes – see (e). However waveform repeatability of deep moonquakes from distinct source regions allows stacking to improve the signal to noise ratio (f)

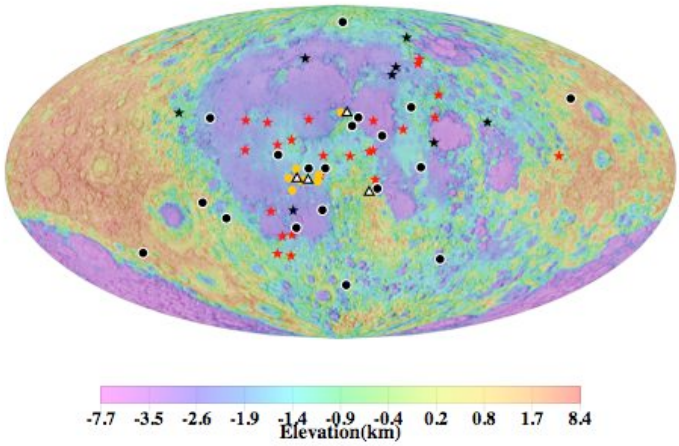

Figure 4: Seismic events located by Lognonné *et al.* (2003) and used in recent velocity models (Lognonné *et al.* 2003; Gagnepain-Beyneix *et al.* 2006), Apollo stations 12, 14, 15, and 16 are shown (white triangles), along with the locations of 24 deep event clusters (red stars), 8 shallow events (black stars), 19 meteoroid impacts (black circles) and 8 artificial impacts (orange circles). Background color map is Clementine topography (Aitoff equal area projection), shaded using a global digital image map (USGS map I-2769, 2002);

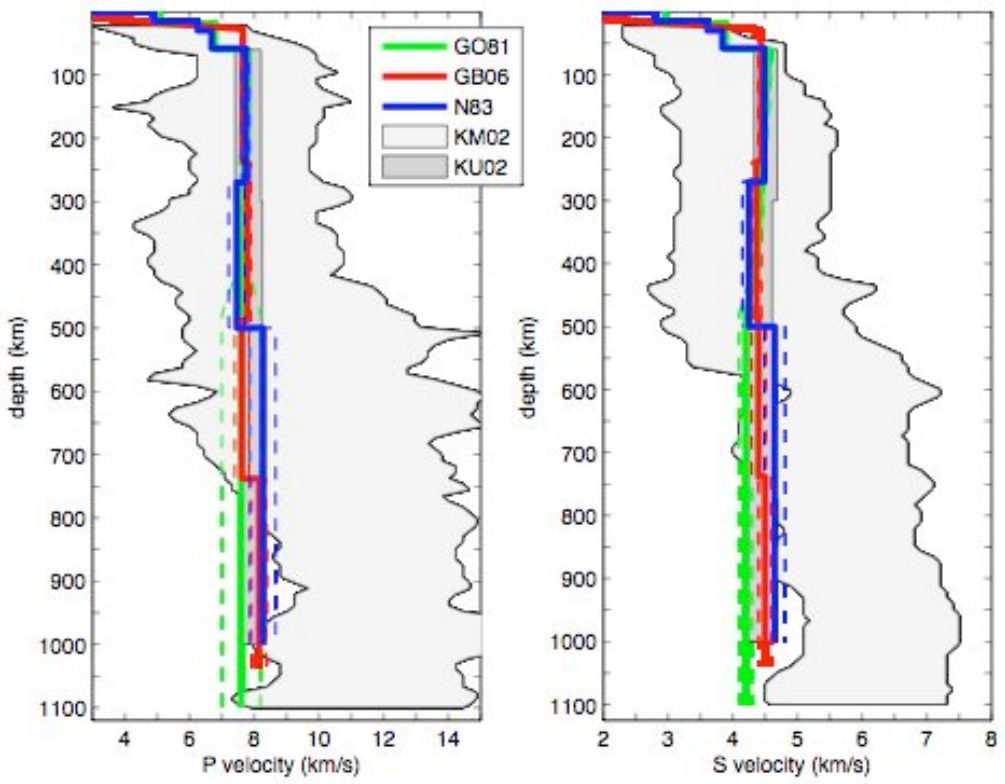

Figure 5: P- and S wave velocity models versus depth: green – Goins *et al.* (1981b), red - Gagnepain-Beyneix *et al.* (2006), blue - Nakamura (1983); The light grew zone is the 80% probability zone of Khan and Mosegaard (2002); The dark grew is the petrology/geochemistry model of Kuskov *et al.* (2002). Values for mantle velocities and associated 1σ uncertainties for each model can be found in Table 1 of Lognonné (2005) and are plotted in dashed line with the same colors for the three first models.

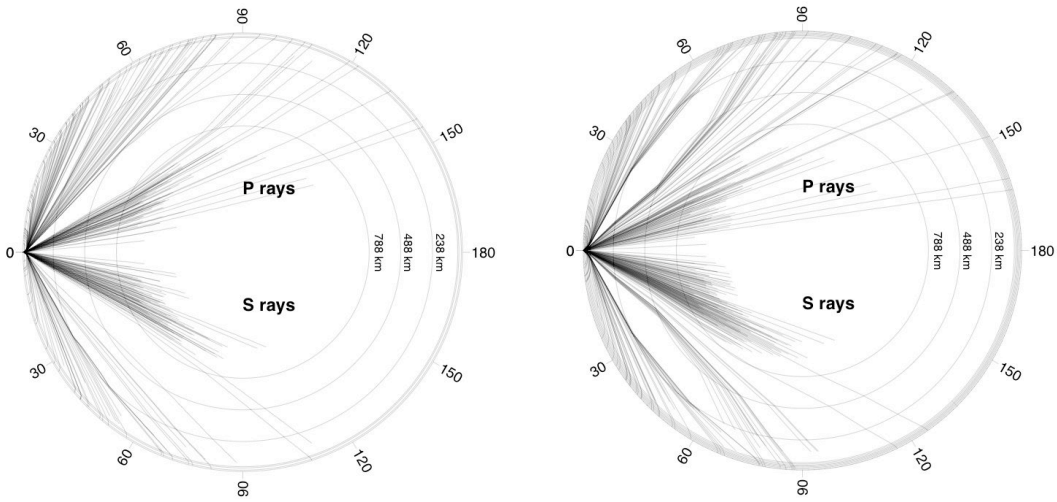

Figure 6a-b: Summary of the source-receiver seismic raypaths for two different seismic models of the Moon determined at the top (a) with the travel times of Gagnepain-Beyneix *et al.* (2006) and at the bottom (b) with the travel times of Nakamura (1983). All pairs of rays are superimposed, with the stations all located at 0° and the source at the actual depth and epicentral distance from the station. (Note the rays associated with deep moonquakes.) The crustal thickness in the left case is 30 km, below which there is a 10 km transition zone in which there is a shear wave gradient. Crustal thickness for the model on the right side is 58 km. Despite differences in the mantle sampling, no rays sound the lunar core for both models. Reprinted from Gagnepain-Beyneix *et al.* (2006) with permission from Physics of the Earth and Planetary Interior.

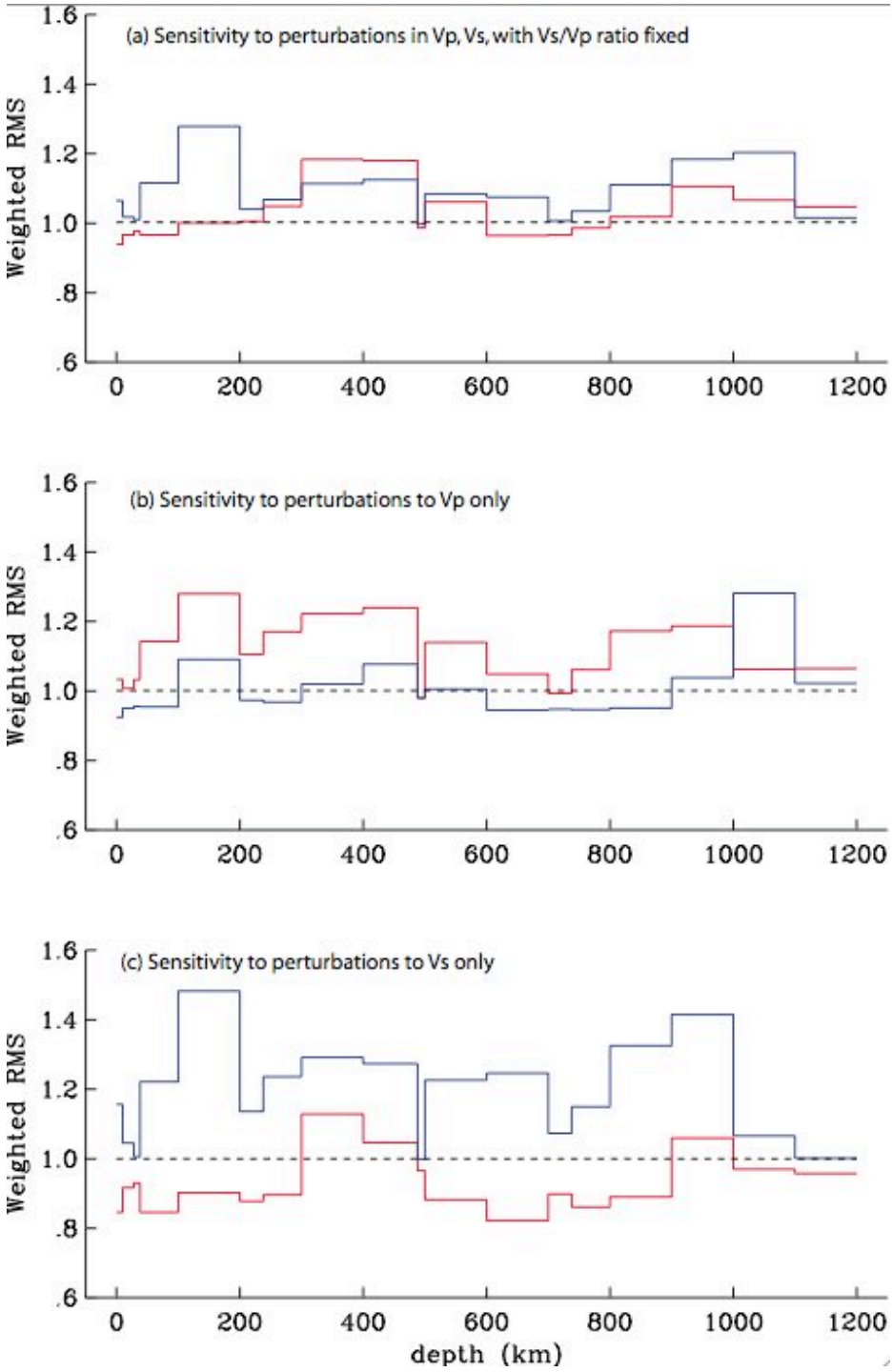

Figure 7: Weighted RMS misfit of the predicted travel times to observed travel times (Lognonné *et al*. 2003) for velocity models in which the velocity model of GB06 is perturbed by 10% in a specified 100 km thick interval. Where the published velocity model comprises layers of thickness less than 100km, the published layer thickness is used. Travel times residuals (observed minus predicted) are weighted by the uncertainty in the travel time pick and the total misfit is normalized such that the misfit to the unperturbed GB06 is 1 (dashed line). GB06 increased by 10% as a function of depth (red); GB06 decreased by 10% (blue). (a) the Vp/Vs ratio is held constant, as specified in GB06, the P-wave velocity is perturbed by ±10% in a specified depth interval and Vs is perturbed using the Vs ratio. RMS misfit is computed using both P and S arrival times. (b) Vp only is perturbed by ±10% and the misfit to the P arrival times computed. (c) Vs only is perturbed by ±10% and the misfit to S arrival times computed.

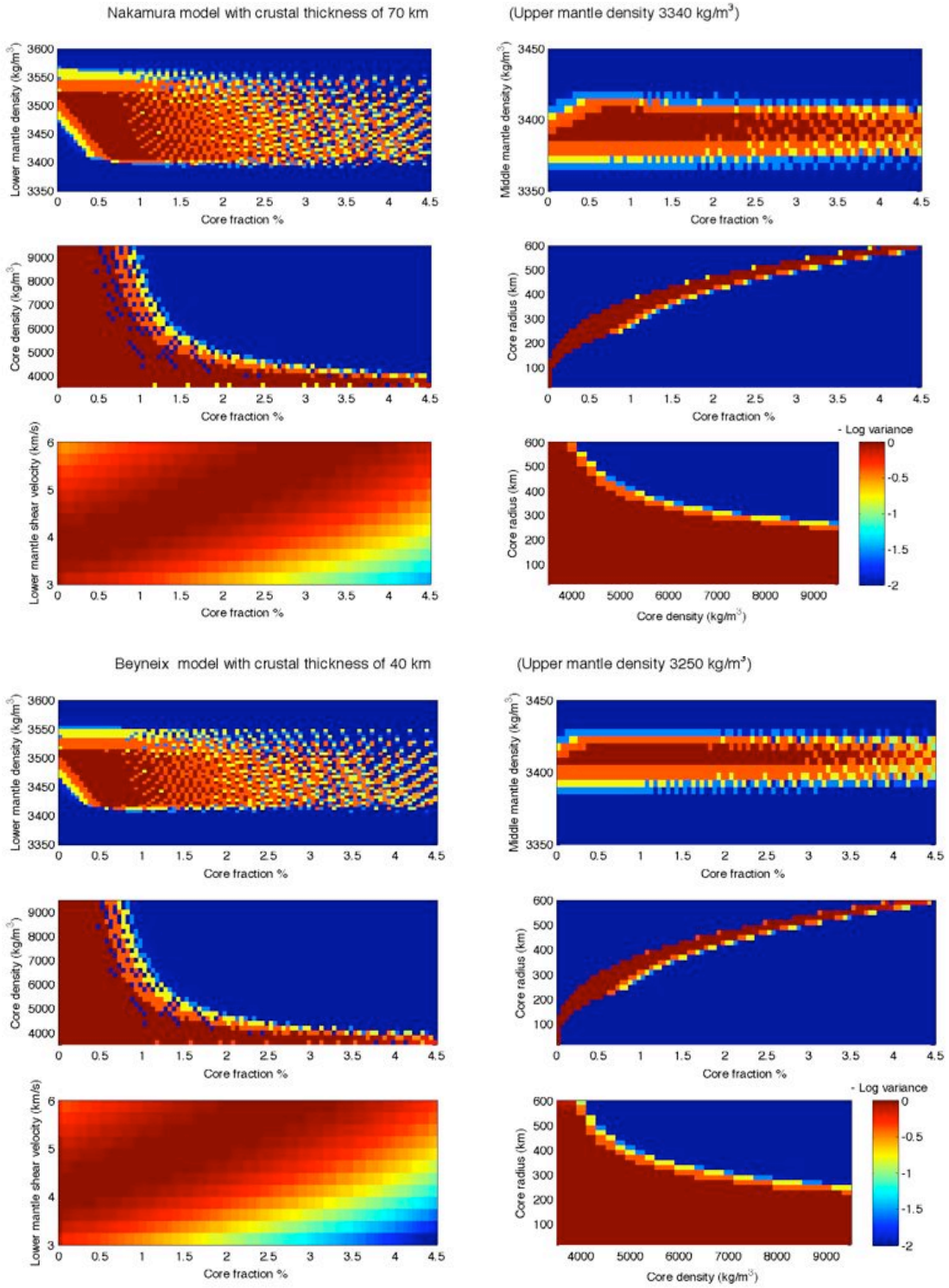

Figure 8a-b: Exploration of the model space for acceptable models for density, inertia factor and Love number k_2 using (a) the seismic models of Gagnepain-Beyneix *et al.* (2006) and (b) Nakamura (1983). The middle mantle is defined between 1500 km and 1000 km radius, while the lower mantle is between 1000 km and the core radius. The color scale represents the decimal logarithm of exp(-var), proportional to the probability, where the variance is between the computed and observed densities, moment of inertia and k_2. For the variance definition, values and errors, see Khan *et al.* (2004). Dark red and red are acceptable models. The model space is sampled in order to identify the range of acceptable solution. In the middle/lower mantle S-wave velocities values are equal to 4.65 km/s and 4.5 km/s in the models of Nakamura (1983) and Gagnepain-Beyneix *et al.* (2006) respectively.

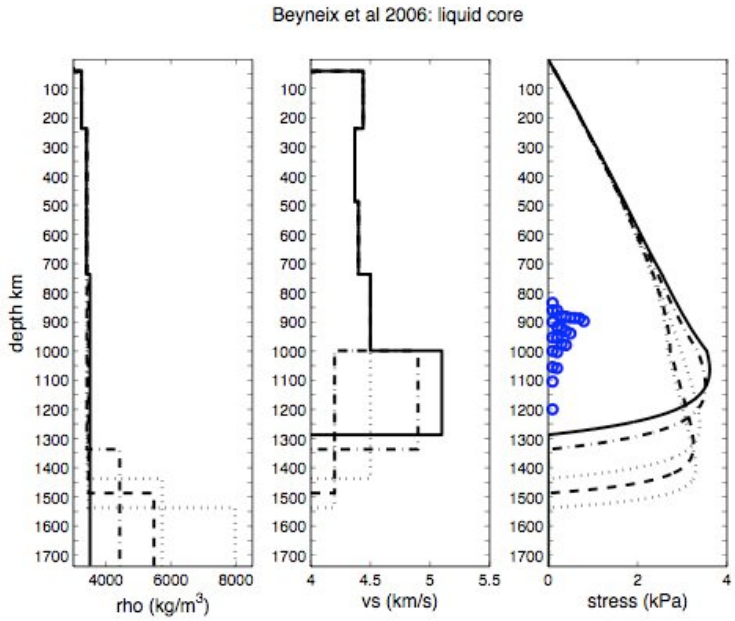

Figure 9: Several seismic and density models of the Moon matching the Apollo seismic travel times, the mean density, moment inertia and k_2 within the data error bars. All models have S-wave velocity values of Gagnepain-Beyneix *et al*. (2006) for the mantle and crust and only the shear velocity in the very deep mantle is modified. Shear velocity in the core is zero, as only models with liquid core are shown. The various lines are each associated with a given core size and minimize the variance. Figures from left to right represent the density, the shear wave velocity and the tidal stresses. Models with the largest core (400 km or more) correspond to an ilmenite core (Wieczorek and Zuber 2002) with core densities lower than 5000 kg m^{-3}. These have correspondingly high shear velocity in the lower mantle. Models with a core radius of 350 km correspond to an FeS core, with densities in the range of 5000-6000 kg m^{-3}. Smaller cores (~200km) of pure Fe are also compatible with the data if associated with a low velocity zone in the lower mantle, in order to match the low k_2 value. On the far right, the maximum horizontal tidal stress, with respect to depth, is shown, defined as $(T_{\theta\theta}+T_{\phi\phi})/2$, where T is the tidal stress tensor, at the latitude and longitude of the deep Moonquake A1 (as found by Gagnepain-Beyneix *et al.* (2006), i.e. -15.27°S, -34.04°E). See Minshull and Goulty (1987) for more details on stress computations. Note that only models with a core radius of 350 km or more produce maximum tidal stresses in the vicinity of the deep moonquakes.

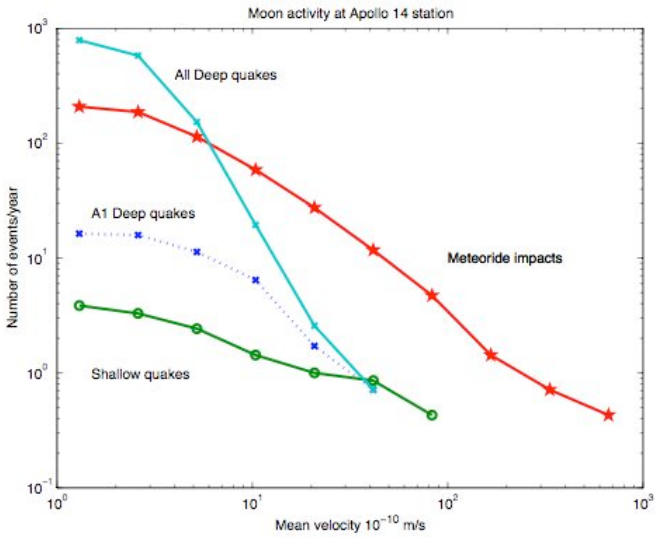

Figure 10: Number of events/year detected on the Apollo 14 station versus amplitude. Amplitudes are from the Nakamura (2004) catalogue and converted approximately as mean velocity, assuming a recording by the long-period horizontal component on the peaked mode and peaked frequency. Note the very high number of events detected, despite their very low amplitudes (See Figure 1 for seismometer sensitivity)

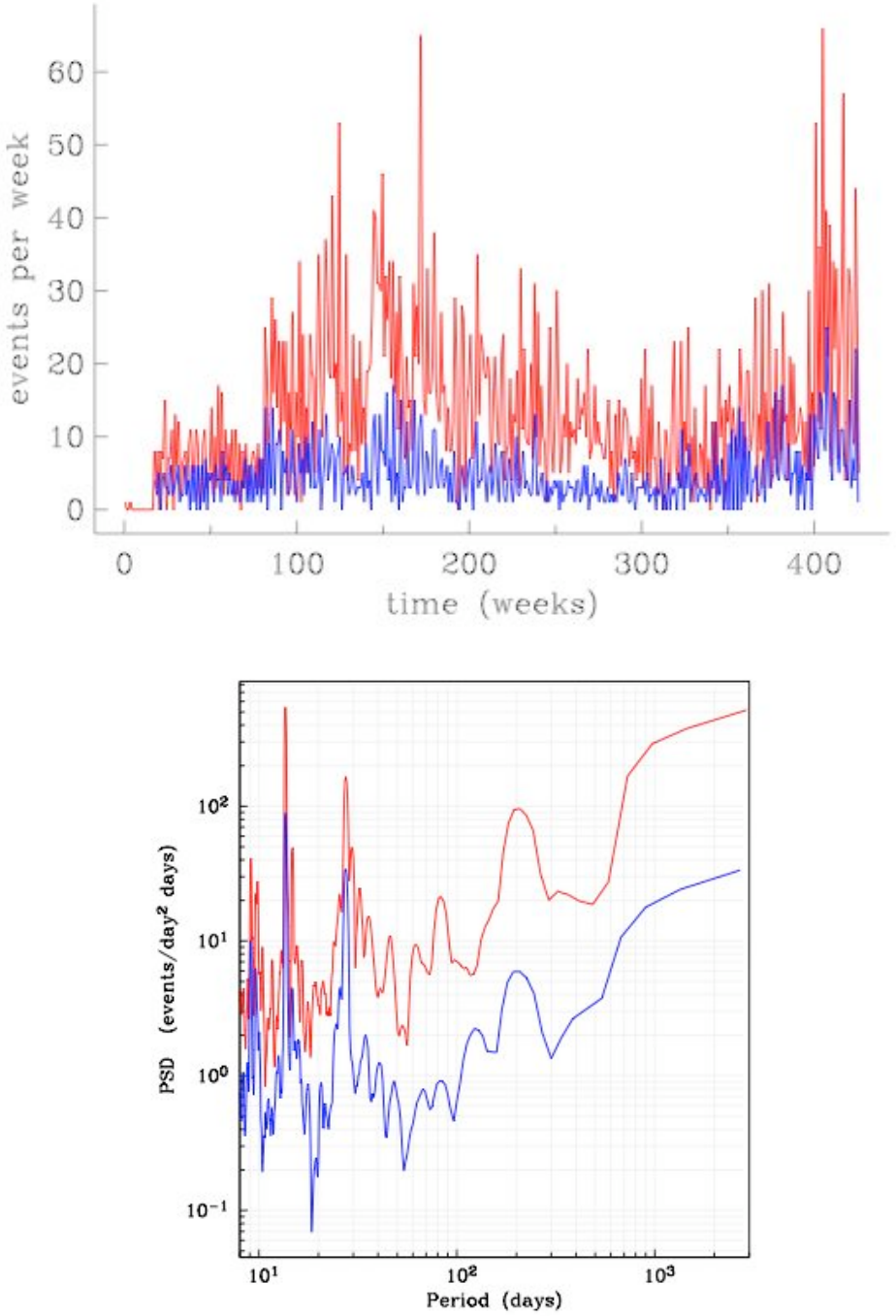

Figure 11: Deep moonquake activity. (a) Number of moonquakes per week versus time in weeks, starting from the beginning of the seismic experiment is shown. Moonquake activity for a recent update of the deep moonquake catalog (Nakamura *et al*. 2004), is shown in red. For comparison, moonquake activity at 9 of the most active deep clusters is shown in blue. This includes new events recently found by Bulow *et al.* (2005, 2006) and not included in the lunar catalog (Nakamura *et al.* 2004). (b): Power spectral density of number of moonquakes per day vs. period in days. Peaks at ~14, 28, and 206 days can be seen, and power at the longest periods likely results from a 6-year modulation of moonquake occurrence times. Red and blue curves are as in Figure 11a.

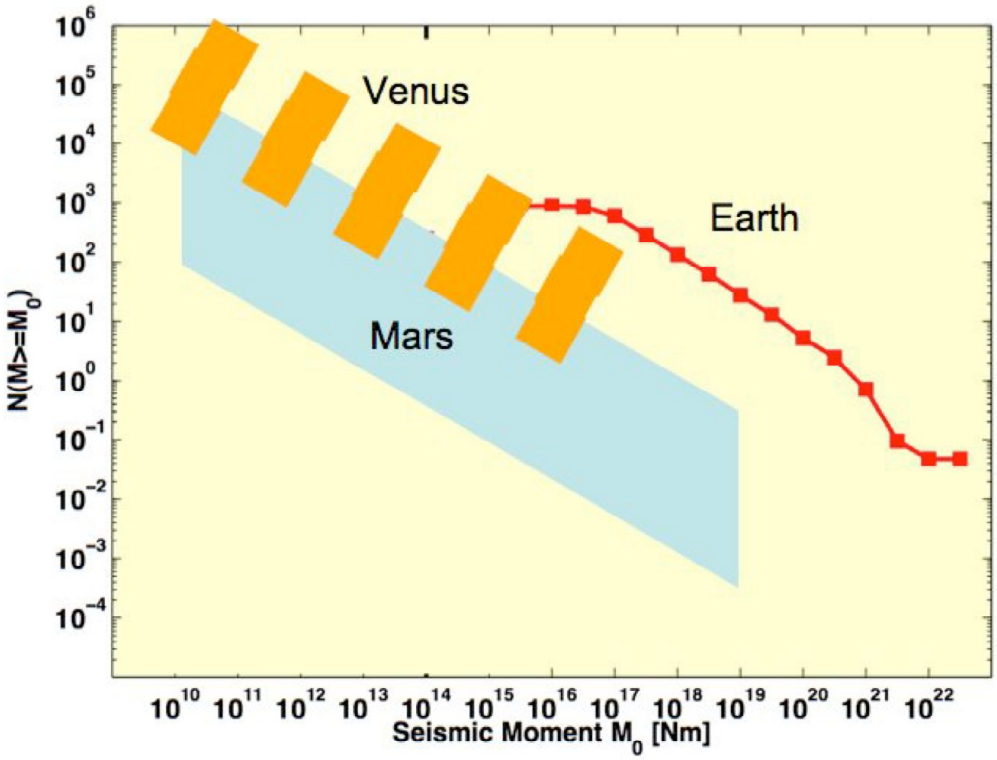

Figure 12 Seismic activity of the telluric bodies. The figure shows the number of events per year larger than a given seismic moment. For the Moon, the estimate is obtained from Oberst (1987) and is only for the shallow moonquakes. For Mars and Venus, the activity is estimated from various published models, based on the thermoelastic cooling of the lithosphere. The terrestrial activity is the mean activity in the period 1984-2004. Figure after Knapmeyer *et al.* (2006)

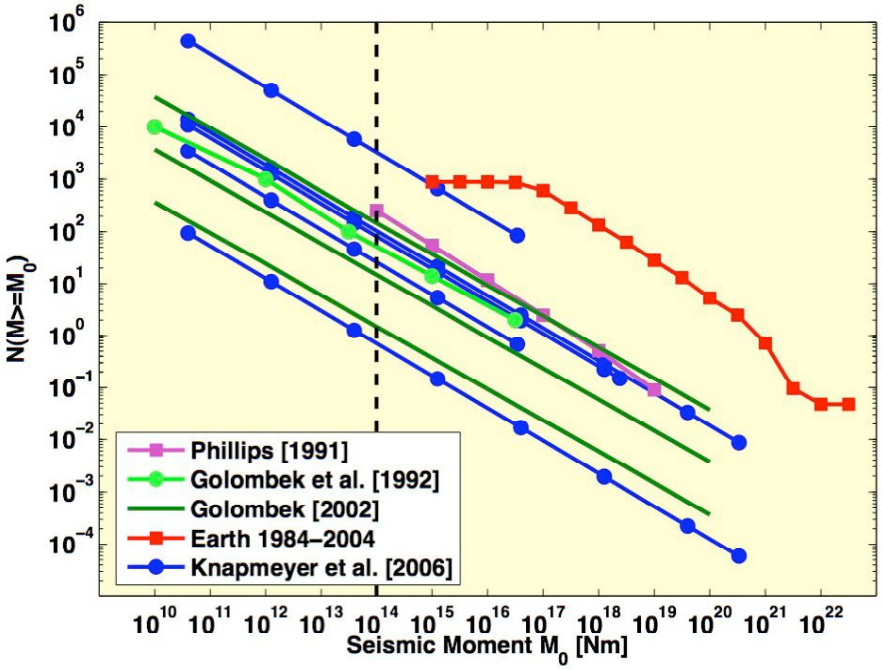

Figure 13: Comparison of models for Martian seismic activity per year with the terrestrial mean annual activity (Knapmeyer, personnal communication). Most models predict a total of 10 to 100 quakes per year with moments larger than 10^{15} Nm. The dashed line is for quakes of Moment 10^{14}, which S, respectively P, body waves have amplitudes in the 0.1-1Hz bandwidth of about 10^{-9} ms^{-2} peak-to-peak and 2 10^{-8} ms^{-2} at 100° of epicentral distance (Mocquet *et al.* 1999) and may therefore be at the limit of detection for estimated martian noise levels (Lognonné *et al.* 2000). The multiple lines shown for Golombek (2002) and Knapmeyer (2006) are for different hypotheses regarding the seismicity.

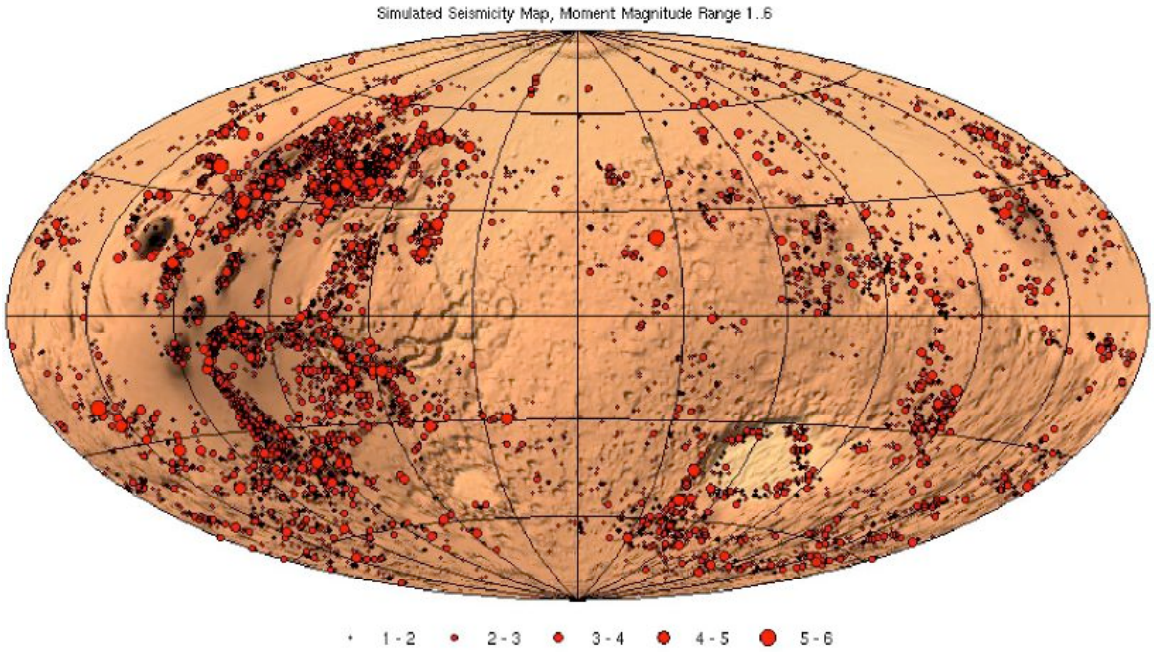

Figure 14: Seismicity map of Mars from Knapmeyer (2006), determined from a MonteCarlo simulation of seismic activity releasing a cumulated moment of 10^{18}-10^{19} Nm per year (from Golombek *et al.* 1992), and with a probability distribution of epicenter locations provided by the density of surface faulting The map shows the distribution of marsquakes that might be expected during one Earth year, with a annual seismic budget between the upper and lower bounds (Knapmeyer, personnal communication).

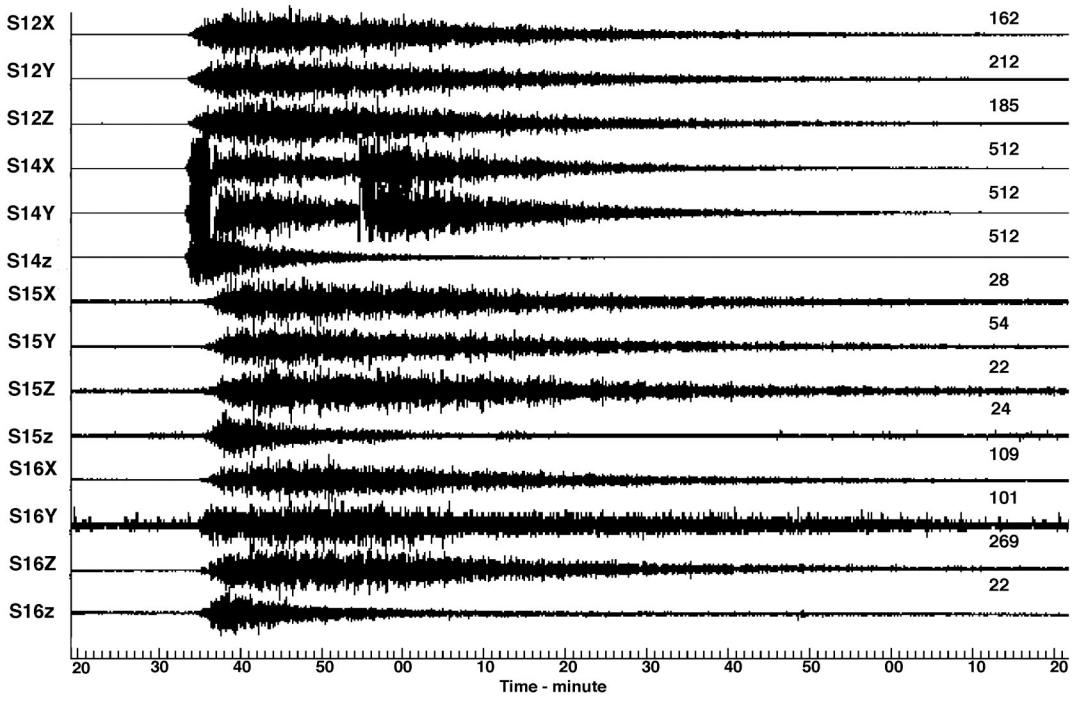

Figure 15: Seismic records, from the Apollo seismic network, of the impact of the Apollo 17 Saturn V upper stage (Saturn IVB) on the Moon on 10 December 1972 at 4.21°S, 12.31°W (at distances of 338, 157, 1032 and 850 km from the Apollo 12, 14, 15 and 16 stations, respectively). X,Y, Z are for the long period seismometers, z is for the short period seismometer. Bit sensitivity is 4×10^{-10} m s^{-2} for the LP (at 0.45 Hz) and 1.3×10^{-7} m s^{-2} for the SP (at 8 Hz). Amplitudes at the Apollo 14 station, 157 km from impact, reach about 10^{-5} m s^{-2} with an amplitude mainly related to S waves trapped in the regolith. The first P arrival is typically 10 times smaller. Note the 10-db gain change at the middle of the 4th and 5th traces. Reprinted from Lognonné (2005) with permission of Annual review in Earth and Planetary Science.

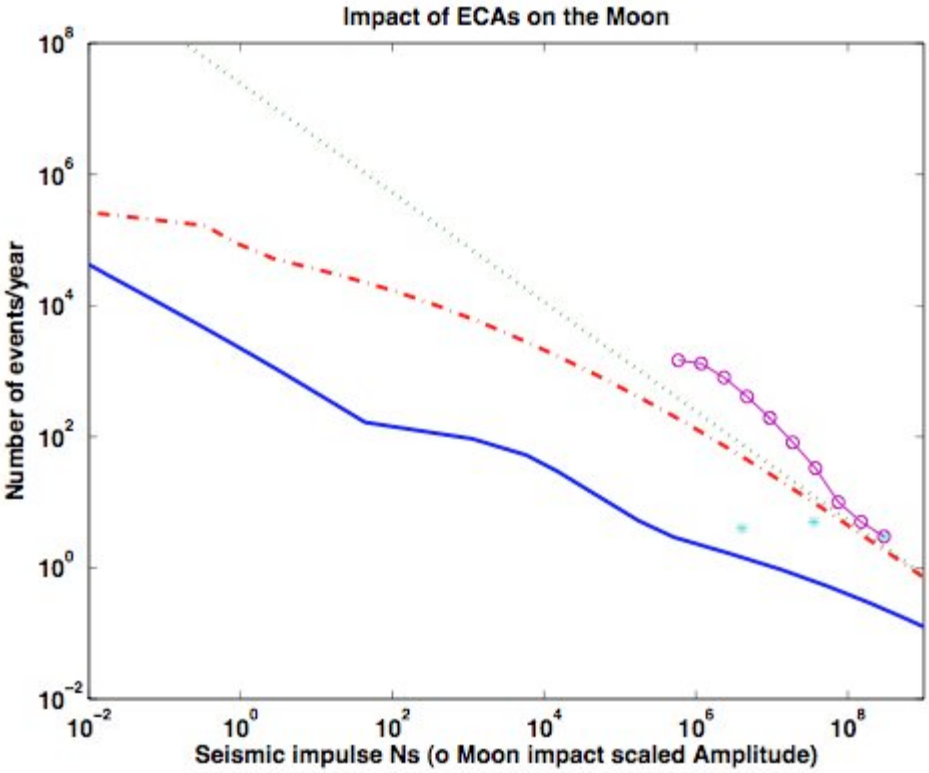

Figure 16: Impact statistics for Earth-crossing asteroids on the Moon. The distribution of impactors is from Poveda *et al.* (1999) and the collision probability is assumed to be 4.2 10^{-9} per year (Shoemaker *et al.* 1990). Lunar case (green dotted line); impactor detection curves at the Apollo 14 station (purple circles and line), with the largest event anchored to a seismic moment of 3 10^{8} N s; Mars (red dot-dashed) and Earth (blue solid) curves, with atmospheric effects included. The latter leads to a reduction of both the mass and velocity of the impactor. Pale blue stars are the seismic impulses, in increasing impulse, of the LEM, the Saturn 5 and the largest natural impacts respectively. The natural impact corresponds to typical impacts expected on NEOs missions. Note that event frequency scales with the squared ratio of the Near Earth Object (NEO) radius (crossing diameter) and the Moon's radius. At 1AU, the number of events, compared to the Moon, are reduced by about 120,000 for a 5 km radius NEO. Entry velocity is taken as 20 km s^{-1}, for impactor mass of 2400 kg m^{-3}.

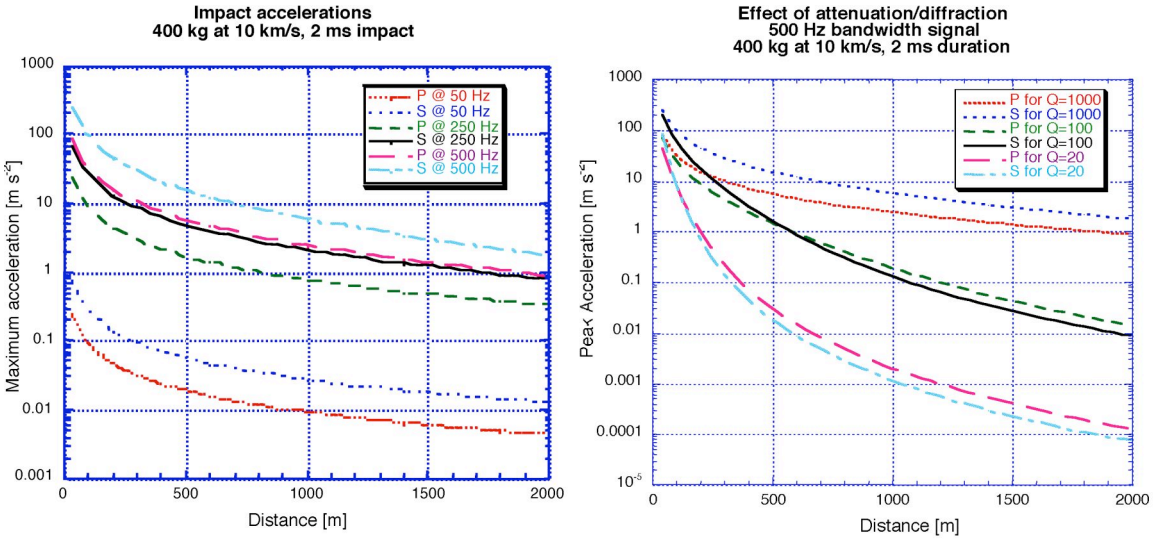

Figure 17a-b: Direct Pand S waves amplitude vs. distance estimates of the P and S waves for an impact of 400 kg at 10 km s^{-1} for different frequency bands (a) and diffraction/attenuation effects (b). Velocities are 3670 m s^{-1} and 2100 m s^{-1} respectively and densities 2600 kg m^{-3}. A Q of 1000 is assumed on the top curve. Figure redrawn after Lognonné *et al.* (2004)

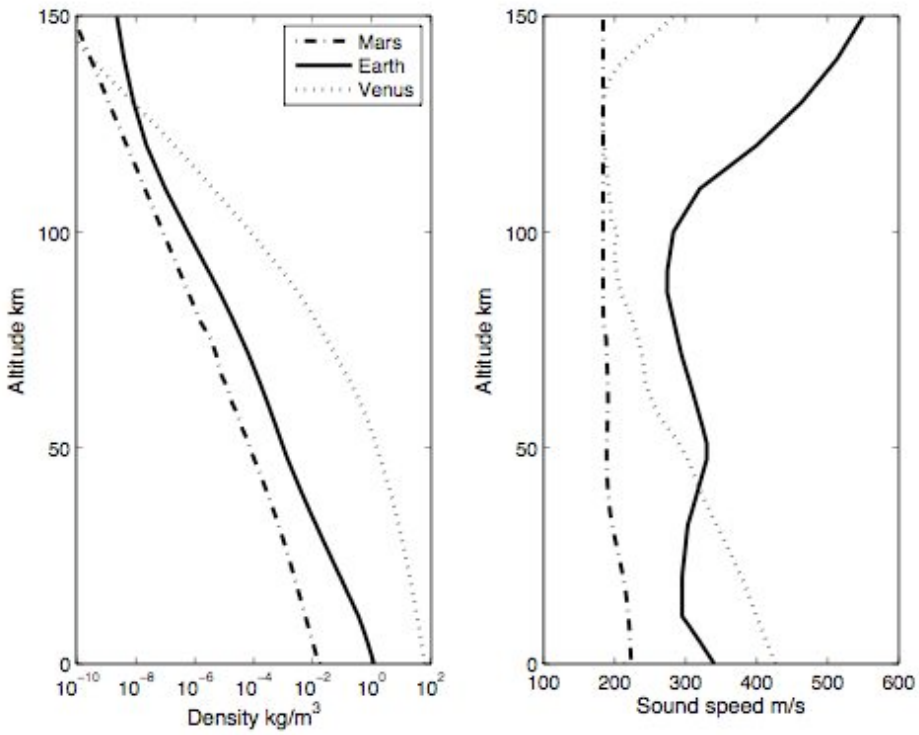

Figure 18: Atmospheric models of the Earth, Mars and Venus used for the computation of the atmospheric coupling. Note that these models are sensitive to the local time and latitude, as well as to the solar environment. US standard atmospheric model (1976) is used for the Earth, whereas the models of Forget *et al.* (1999) and Hunten *et al.* (1983) are used for Mars and Venus respectively.

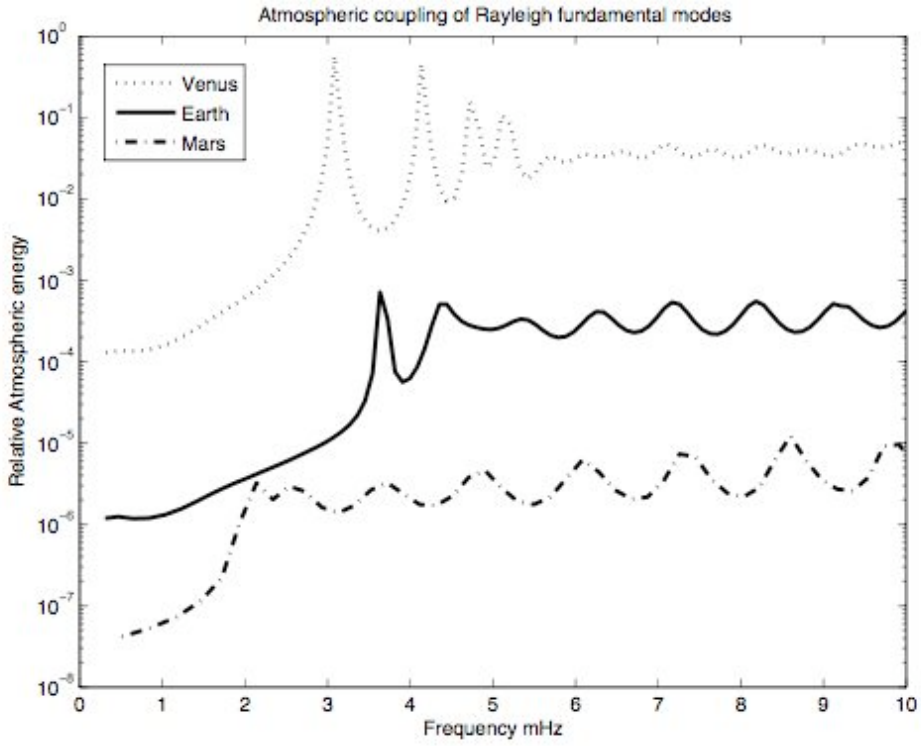

Figure 19: Fraction of the energy of surface waves in the Venus, Earth and Mars atmospheres for Rayleigh surface waves. Only the first peaks are due to atmospheric resonances. Note that the amplitudes on Mars and Earth are comparable at low frequency (2-3 mHz), due to differences in the atmospheric resonance frequency.

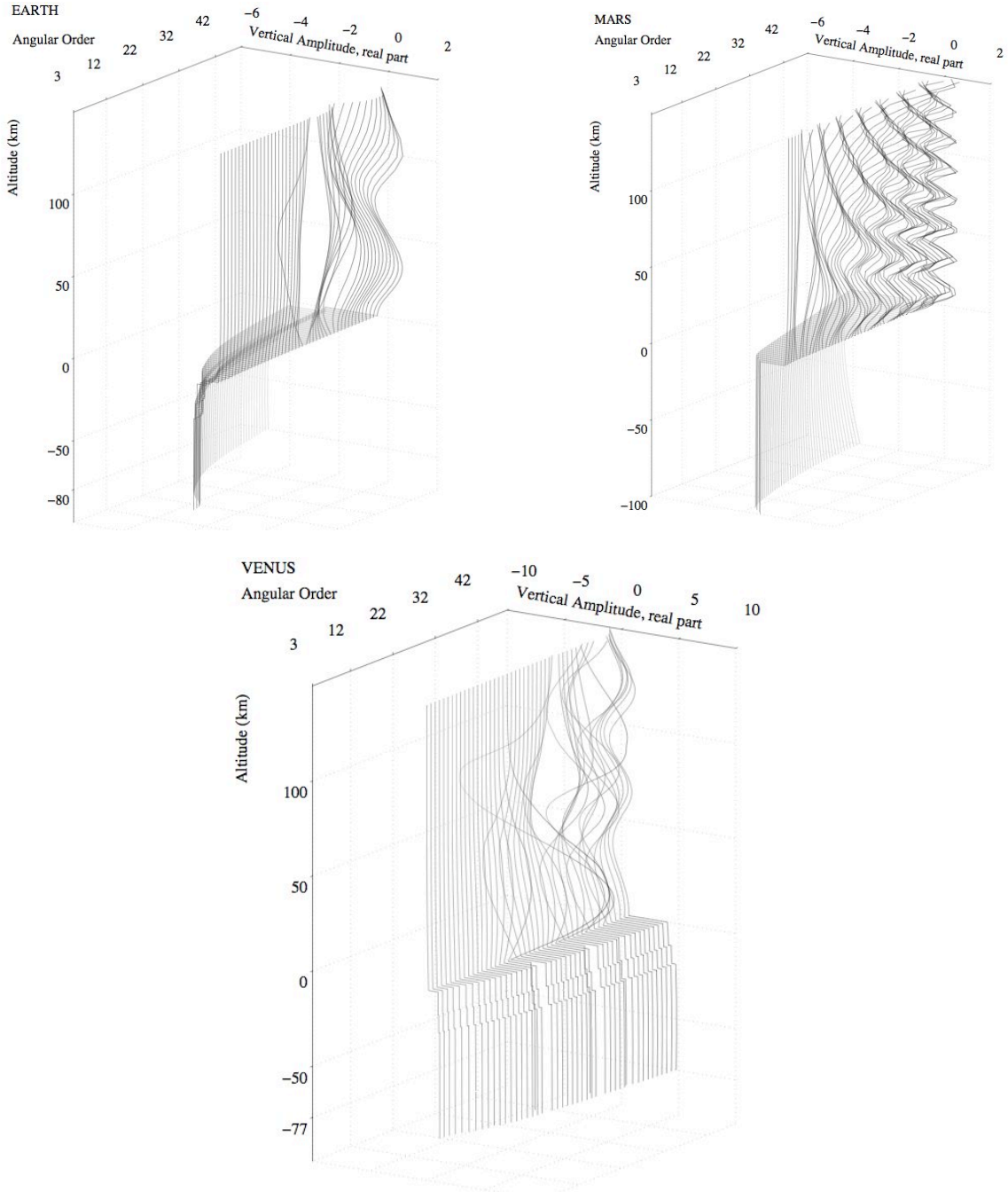

Figure 20a-c: Rayleigh normal modes for the Earth, Mars and Venus. The amplitudes shown are the vertical displacement, multiplied by the square root of density. Amplitudes are multiplied by 5 for the Earth and by 50 for Mars. For Venus, amplitudes are not amplified. Amplitudes are shown over a vertical scale from 100 km depth to 150 km altitude. Note in all cases the exponentially decaying amplitudes close to the surface for the low angular orders below the cutoff frequency, the single oscillation at the resonance comparable to the amplitude of the atmospheric fundamental modes and the oscillating amplitudes above the resonance frequency.

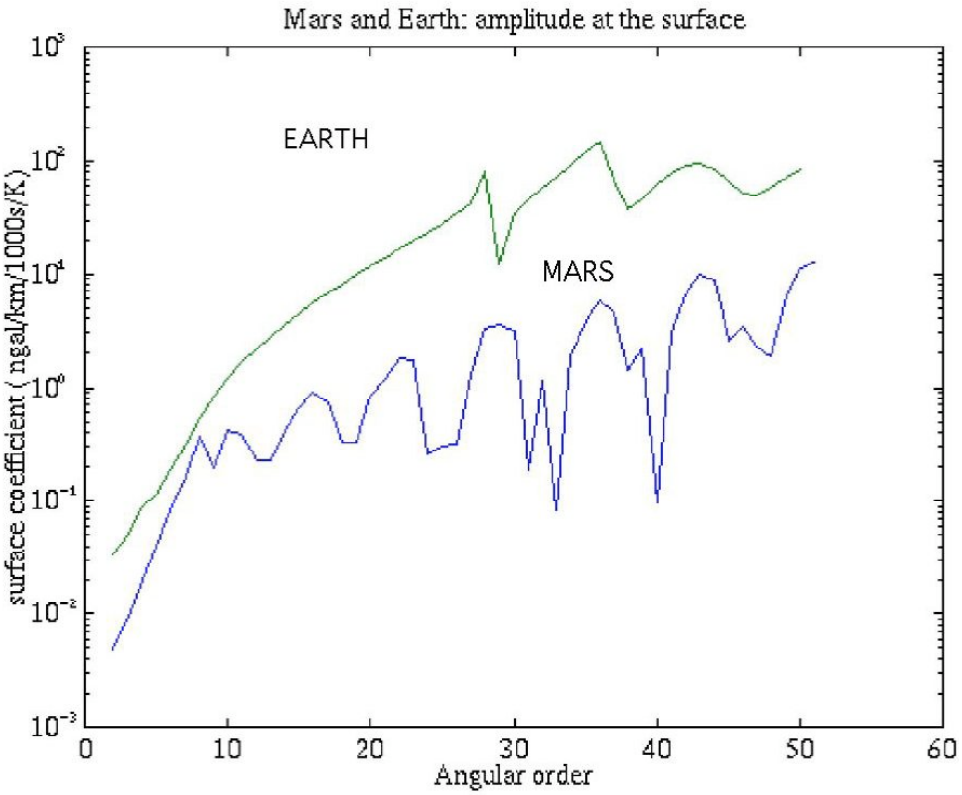

Figure 21: Excitation term $A_\ell(z)$ versus angular order for Earth and Mars (equation (14)) at the surface of the planet (z=0). Note that at low order, the excitation terms for the two planets are comparable. Due to the high temperature variations, the Martian hum might therefore be more efficient for these low order terms than on Earth.

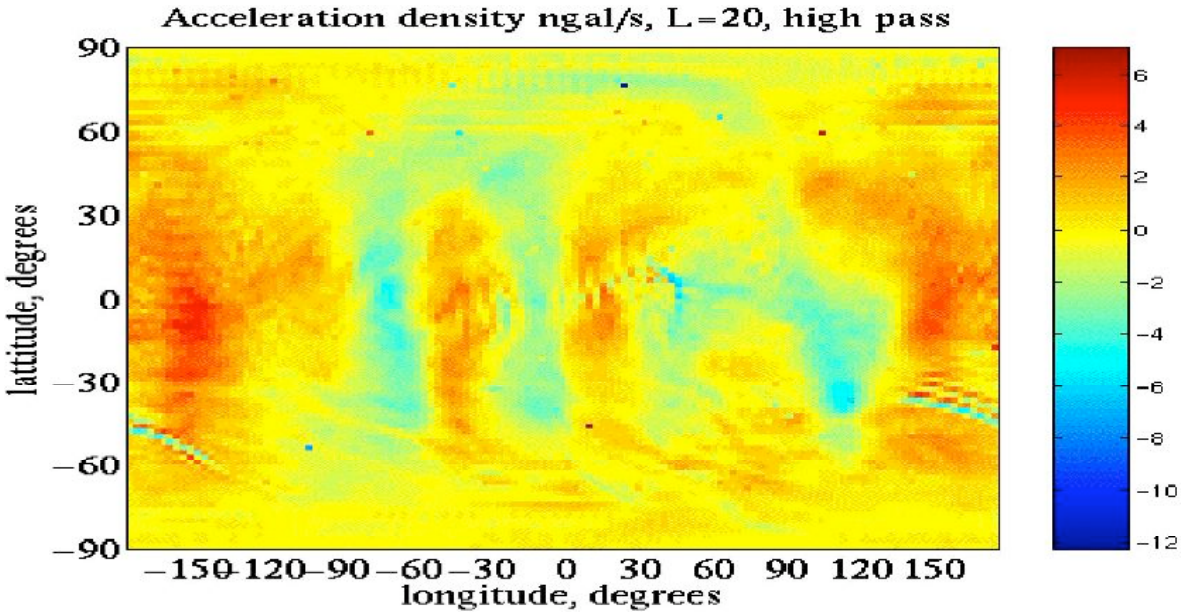

Figure 22: Acceleration field of a Martian GCM model at a given time on the planet, obtained for a 30 days run of the GCM (Forget *et al*. 1999), corresponding to the term $a_\ell^m(t)$ in equation (14) The field is computed for the spheroidal mode ${}_0S_{20}$ and includes the vertical most right integration of equation 14, but not the Legendre transformation nor the time integration. Note the presence of atmospheric front in the south hemisphere, which provides highly localized excitation of the normal modes, as well as the large scale pressure field associated with the daily variation.

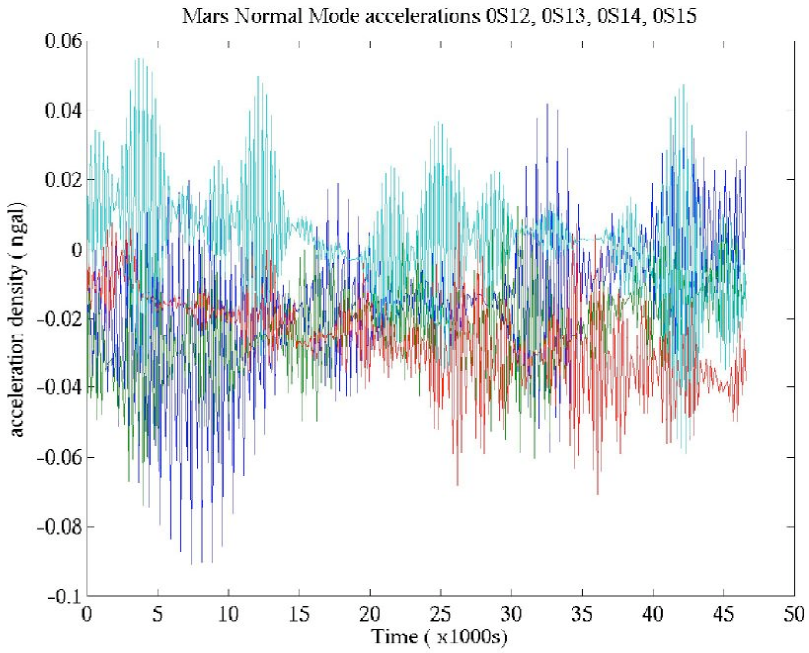

Figure 23: Simulations of the permanent excitation of normal modes, for the spheroidal modes ${}_0S_{12\text{-}15}$ on Mars, with a GCM model during 2 weeks. A fraction of only about 14 hours is shown, illustrating the typical amplitudes variations for these modes, with typical periods from 400 sec to 300sec. Color code is blue, green, red and cyan respectively for increasing angular orders. Observed amplitudes on the Earth below angular order of 20 are 0.2 ngals.

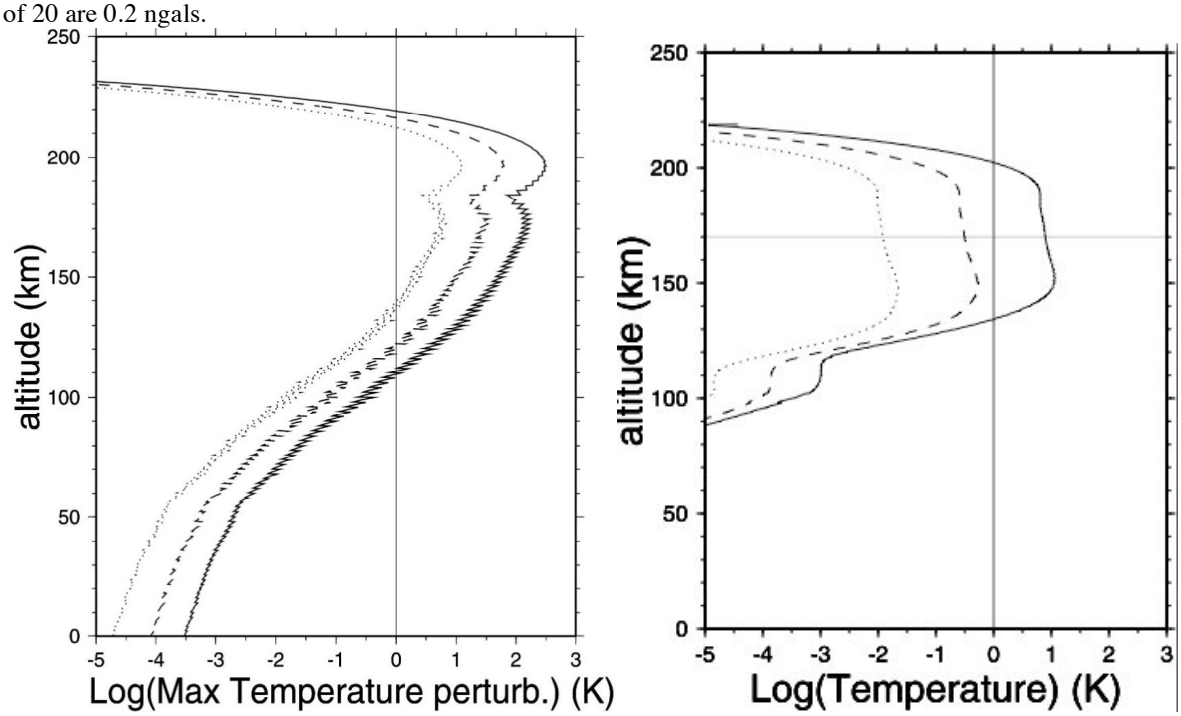

Figure 24a-b: Logarithm of (a) the maximum adiabatic temperature perturbation (in K), as a function of altitude (in km) for different earthquake moment magnitudes: M_w=5 (dotted line), M_w=5 (dashed line) and M_w=6 (plain line). Vertical bars are visual. The signals have periods corresponding to the acoustic waves. (b): Same but for the non-adiabatic heating, associated to the acoustic energy deposition in the atmosphere. The temperature anomalies remain for about 4 minutes, before their atmospheric diffusion. Reprinted from Garcia *et al.* (2005) with permission of the Geophysical Research Letters.

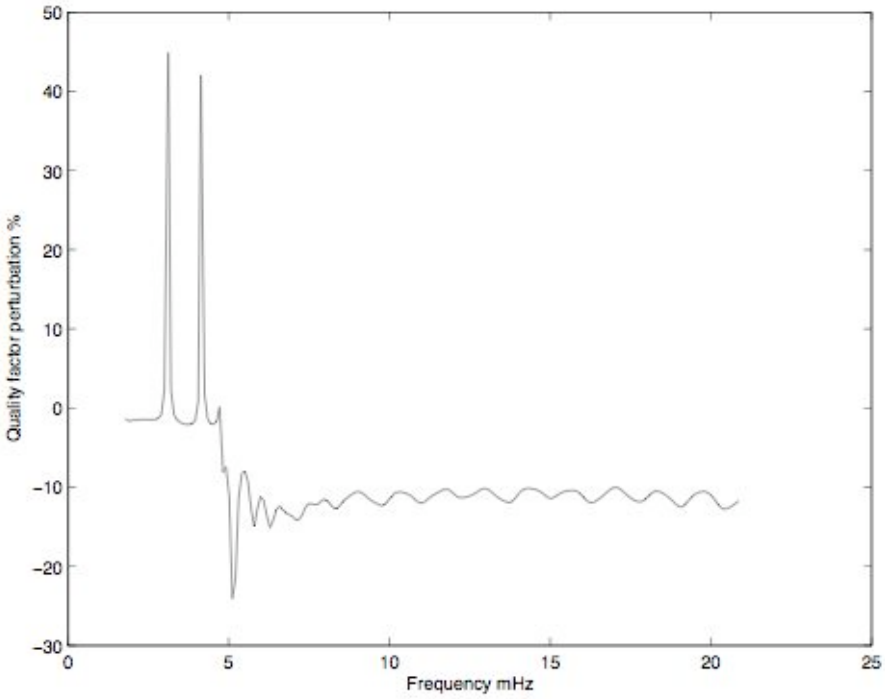

Figure 25: Perturbation of the quality factor for the spheroidal fundamental normal modes. The two peaks are associated to resonances where a significant energy is transferred in the atmosphere instead of the solid planet, leading to a reduced attenuation. After 5 mHz however, modes loose a significant fraction of their energy in the atmosphere.

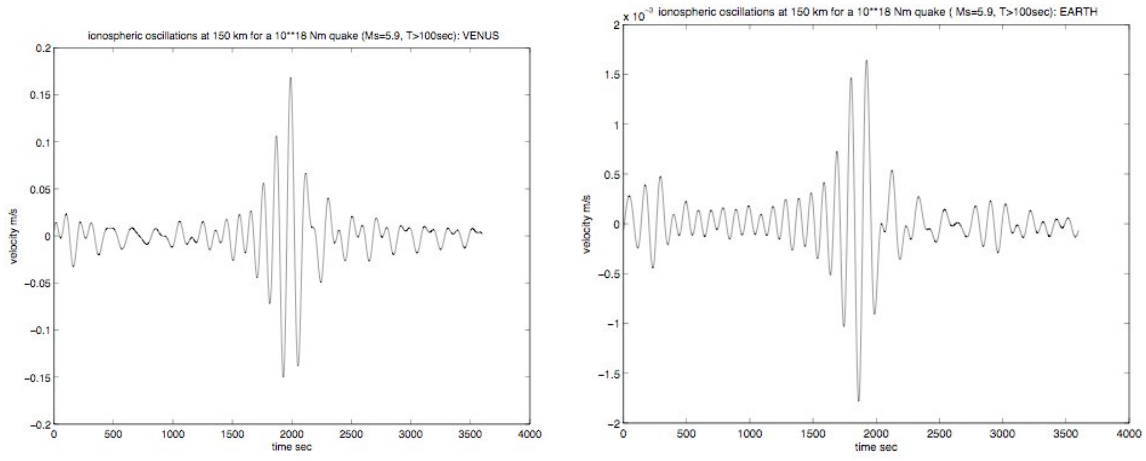

Figure 26a-b: Long period vertical atmospheric oscillations, for a 10^{18} Nm quake (M_w=5.9) and for period larger than 100 sec on Venus (a) and on the Earth (b). Due to the difference in the acoustic coupling at the ground, ionospheric signals at 150 km of altitude are about 100 stronger on Venus for the same magnitude. This is about 1.3 M_w magnitude. Ionospheric velocity oscillations are about 0.3 m s^{-1} peak-to-peak at these periods, corresponding to wavelength larger than 300 km. They will be about one order of magnitude larger at 20 sec

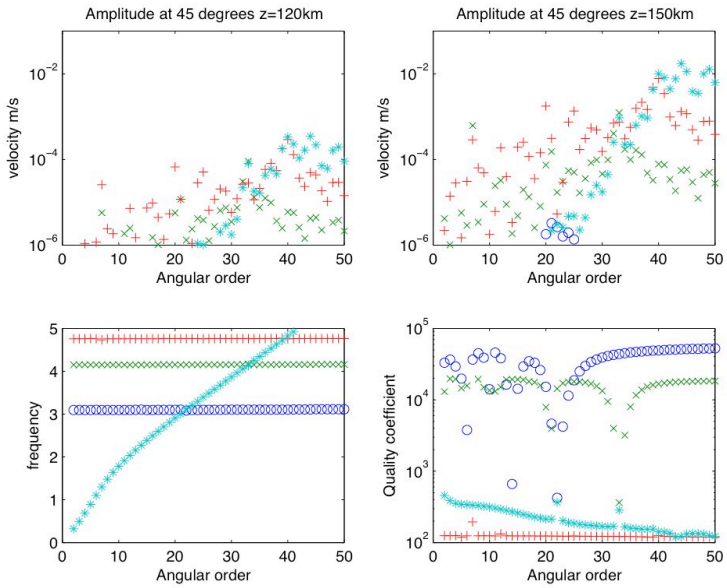

Figure 27: Free oscillations amplitudes (in term of vertical velocities, in m s^{-1}) with respect to angular orders, for a quake with a seismic moment of 10^{18} Nm (M_w=5.9). All these amplitudes are expected to be multiplied by the spherical harmonics values at the location of observations. Sky blue stars are for the Rayleigh fundamental modes. Dark blue circles for the fundamental accoustic modes. Green x and red + for the first and second acoustic modes respectively. For angular orders below 20, the order of the branches are first the Rayleigh fundamental modes, and then the fundamental, 1st and second acoustic overtones. In the intra-plate cooling hypothesis, such quakes are expected at a rate of 2 per months (and quakes with moment and therefore amplitudes 10 times larger are expected at a rate of 5 per year). The top left figure shows the amplitudes of the modes at 120 km of altitude (which can be sounded by optical imaging systems) while the right one shows the amplitudes at 150 km of altitude (which can be achieved by Doppler sounder). The two bottom figures shows the frequencies and quality coefficient of the modes. As no viscosity is taken into account in the model, Q for the fundamental and first acoustic modes are high. The Q of the second overtone is much lower, due to the partial traping of the modes, while the Q of the Rayleigh modes is also low, due to attenuation in the solid part.

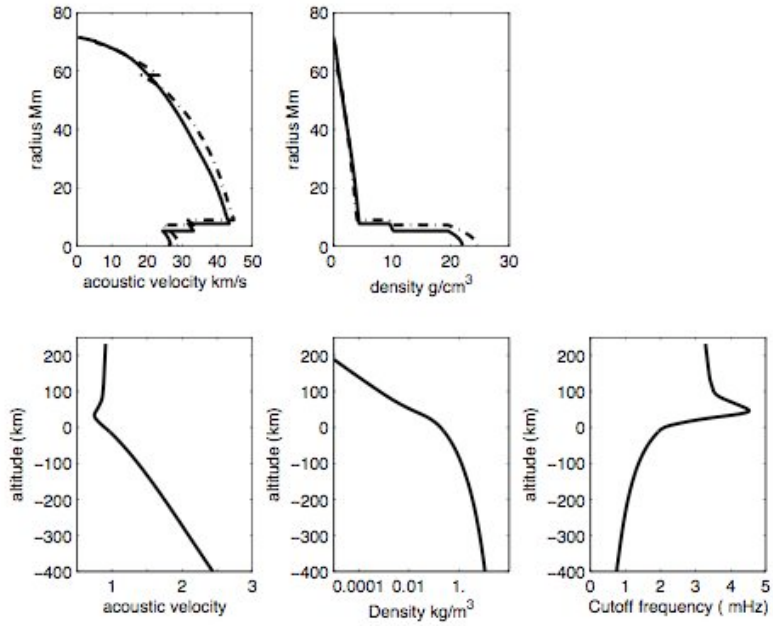

Figure 28: Seismic properties for two different models of Jupiter (Mosser 1996). The continuous line is a model without PPT discontinuity, while the dashed line is with a plasma phase transition (PPT). The two upper figures are for the whole Jupiter, while the three bottom ones are for the atmosphere, with the acoustic velocity, the density and the cutoff frequency respectively.

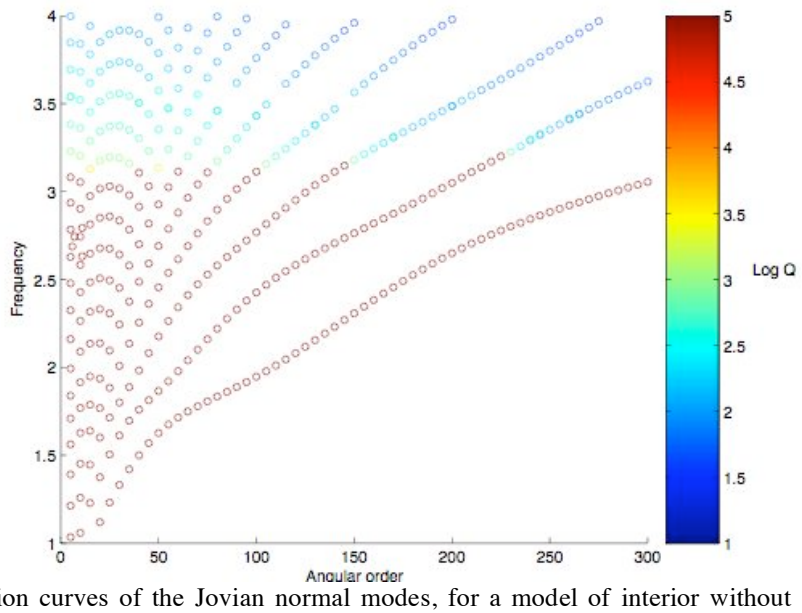

Figure 29: Dispersion curves of the Jovian normal modes, for a model of interior without PPT. Modes are shown with l values from 5 to 300, increasing by 5. The color gives the decimal logarithm of the Q. Note that Q strongly decreases for frequencies higher that 3 mHz, as a consequence of the lack of trapping. The tropospheric guided modes, at about 3.50 mHz, are not shown on the figure.

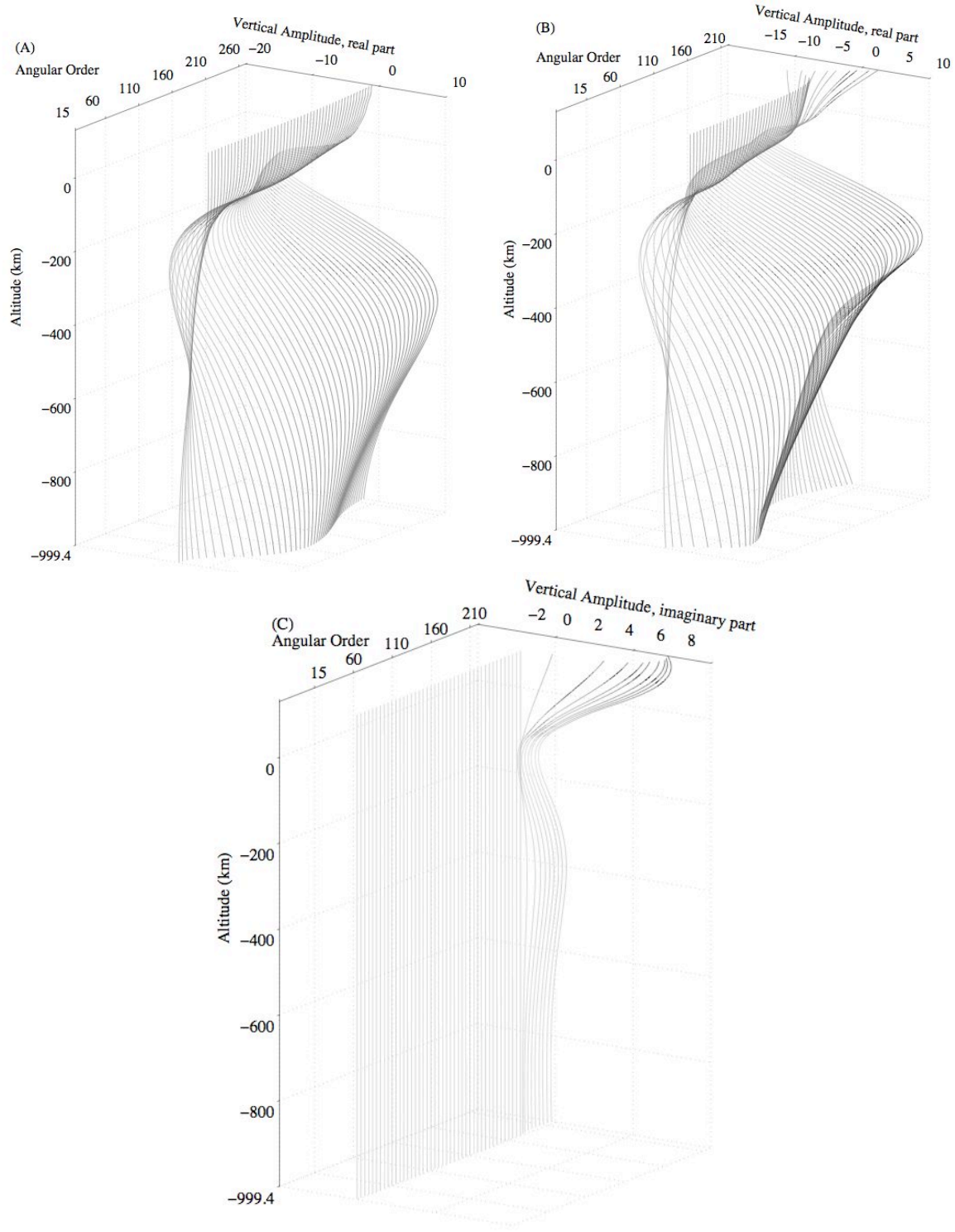

Figure 30a-c: Amplitude of the Jovian Normal modes from 1000 km below the 1 bar level to 150 km of altitude. Figure a shows the vertical amplitude of the fundamental mode. All modes are below the cutoff frequency and the imaginary component is almost zero. Figures b and c show the real and imaginary parts of the vertical amplitude of the first overtone, the first seismic modal branch. Note that the energy is focused closed to the surface for the first overtone. Note also the increasing imaginary part, for frequency higher that the cutoff frequency.

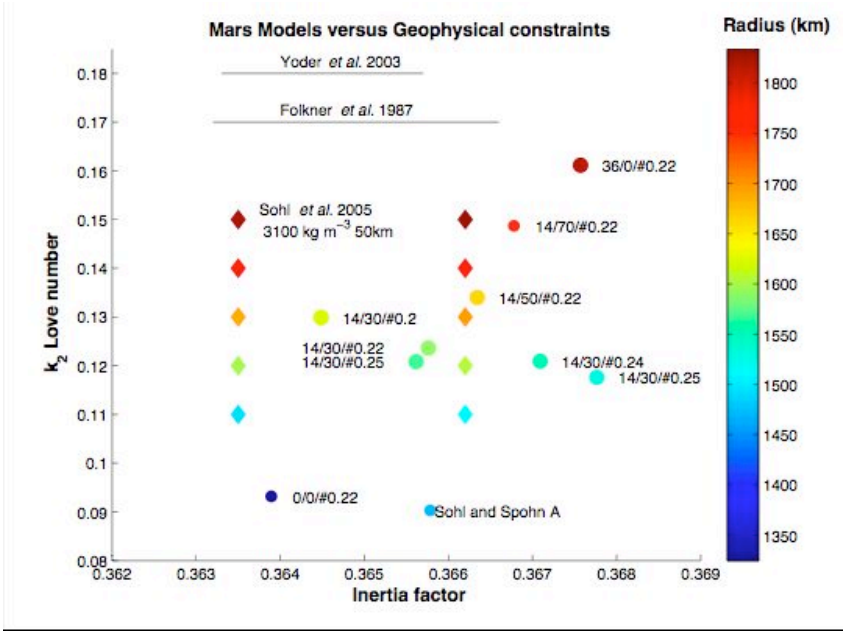

Figure 31: Fit of the computed k_2 and inertia factors for several models of Sohl and Spohn (1997) and Gudkova and Zharkov (2004) (circles) and Sohl *et al.* (2005) (diamonds), the latter for a crust of about 50 km and a crustal density of 3100 kg m^{-3}. Only model A of Sohl and Spohn (1997) is shown, model B with a 0.3566 value for the inertia factor being too far from the observation range. The black horizontal lines are, from right to left, the determinations of I/Ma^2 from Folkner *et al.* (1997) and Yoder *et al.* (2003) after correction for the extrapolated value of I/Ma^2 given by Sohl *et al.* (2005). The core radius is given by the color scale and note that a change of about 10 km is able, for the models taken from Sohl *et al.* (2005) to change the moment of intertia from 0.3635 to 0.3662. For the Gudkova models, the amount of sulfur, hydrogen and #Fe are given. The two first are in weight % and molar % respectively, while the third is the molar Fe ratio, defined as $Fe\# = Fe^{2+}/(Mg+Fe^{2+})*100$.

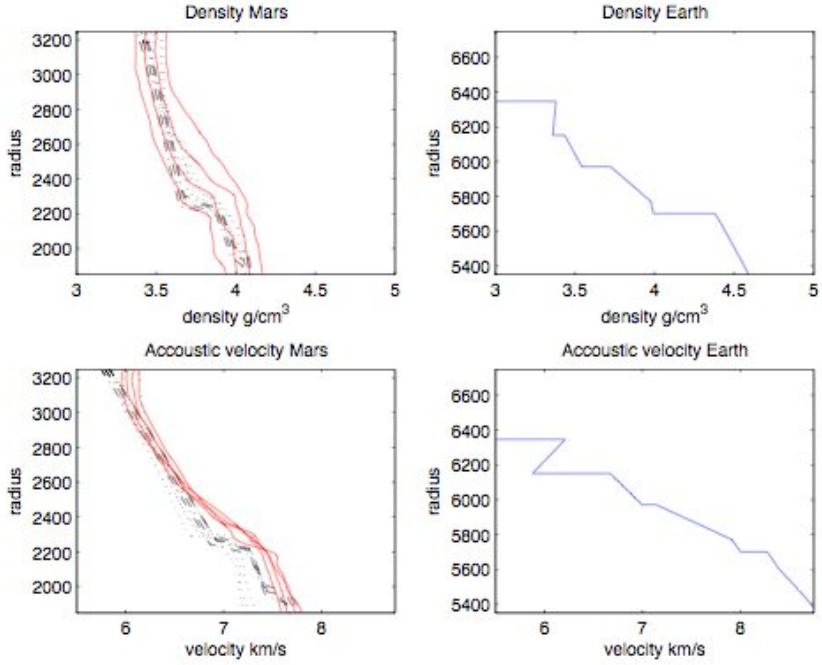

Figure 32: Model M1 to M4 of Gudkova and Zharkov (2004) with Fe contents from 0.20 to 0.25 (0.20-0.22-0.24-0.25)(dash-dot lines), models of Mocquet *et al.* (1996) with Fe content from 10 to 40% (0.1-0.2-0.3-0.4)(solid line) and models of Verhoeven *et al.* (2005) with Fe contents from 0.09 to 0.28 (0.09-0.2-0.25-0.28)(dotted line). The difference in depth of the discontinuities is mainly related to change in the core mantle boundary temperature. A temperature of approximately 2100K is taken at the core mantle boundary for the model of Gudkova and Zharkov (2004), whereas a more complex model, with temperature inversion in the mantle and mantle temperature approximately 500K colder at the depth of the discontinuities, is taken by Mocquet *et al.* (1996). These colder temperatures shift the discontinuity to a shallower depth. The temperatures for models of Verhoeven *et al.* (2005) are those of Breuer and Spohn (2003)

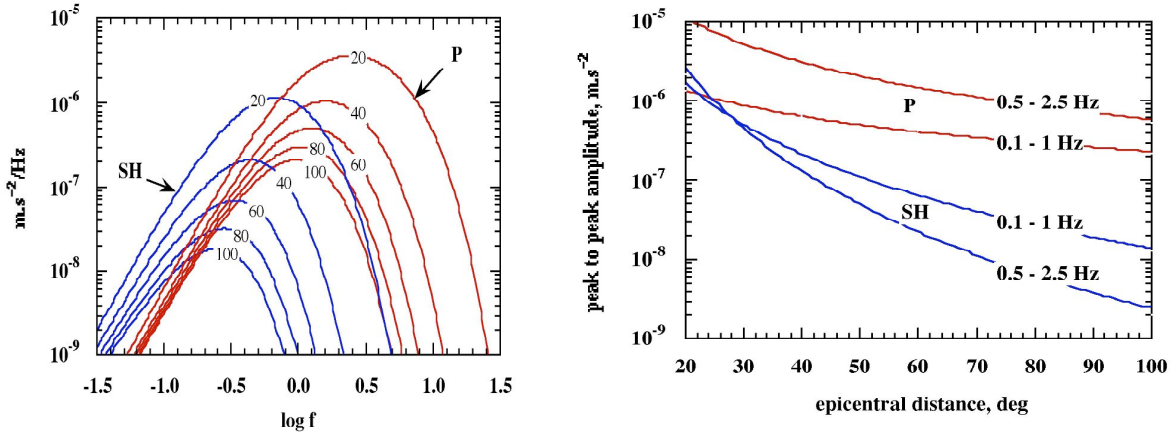

Figure 33a-b: (a)Fourier transformed amplitude of the P and S body wave packet. Amplitude is plotted with respect to frequency for different epicentral distances, in degree. (b) Maximum peak-to-peak amplitude in the frequency band with respect to epicentral distance for a 10^{15} Nm seismic moment quake at the surface. For a source below the surface, the amplitudes are divided by 2, assuming both P and pP arrivals. Reprinted from Mocquet (1999) with permission of Planetary Space Science.

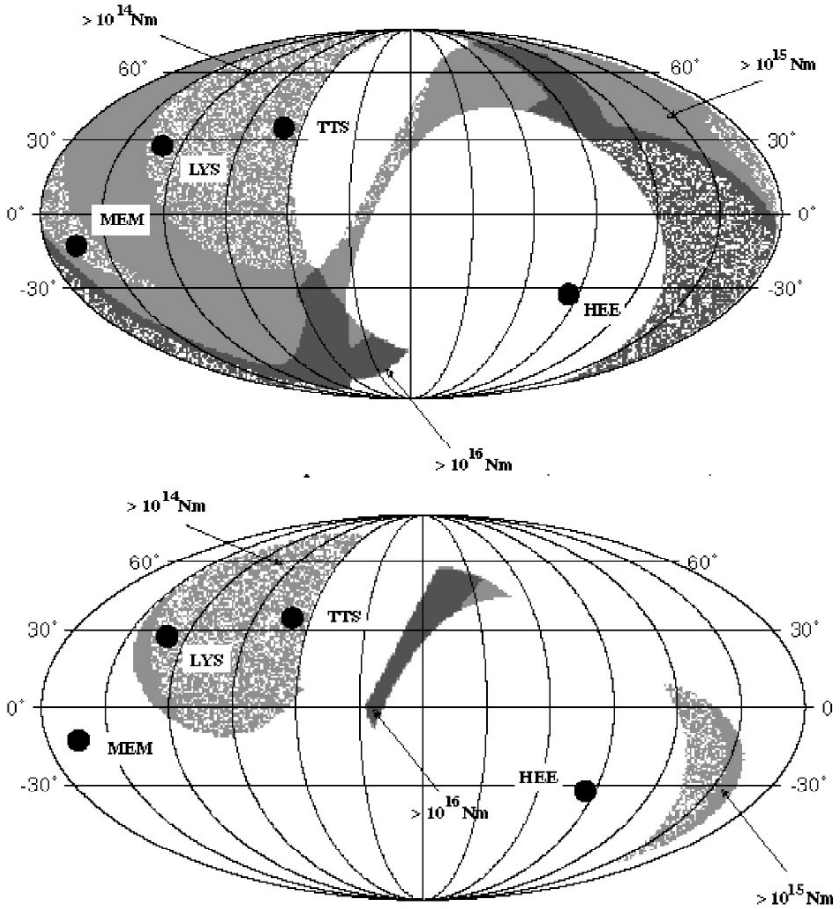

Figure 34a: (Top) Detection zone of P and S waves for one of the studied configuration in the former Netlander project (MEM, LYS, TTS and HEE are respectively Menomnia Fosae, Lycus Sulci, Tempe Terra South and Hellas East). The white zone on to the east of TTS corresponds to the joint shadow zone of MEM and HEE. Note that the detection efficiency is very high in the Tharsis area, where small quakes of seismic moment of 10^{14} Nm might be detected. (Bottom) Detection zone for a detection of a PKP wave in at least one station and of PandS waves in the three other stations. The success rate is 16%, leading to about 22 quakes detected during the two years of operation. Reprinted from Lognonné *et al.* (2000) with permission of Planetary Space Science.

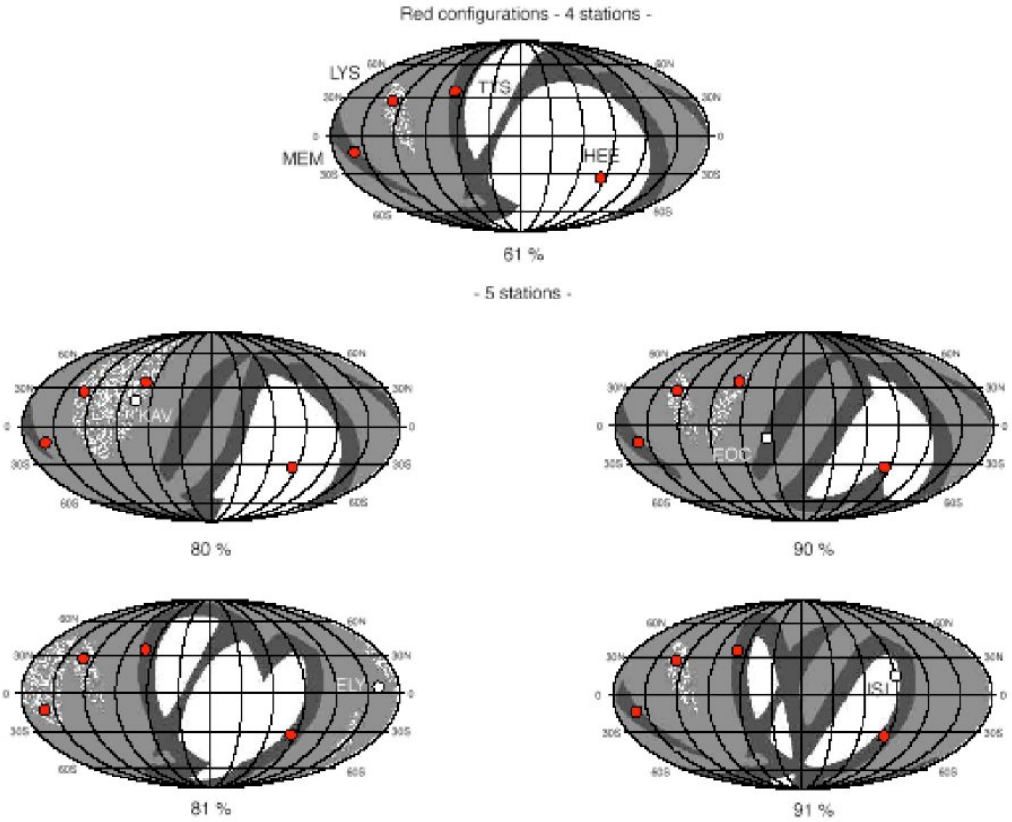

Figure 34b: Zone covered by a successful detection of P and S waves on at least three stations for a Network with 4 or 5 stations. The top figure recalls the detection zones with only 4 stations, while the other are for 5 stations. In this case, the red dots are the 4 nominal landing sites of the Netlander mission. The white dot is a possible new landing site. The shaded zone corresponds (from grey to black) to detection threshold from magnitude 3.5 to 5. Note the large increase of the total surface covered by the network given below each figure. Note also that the dashed grew zone, corresponding to the detection of small quakes of seismic moment of 10^{14} Nm, has either a larger surface or appears in several different spots, each of them being associated with a successive detection on the 3 closer stations.

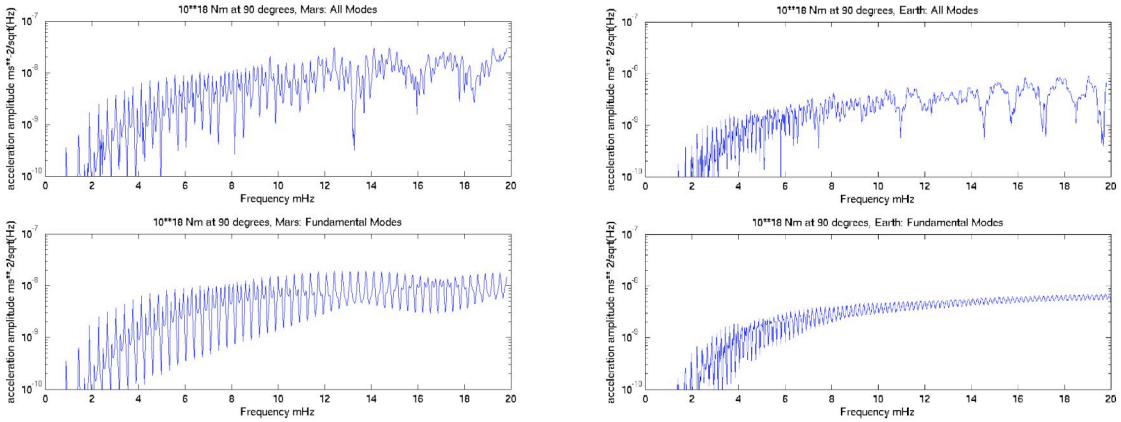

Figure 35a-b: Acceleration amplitude spectrum for a quake with strike, deep, rake angles of 45°, 45°, 45° and a seismic moment of 10^{18} Nm. Azimuth is 20° and the epicentral distance is 90°. The depth of the event is 30 km. Spectrum for Mars are shown on (a). Those for the Earth are on (b). At 5 mHz, the amplitudes exceed 1 ng $Hz^{-1/2}$ and are a factor 4 greater than those observed on the Earth. Note that below 10 mHz, the fundamental modes are associated to most of the signal.

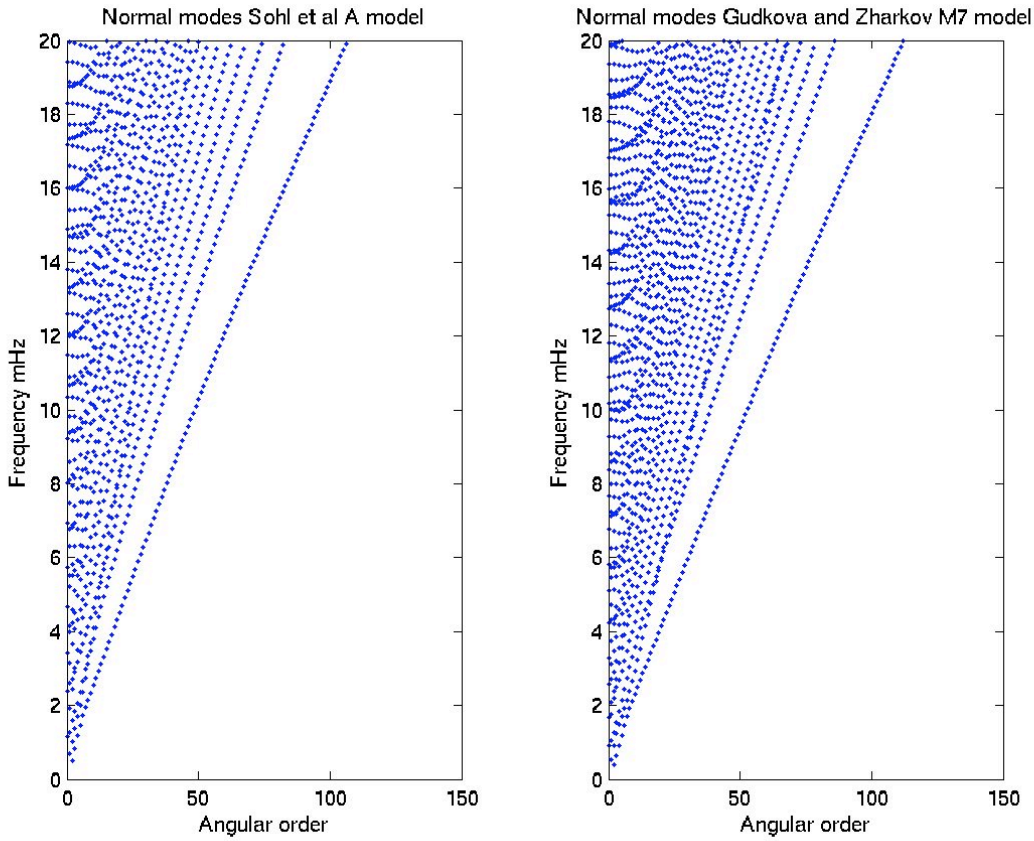

Figure 36: Normal modes for two Mars model (Model A from Sohl and Spohn and model M7 from Gudkova and Zharkov (2004). Differences in the frequencies are about 5-10 %

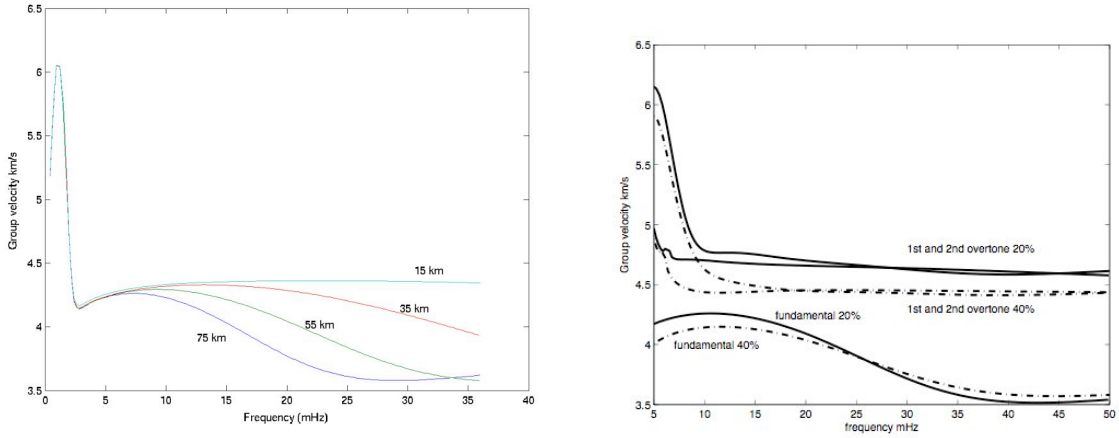

Figure 37: (a) Sensitivity of the Rayleigh waves to the crustal thickness. Model B of Sohl and Spohn (1997) is used and velocity and density in the crust, assumed tobe homogeneous, are those of this model. Variations of 10% in the group velocity are found for about 20km of crustal thickness variation for frequencies in the range of 10 to 30 mHz. (b) Group velocities for two models of Mocquet et al (1996) and for the fundamental, first and second overtones. The iron content of the mantle is indicated in percent. Note that we have added to these models a crust of 50 km thickness, using the Sohl and Spohn (1997) crustal structure. Group velocities without this crust can be found in Lognonné (2005).

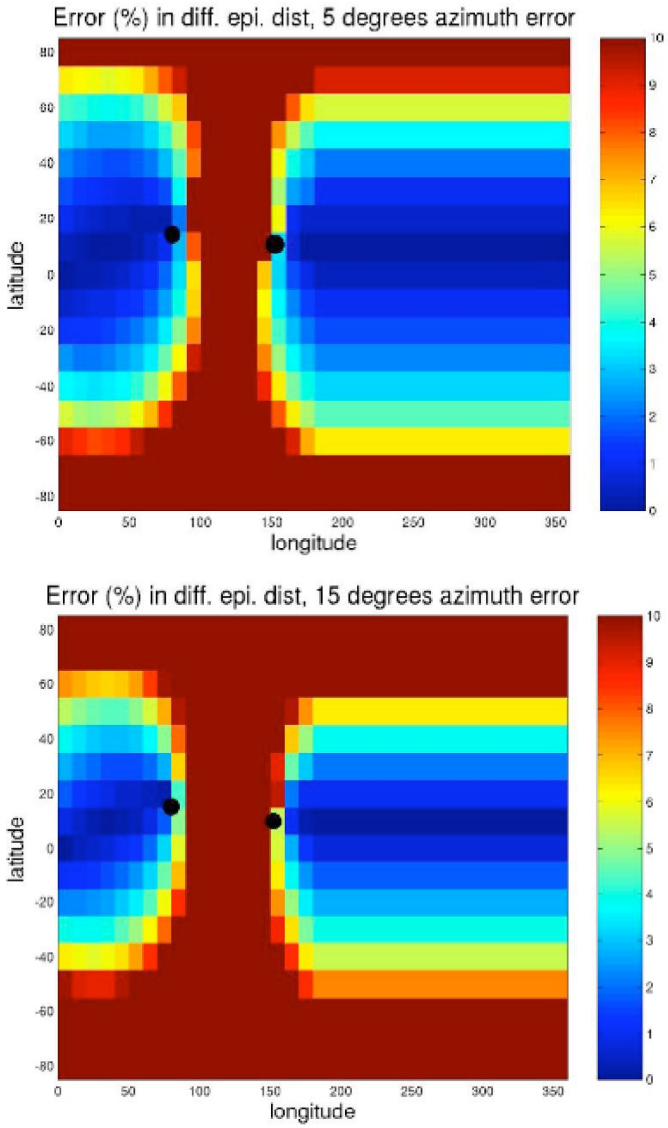

Figure 38a-b: Relative error in the differential epicentral distance for surface waves analysis based on the back-azimuth determination in two cases. The differential epicentral distance is the difference of epicentral distances between the epicenter and the two stations. Left is for a 5 degree error, right is for a 15 degree error. The location of the two stations is 11° North, 152°W and 15°North, 80°W, corresponding to two landing sites proposed for the NetLander Network mission. Only locations with an error smaller than 10% are shown, the latter limit being the a-priori difference between the seismic values proposed by the models shown on Figure 32.

8. REFERENCES

A'Hearn M F, Belton M J S, Delamere W A, Kissel J, Klaasen K P, McFadden, L A, Meech K J, Melosh H J, Schultz P H, Sunshine J M, Thomas P C, Veverka J, Yeomans D K, Baca, M W, Busko I, Crockett C J, Collins S M, Desnoyer M, Eberhardy C A, Ernst C M, Farnham T L, Feaga L, Groussin O, Hampton D, Ipatov S I, Li J Y, Lindler D, Lisse C M, Mastrodemos N, Owen W M, Richardson J E, Wellnitz D D, White R L 2005 Deep Impact: Excavating Comet Tempel 1. *Science*, **310**, 258-64.

Aki K, Richards P G 1980. *Quantitative seismology*. Freeman, San Fransisco

Aki K 1992. Scattering conversions P to S versus S to P. *Bull. Seism. Soc. Am*., **82**, 4, 1969-72.

Anderson D L, Miller W F, Latham G V, Nakamura Y, Toksöz M N, Dainty A M, Duennebier F K, Lazarewicz A R, Kowach R L, Knight T C 1977a. Seismology on Mars. *J. Geophys. Res*., **82**, 4524-46.

Anderson D L, Duennebier F K, Latham G V, Toksöz M N, Kovach R L, Knight T C D, Lazarewicz A R, Miller, W F, Nakamura Y, Sutton G H 1977b Viking seismology experiment. *Bull, American Astro. Soc*., **9**, 447

Anderson D L, Given J, Absorption band Q model for the earth. 1982 *J. Geophys. Res*., **87**, 3893-3904.

Abercombie, Rachel E, Göran E 2001 Earthquake slip on oceanic transform faults. *Nature,* **410***,* 74-77.

Artru J, Lognonné P, Blanc E 2001 Normal modes modeling of post-seismic ionospheric oscillations. *Geophysical Res. Lett.,* **28**, 697-700.

Artru J, T Farges, P Lognonné. 2004 Acoustic waves generated from seismic surface waves: propagation properties determined from doppler sounding observation and normal-modes modeling. *Geophys. Jour. Int*., **158**, 1067-1077.

Assessment of NASA's Mars Architecture, 2007-2016, National Research Council of the National Academies,

Balmino G, Duron J, Marty J 2005 A new martian gravity field mean model and its time variations, American Geophysical Union. Fall Meeting 2005 abstract #G53C.

Ball A J, Lognonné P, Seiferlin K, Spohn T, Zarnecki J C 2003 Lander and penetrator science for NEO mitigation studies. chapter 13, in Belton, M.J.S., Yeomans DK, Morgan TH (editors), Mitigation of Hazardous Impacts due to Asteroids and Comets. Cambridge University Press, ISBN: 0521827647.

Banerdt W B, Chui T, Herrin E T, Rosenbaum D, Teplitz V L 2006 Lunar seismic search for strage quark matter. *Adv. Space. Res*., **37**, 1889-93.

Beauduin R, Lognonné P, Montagner J P, Cacho S, Karczewski J F, Morand M 1996 The effect of the atmospheric pressure changes on seismic signals or how to improve the quality of a station. *Bull. Seism. Soc. Am.,* **86**, 1760-1769.

Beer T 1974 Atmospheric waves. New York, Halsted Press; London, Adam Hilger, Ltd. 1974. 315 pages.

Benioff H, Press F, Smith S W 1961 Excitation of the free oscillations of the earth by earthquake. *J. Geophys. Res*., **66**, 605-20.

Belleguic V, Lognonné P, Wieczorek M 2005 Constraints on the martian lithosphere from gravity and topography data. *J. Geophys. Res*., **110**, E11005, doi:10.1029/2005JE002437.

Bills B G, Ferrari A J 1977 A lunar density consistent with topographic, gravitational, librational and seismic data. *J. Geophys. Res.,* **82**, 1306-14.

Bills B G, Rubincam D P 1995 Constraints on density models from radial moments: applications to earth, Moon, and Mars, *J. Geophys. Res*.,**100**, 26305—16.

Bills B G, Neumann G A, Smith D E, Zuber M 2005 Improved estimate of tidal dissipation within mars from MOLA observations of the shadow of Phobos. *J. Geophys. Res.*, **110**, E07004, doi:10.1029/2004JE002376.

Bois E, Boudin F, Journet A 1996 Secular variation of the moon's rotation rate. *Astronomy and Astrophysics*, **314**, 989-94.

Bratt S R, Bergman E A, Solomon S C 1985 Thermoelastic stress: how important as a cause of earthquakes in young oceanic lithosphere; *J. Geophys. Res*., **90**, 10249-260.

Breuer D, Spohn T 2003 Early plate tectonics versus single-plate tectonics on mars: evidence from magnetic field history and crust evolution. *J. Geophys Res. Plan.,* **108**, CiteID 5072, DOI 10.1029/2002JE001999.

Breuer D, Spohn T 2006 Viscosity of the martian mantle and its initial temperature: constraints from crust formation history and the evolution of the magnetic field. *Planet. Space Sci.*, **54**, 153-69.

Bullen, K E 1947 An Introduction to the Theory of Seismology, *Cambridge University Press*.

Bulow R, Johnson C L, Shearer P 2005 New events discovered in the lunar Apollo seismic data. *J. Geophys. Res. Planets*, **110**, E10003, doi:10.1029/2005JE002414.

Bulow R, Johnson C L, Bills B Shearer P 2006a Characteristics of Deep Moonquakes, *J. Geophys. Res. Planets.,* submitted

Bulow R, Johnson C L, Bills B G 2006b Tidal stress and deep moonquakes. LPSC 37th, Abstract 1183

Cailleau B, Walter T R, Janle P, Hauber E 2003 Modeling volcanic deformation in a regional stress field : implications for the formation of graben structures on alba patera, mars. *J. Geophys. Res.*, **108**, No. E12, 5141, doi:10.1029/2003JE002135.

Cameron A G 2000 Higher-resolution simulations of the giant impact, in: R.M. Canup, K. Righter (Eds.), Origin of the Earth and Moon. Univ. of Arizona Press, Tucson, Arizona, 133–44.

Canup R M, Asphaug E 2001 Origin of the moon in a giant impact near the end of the earth's formation. *Nature*, **412**, 708-712.

Calais E, Minster J B, 1995 GPS detection of ionospheric perturbations following the January 17, 1994, northridge earthquake. *Geophys. Res. Lett.,* **22**, 1045-48.

Cacciani A, Dolci M, Moretti P F, D'Alessio F, Giuliani C, Micolucci E, Di Cianno A 2001 Search for global oscillations on jupiter with a double-cell sodium magneto-optical filter. *Astronomy and Astrophysics*, **372**, 317-25.

Chenet H, Lognonné P, Wieczorek M, Mizutani H 2006 Lateral variations of lunar crustal thickness from Apollo seismic dataset. *Earth Planet. Sci. Lett.,* **243**, 1-14.

Chyba C F, Thomas P J, Zahnle K J 1993 The 1908 Tunguska explosion - atmospheric disruption of a stony asteroid. *Nature*, **361**, p. 40-44.

Cisowski S M, Collinson D W, Runcorn S K, Stephenson A 1983 A review of lunar paleonintensity data and implications for the origin of lunar magnetism. *J. Geophys. Res.*, **88**, A691-A704.

Davis K, Baker D M 1965 Ionospheric effects observed around the time of the alaskan earthquake of march 28, 1964. *J. Geophys. Res.*, **70**, 1251-53.

Dainty A M, Toksöz N M 1977 Elastic wave propagation in a highly scattering medium : a diffusion approach. *J. Geophys.*, **43**, 375- 88.

Davis P M 1993 Meteoroid impacts as seismic sources on Mars. *Icarus*, **105**, 469-78.

Deming D, Mumma M J, Espenak F, Jennings D E, Kostiuk T, Wiedemann G, Loewenstein R, Piscitelli J 1989 A search for p-mode oscillations of jupiter~: serendipitous observations of non-acoustic thermal wave structure. *Astrophysical Journal*, **343**, 456-67.

De Pater I, Lissauer J J 2001 Planetary sciences. cambridge university press, page 66.

Dragoni M, Piombo A 2003 A model for the formation of wrinkle ridges in volcanic plains on venus. *Phys. Earth Planet. Inter.,* **135**, 161 – 71.

Dreibus G, Wanke H 1985 A volatile-rich planet. *Meteoritics*, **20**, 367—82.

Drossart P, Piccioni G, Coradini A, Reess J M, Semery A, Suetta E, Cosi M, Dami M, Arnold G, Peter G, Henry F 2004 VIRTIS imaging spectrometer for the ESA/venus express mission, earth observing systems IX. Edited by Barnes, William L, Butler James *J. Proceedings of the SPIE*, **5543**, 175-85

Ducic V, Artru J, Lognonné P, Ionospheric remote sensing of the denali earthquake rayleigh surface waves 2003 *Geophys. Res. Lett.*, **30(18)**, 1951, doi:10.1029/2003GL017812.

Duennebier F, Sutton G H 1974 Thermal moonquakes. *J. Geophys. Res.*, **79**, 4351-64.

Dziewonski A, Anderson D L 1981 Preliminary reference earth model. *Phys. Earth Planet. Inter.,* **25**, 297-356.

Dziewonski A M, Hager B H, O'Connell R J 1977 Large-scale heterogeneities in the lower mantle. *J. Geophys. Res.*, **82**, 239-55.

Ewing M, Latham G, Press F, Sutton G, Dorman J, Nakamura Y, Meissner R, Duennebier F, Kovach R 1971
Seismology of the Moon and implications on internal structure, origin and evolution, in Highlights of
Astronomy, edited by De Jager, 155-172, D. Reidel, Dordrecht.

Folkner W M, Yoder C F, Yuan D N, Standisch E M, Preston R A 1997 Interior structure and seasonal mass redistribution of mars from radio tracking of mars pathfinder. Science, **278**, 1749-51.

Forget F, Hourdin F, Fournier R, Hourdin C, Talagrand O, Collins M, Lewis S, Stephen R, Read P L, Huot J-P 1999 Improved general circulation models of the martian atmosphere from the surface to above 80 km. *J. Geophys. Res.*, **104**, 24155-76.

Fuller M, Stanley M C 1987 Lunar paleomagnetism. in *Geomagnetism*, **2**, 307-455.

Gagnepain-Beyneix J, Lognonné P, Chenet H, Spohn T 2006 Seismic models of the moon and their constraints on the mantle temperature and mineralogy. *Phys. Earth Planet. Int.,* **159**, 140-66

Garcia R, Lognonné P, Bonnin X 2005 Detecting atmospheric perturbations produced by Venus quakes. *Geophys. Res. Lett.*, **32**, L16205

Garcia R, Crespon F, Ducic V, Lognonné P 1995 3D ionospheric tomography of post-seismic perturbations produced by the denali earthquake from GPS data. *Geophys. J. Int*, **163**, 1049-64

Goins N R, Lazarewicz A R 1979 Martian seismicity. *Geophys. Res. Lett.,* **6**, 368-70.

Goins N R, Dainty A M, Toksöz M N 1981 a Seismic energy release of the moon. *J. Geophys. Res*., **86**, 378-88.

Goins N R, Dainty A M, Toksöz M N 1981 b. Lunar seismology : the internal structure of the moon. *J. Geophys. Res*., **86**, 5061-74,

Golombek MP, Banerdt W B, Tanaka K L, Tralli D M 1992 A prediction of mars seismicity from surface faulting. *Science*, **258**, 979—81.

Gough D O 1986 Seismology of the sun and the distant stars; proceedings of the NATO advanced research workshop,Dordrecht, D Reidel Publishing Co. (NATO ASI Series. Volume C169). 491 p., Cambridge University, England.

Grimm R E, Hess P C 1997 The crust of venus, in Venus II : geology, geophysics, atmosphere, and solar wind environment. Edited by S W Bougher, D M Hunten, R J Philips. Tucson, AZ : University of Arizona Press, p.1205.

Gudkova T, Mosser B, Provost J, Chabrier G, Gautier D, Guillot T 1995 Seismological comparison of giant planet interior models, astronomy and astrophysics. 303, 594-603.

Gudkova T V, Zharkov V N 1997 Models of jupiter and saturn with water-depleted atmospheres. *Astronomicheskii Vestnik*, **31**, 99.

Gudkova T V, Zharkov V N 1998 The free oscillations of jupiter. *Planetary and Space Science*, **47**, 1211-1224.

Gudkova T V, Zharkov V N 2004 Mars: interior structure and excitation of free oscillations. *Phys. Earth Planet. Int.* **142**, 1–22.

Guillot T 2005 The interiors of giant planets: models and outstanding questions. *Annual Rev. of Earth and Planet. Sci.*, **33**, 493-530.

Gusev G A, Kurlachev M I 1976 The possibility of observing the lunar microseismic background. Akademiia Nauk SSSR, Izvestiia, Fizika Zemli, Dec. 1976, p. 84-86. In Russian.

Hammel H B, Beebe R F, Ingersoll A P, Orton G S, Mills J R, Simon A A, Chodas P, Clarke J T, de Jong E, Dowling T E, Harrington J, Huber L F, Karkoschka E, Santori C M, Toigo A, Yeomans D, West R A 1995 HST imaging of atmospheric phenomena created by the impact of comet shoemaker-levy 9. *Science*, **267**, 1288-96.

Hanks T C, Kanamori H 1979. A moment magnitude scale, *J. Geophys. Res*., **84**, 2348-50.

Harder H, Christensen U R1996 A one plume model of martian mantle convection. *Nature*, **380**, 507—9.

Hood L L 1995 Frozen fields. *Earth, Moon and Planets*, **67**, 131-142.

Hood L L, Mitchell D L, Lin R P, Acuna M H, Binder A B 1999 Initial measurements of the lunar induced magnetic dipole moment using lunar prospector magnetometer data. *Geophys. Res. Lett*., **26**, 2327—30.

Hood L L 1986 Geophysical constraints on the lunar interior, in *Origin of the moon*, W K Hartmann, R J Philips, G J Taylor (Eds.). Lunar and Planetary Institute, pp. 361-410.

Hood L L, Zuber M T 1986 Recent refinements in geophysical constraints on Lunar origin and Evolution, in: R.M. Canup and K. Righter (Ed.). *Origin of the Earth and Moon*, Lunar and Planetary Institute, Houston, 397-409, 2000.

Hood L L, Jones J H 1987 Geophysical constraints on lunar bulk composition and structure: a reassessment. *J. Geophys. Res*., 92, E396-E410.

Hunten D M, Colin L, Donahue T M 1983 Venus, 1143 pp., Univ of Ariz. Press, Tucson.

Ingersoll A P, Kanamori H, Dowling T E 1994 Atmospheric gravity waves from the impact of comet

Shoemaker-Levy 9 with Jupiter. *Geophys. Res. Lett*., **21**, 1083-86.

Ingersoll A P, Kanamori H 1995 Waves from the collisions of comet shoemaker-levy-9 with jupiter. *Nature*, **374**, 706-8.

Jolliff B L, Gillis J J, Haskin L A, Korotev R L, Wieczorek M A 2000 Major lunar crustal terranes: surface expression and crust mantle origins. *J. Geophy. Res*., **105**, 4197-4216.

Johnson C L, Stixrude L, Lithgow-Bertelloni C, Bulow R C, Shearer P M 2005 Mineralogical and seismological models of the lunar mantle, in 36th. *Annual Lunar and Planetary Science Conference*, March 14-18, 2005, in League City, Texas, abstract no.1565.

Kanamori H, Mori J 1992 Harmonic excitation of mantle rayleigh waves by the 1991 eruption of mount pinatubo, philippines. *Geophys. Res. Lett.*, **19**, 721-24.

Kanamori H 1993 Excitation of jovian normal modes by an impact source. *Geophys. Res. Lett*., **20**, 2921-24.

Kanamori H, Mori J, Harkrider D G 1994 Excitation of atmospheric oscillations by volcanic eruptions. *J. Geophys. Res*., **22**, 21947-61.

Kanamori H 2004 Some fluid-mechanical problems in geophysics-wave in the atmosphere and fault lubrification. *Fluid dynamics Res*., **34**, 1-19.

Kaula W M 1979 The moment of inertia of mars. *Geophys. Res. Let*t., **6**, 194-196.

Kelley M, Livingston R, M McCready 1985 Large amplitude thermospheric oscillations induced by earthquakes. *Geophys. Res. Lett*., **12**, 577-580.

Khan A, Mosegaard K, Rasmussen K L 2000 A new seismic velocity model for the moon from a monte carlo inversion of the apollo lunar seismic data. *Geophys. Res. Lett.,* **27**, 1591-94.

Khan A, Mosegaard K 2001 New information on the deep lunar interior from an inversion of lunar free oscillation periods. *Geophys. Res. Lett*., **28**, 1791-1794.

Khan A, K Mosegaard 2002 An inquiry into the lunar interior- a non linear inversion of the apollo seismic data. *J. Geophy. Res.*, **107**, doi:10.1029/2001JE001658.

Khan A, Mosegaard K, Williams J G, Lognonné P 2004 Does the moon possess a molten core? probing the deep lunar interior using results from LLR and lunar prospector. *J. Geophys. Res*., **109**, E09007, doi:10.1029/2004JE002294 .

Khan A, Maclennan J, Taylor S R, Connolly J A D 2006 Are the earth and the moon compositionally alike? inferences on lunar composition and implications for lunar origin and evolution from geophysical modeling. *J. Geophys. Res*., **111**, E05005, doi: 10.1029/2005JE002608.

Knapmeier M, Oberst J, Hauber E, Wählisch M, Deuchler C, Wagner R 2006 Implications of the martian surface fault distribution and lithospheric cooling for seismicity: a working model. submitted to *J. Geophys. Res*.

Kobayashi N, Nishida K 1998 Continuous excitation of planetary free oscillations by atmospheric disturbances. *Nature*, **395**, 357-360.

Konopliv A S, Binder A B, Hood L L, Kucinskas A B, Sjogren W L, Williams J G 1998 Improved gravity field of the moon from lunar prospector. *Science*, **281**, 1476-79.

Koyama J, Nakamura Y 1980 Focal mechanism of deep moonquakes. *Proc. Lunar Planet. Sci. Conf*., **11th**, 1855-65.

Kovach RL, Chyba C F 2001 Seismic detectability of a subsurface ocean on europa. *Icarus* **150**, 279—87.

Kovach R L, Watkins J S 1973a Apollo 17 seismic profiling-probing the lunar crust. *Science*, **180**, 1063-64.

Kovach R L, Watkins J S 1973b The structure of the lunar crust at the apollo 17 site. *Geochim. Cosmochim. Acta*, **37**, Suppl. 4, 2549-60.

Khavroshkin OB, Tsyplakov V V 1996 Penetrator « Mars-96 », reality and possibilities of seismic experiment, in experimental problems in planetology. 1 united institute of physics of the earth, Russian academy of Science, Moscow.

Kochan H, Feibig W, Konopka U, Kretschmer M, Möhlmann D, Seidensticker K J, Arnold W, Gebhardt W, Licht R 2000 CASSE -- The ROSETTA lander comet acoustic surface sounding experiment -- status of some aspects, the technical realisation and laboratory simulations. *Planet. Space Sci*., **48**, 385-99.

Konopliv A S, Binder A B, Hood L L, Kucinskas A B, Sjogren W L, Williams J G 1998 Improved gravity field of the moon from lunar prospector. *Science*, **281**, 1476-80.

Kuramoto K 1997 Accretion, core formation, H and C evolution of the earth and mars. *Phys. Earth Planet. Int*., **100**, 3-20.

Kuskov O L, Fabrichanaya O B 1994 Constitution of the Moon: 2. composition and seismic properties of the lower mantle. *Phys. Earth. Planet. Int*., **83**, 197-216.

Kuskov O L, Kronrod V A 1998 Constitution of the Moon: 5. constraints on composition, density, temperature and radius of a core. *Phys. Earth. Planet. Int*., **107**, 285—306.

Kuskov O L 1995 Constitution of the Moon: 3. composition of middle mantle from seismic data. *Phys. Earth and Planet. Int*. **102**, 239-57.

Kuskov O L 1997 Constitution of the Moon: 4. composition of the mantle from seismic data. *Phys. Earth and Planet. Int*. **90**, 55-74.

Kuskov O L, Kronrod V A 2000 Resemblance and difference between the constitution of the Moon and Io.
Planet. Space Sci., **48**, 717-26

Kuskov O L, Kronrod V A, Hood L L 2002 Geochemical constraints on the seismic properties of the lunar mantle. *Phys. Earth. Planet. Int*. **134**, 175—89.

Kuskov O L, Kronrod V A, Hood L L 2003 Geochemical constraints on the seismic properties of the lunar mantle. *Phys. Earth and Plan. Int*, **134**, 175-89.

Lammlein D R 1973 Lunar seismicity, structure and tectonics. PhD. Dissertation, Columbia University, New York, 99 pp.

Lammlein D, Latham G V, Dorman J, Nakamura Y, Ewing M 1974 Lunar seismicity, structure and tectonics. *Rev. Geophys. Space Phys.,* **12**, 1-21.

Lammlein D 1977 Lunar seismicity and tectonics. *Phys. Earth Planet. Inter.,* **14**, 224-73.

Larmat C, Montagner J P, Capdeville Y, Banerdt W B, Lognonné P, Vilotte J P 2006 Numerical assessment of the effects of topography and crustal thickness on martian seismograms using a coupled modal solution–spectral elements method. submitted to *Icarus*.

Larose E, Khan A, Nakamura Y, Campillo M 2005 Lunar subsurface investigated from correlation of seismic nois. *Geophys Res. Let*., **32**, CiteID L16201

Latham G, Ewing M, Press F, Sutton G 1969 The apollo passive seismic experiment. *Science*, **165**, 241-50.

Latham G V, Ewing M, Press F , Sutton G, Dorman J, Nakamura Y, Toksöz N, Wiggings R, Derr J, Duennebier F 1970a Passive seismic experiment. *Science*, **167**, 455-57.

Latham G V, Ewing M, Dorman J, Press F, Toksöz N, Sutton G, Meissner R, Duennebier F, Nakamura Y, Kovach R, Yates M 1970b Seismic data from man-made impacts on the moon. *Science*, **170**, 620-26.

Latham GV, Ewing M, Dorman J, Lammlein D, Press F, Toksöz N, Sutton G, Duennebier F, Nakamura Y 1971 Moonquakes. *Science*, **174**, 687-92.

Lederer SM, Marley MS, Mosser B, Maillard J P, Chanover N J, Beebe R F 1995 Albedo features and jovian seismology. *Icarus* , **114**, 269-77.

Lee S, Zanolin M, Thode A M, Pappalardo R T, Makris N C 2003 Probing europa's interior with natural sound sources. *Icarus* **165**, 144—67.

Lehner F E, Witt E O, Miller W F , Gurney R D 1962 A seismometer for lunar experiments. *J. Geophys. Res.,* **67**, 4779-86.

Leonard R S, Barnes Jr R A 1965 Observation of ionospheric disturbances following the alaska earthquake. *J. Geophys. Res*., **70**, 1250.

Libbrecht K G, Woodard M F 1991 Advances in helioseismology *Science*, **253**, 152-57.

Linkin V, Harri A M, Lipatov A, Belostotskaja K, Derbunovich B, Ekonomov A, Khloustova L, Krmenev R, Makarov V, Martinov B, Nenarokov D, M Prostov M, Pustovalov A, Shustko G, Jarvine I, Kivilinna H, Korpela S, Kumpulainen K, Pellinen R, Pirjola R, Riihela P, Salminen A, Schmidt W, Siili T, Blamont J, Carpentier T, Debus A, Hua CT, Karczewski J F, Laplace H, Levacher P, Lognonné P, Malique C, Menvielle M, Mouli G, Pommereau J P, Quotb K, Runavot J, Vienne D, Grunthaner F, Kuhnke F, Mussman G, Rieder R, Wanke H, Economou T, Herring M, Lane A, McKay C 1998 A sophisticated lander for scientific exploration of mars: scientific objectives and implementation of the mars96 small station. *Planetary Space Sciences*, **46**, 717-37

Lodders K, Fegley B 1997 An oxygen isotope model for the composition of mars. *Icarus*, **126**, 373—9

Lodders K 2000 An oxygen isotope mixing model for the accretion and composition of rocky planets, *Space Science Reviews*, **92**, 341-54

Lognonné P, Mosser B 1993 Planetary seismology, *Survey in Geophysic*., **14**, 239-302

Lognonné P, Mosser B, Dahlen F A 1994 Excitation of the jovian seismic waves by the shoemaker-levy 9 cometary impact, *Icarus*, **110**, 186-95

Lognonné P, Gagnepain-Beyneix J, W B Banerdt W B, Cacho S, Karczewski J F, Morand M 1996 An ultra-broad band seismometer on inter marsnet, *Planetary Space Sciences*, **44**, 1237-49

Lognonné P, Zharkov V N, Karczewski J F, Romanowicz B, Menvielle M, Poupinet G, Brient B, Cavoit C, Desautez A, Dole B, Franqueville D, Gagnepain-Beyneix J, Richard H, P Schibler P, Striebig N 1998a The seismic optimism experiment, *Planetary Space Sciences*, **46**, 739-47

Lognonné P, Clévédé E, Kanamori H 1998b Normal mode summation of seismograms and barograms in an spherical earth with realistic atmosphere, *Geophys. J. Int*., **135**, 388-406

Lognonné P, Giardini D, Banerdt B, Gagnepain-Beyneix J, Mocquet A, Spohn T, Karczewski J F, Schibler P, Cacho S, Pike W T, Cavoit C, Desautez A, Pinassaud J, Breuer D, Campillo M, Defraigne P, Dehant V, Deschamps A, Hinderer J, Lévéque J J, Montagner J P, Oberst J 2000 The NetLander very broad band seismometer, *Planet. Space Sc.*, **48**,1289-1302

Lognonné P, Clévédé E 2002 Chapter 10: normal modes of the earth and planets, handbook on earthquake and engineering seismology, IASPEI centennial publications, H Kanamori, P Jennings, W Lee editors, *International Geophysics series*, **81A**, Academic Press.

Lognonné P, Gagnepain-Beyneix J, Chenet H 2003 A new seismic model of the Moon : implication in terms of structure, formation and evolution, *Earth Plan. Sci. Let.*, 6637, 1-18

Lognonné P 2005 Planetary seismology, *Annual Review in Earth Planet. Sci*., **33**, 19.1-19.34, doi :10.1146/annurev.earth.33.092203.122605

Lognonné P, Artru J, Garcia R, Crespon F, Ducic V, Jeansou E, Occhipinti G, Helbert E, Moreaux G, Godet P-E 2006 Ground based GPS tomography of ionospheric post-seismic signal during demeter: the SPECTRE project, *Planet. Space. Science,* **54**, 528-40

Loudin M G, Alexander S S 1978 Observed estimates of spheroidal free oscillations of the moon and their interpretation. *EOS Trans. Am. Geophys. Union*, **59**, 1124

Mackwell S J, Zimmerman M E, Kohlstedt D L 1998 High-temperature deformation of dry diabase with application to tectonics on venus, Journal of Geophys. Res., **103**, 975-84

Marley Mark S, Porco Carolyn C 1993 Planetary acoustic mode seismology - saturn's rings,Icarus, 106, p. 508-524

Marley M S 1994 Seimological consequences of the impact of comet shoemaker-levy 9, *Astrophys., J.*, **427**, L63-L66

Miller W F 1963 The caltech digital seismograph, *J. Geophys. Res.*, **68**(3), 841-47

Minshull TA, Goulty N R 1988 The influence of tidal stresses on deep moonquake activity, *Physics Earth Planet. Int.*, **53**, 41-55.

Mosser B, Schmider F-X, Delache P, Gautier D 1991 A tentative identification of jovian global oscillations, *Astron.Astroph*, **251**, 356-64.

Mocquet A, Vacher P, Grasset O, Sotin C 1996 Theoretical seismic models of mars: the importance of the iron content of the mantle. *Planet. Space Sci.,* **44**, 1251-68

Mocquet A 1998 A search for the minimum number of stations needed for seismic networking on mars, , *Planet. Space Sci.*, **47**, 397–409

Mosser B, Mekarnia D, Maillard J P, Gay J, Gautierand D, Delache P 1993 Seismological observations with a Fourier transform spectrometer - detection of jovian oscillations, *Astronomy and Astrophysics*, **267**, 604-22.

Mosser B 1995 Propagation and trapping of global oscillations in the Jovian troposphere and stratosphere, *Astron. Astrophys.*, **293**, 586-93

Mosser B, Galdemard P, Lagage P, Pantin E, Sauvage M, Lognonné P, Gautier D, Billebaud F, Livengood T, Kaüfl H 1996 Impact seismology: a search primary pressure waves following impacts A and H, *Icarus*, **121**, 331-40

Mosser B, Giant planets seismology 1996 in sounding solar and stellar interiors, proceedings of the 181st symposium of the international astronomical union, J Provost, F-X Schmider editors, Dordrecht Kluwer Academic Publishers, page 251

Mosser B, Maillard J P, Mékarnia D 2000 New attempt at detecting the jovian oscillations, *Icarus*, **144**, 104-13

Mueller S, Taylor G J, Phillips R J 1988 Lunar composition - a geophysical and petrological synthesis, *J. Geophys. Res.*, **93**, 6338-52

Nakamura Y, Anderson D L 1979 Martian wind activity detected by a seismometer at viking lander 2 site, *Geophysical Research Letters*, 6, 499-502

Nakamura Y 1976 Seismic energy transmission in the lunar surface zone determined from signals generated by movement of lunar rovers, *Bull. Seismol. Soc. Am.*, **66**, 593-606

Nakamura Y 1977 Seismic energy transmission in an intensely scattering environment*, J. Geophys. Res.*, 43**,** 389-99

Nakamura Y 1978A1 Moonquakes: source distribution and mechanisms, *Proc. Lunar Sci. Conf.*, **9th**, 3589-607.

Nakamura Y 1983 Seismic velocity structure of the lunar mantle, *J. Geophys. Res.,* **88**, 677-86.

Nakamura Y 2003 New identification of deep moonquakes in the Apollo lunar seismic data, *Phys. Earth Planet. Inter.,* **139**, 197–205.

Nakamura Y 2005 Farside deep moonquakes and deep interior of the moon, *J. Geophys. Res.,* **110**, E01001, doi:10.1029/2004JE002332.

Nakamura Y, Koyama J 1982 Seismic Q of the lunar upper mantle, *J. Geophys. Res.*, **87**, 4855-61

Nakamura Y, Latham G, Lammlein D, Ewing M, Duennebier F, Dorman J 1974 Deep lunar interior inferred from recent seismic data, *Geophys. Res. Lett.*, **1**, 137-40

Nakamura Y, Dorman J, Duennebier F, Lammlein D, Latham G 1975 Shallow lunar structure determined from the passive seismic experiment, *Moon*, **13**, 57-66

Nakamura Y, F K Duennebier, G V Latham, H J Dorman 1976 Structure of the lunar mantle, *J. Geophys. Res.*, **81**, 4818-24

Nakamura Y, Latham G V, Dorman H J, How we processed apollo lunar seismic data 1980. *Phys. Earth.Plan. Int.,* **21**, 218-24

Nakamura Y, Latham G V, Dorman H J 1982 Apollo lunar seismic experiment- final summary. proc. lunar planet. Sci. Conf. 13th, *J. Geophys. Res.*, **87**, A117-A123

Nakamura Y, Latham G V, Dorman J, Harris J 1981 Passive seismic experiment long-period event catalog, final version, *Technical report* **No 18**, Galveston Geophysics Laboratory, University of Texas at Austin.

Nakamura Y, Latham G V, Dorman H J, Harris J E 2004 Passive seismic experiment long-period event catalog, Tech. Rep. 118, rev. ed., Univ. of Tex. Inst. for Geophys., Austin.

Nataf H, Ricard Y 1996 3SMAC: an a priori tomographic model of the upper mantle based on geophysical

modeling, *Physics Earth and Planet. Int.*, **95**, 101-22
Neukum G, Jaumann R, Hoffmann H, Hauber E, Head J W, Basilevsky A T, Ivanov B A, Werner S C, van Gasselt S, Murray J B, McCord T, the HRSC Co-Investigator team 2004 Recent and episodic volcanic and glacial activity on mars revealed by the high resolution stereo camera, *Nature*, **432**, 971-79
Nimmo F, Schenk P 2005 Normal faulting on europa: implications for ice shell properties, *J. Struct. Geol.*, in press, doi:10.1016/j.jsg.2005.08.009.
Nishida K, Kobayashi N, Fukao Y 2000 Resonant oscillations between the solid earth and the atmosphere, *Science*, **287**, 2244-46
Oldham R D 1906 The constitution of the earth, quart. *J. Geological Soc. Lond.,* 62, 456-75
Oberst J 1987 Unusually high stress drop associated with shallow moonquakes, *J. Geophys. Res.*, **92**, 1397-405
Okal E, Anderson D J 1978 Theoretical models for mars and their seismic properties, *Icarus*, **33**, 514-28
Panning M, Lekic V, Manga M, Cammarano F, Romanowicz B 2007 Long-period seismology on europa: II. predicted seismic response , *J.Geophys. Res.,* in press.
Papanicolaou G, Ryzhik L, Keller J B 1996 Stability of the P to S-energy ratio in the diffusive regime, *Bull. Seism. Soc. Amer*, **86**, 1107-15
Peterson J 1993 Observation and modeling of seismic background noise, *U.S. Geol. Surv. Open-file Rep.*, **93-322**, 1-45
Phillips R J 1991 Expected rate of marsquakes in scientific rationale and requirements for a global seismic network on mars. *LPI Tech. Rept.*, **91-02**, Lunar and Planetary Inst., Houston. pp. 35-38.
Poveda A, Herrera M A, García J L, Hernández-Alcántara A, Curioca K 1999 The expected frequency of collisions of smallmeteorites with cars and aircraft, *Planetary and Space Science*, **47**, 715-19
Press F, Buwalda P, Neugebaue Mr, A lunar seismic experiment 1960 *J. Geophys. Res.,* **65**, 3097-105
Richardson JE, Melosh H J, Greenberg R 2004 Impact-induced seismic activity on asteroid 433 eros: a surface modification, *Science*, **306**, 1526—29
Righter K 2002 Does the moon have a metallic core? constraints from giant impact modeling and siderophile elements, *Icarus*, **158**, 1-13.
Rhie A, Romanowicz B 2004 Excitations of the earth's incessant free oscillation by atmosphere/ocean/solid earth coupling, *Nature* , **431**, 552—6.
Rhie J, Romanowicz B 2006 A study of the relation between ocean storms and the earth's hum, geochemistry geophysics geosystems, 7, 10, CiteID Q10004.
Riedel K S, Sidorenko A 1995 Minimum bias multiple taper spectral estimation, *IEEE Trans. Sig. Proc.*, **43**, 188-95
Rubie DC, CGessmann C K, Frost D J 2004 Partitioning of oxygen during core formation on the earth and mars, *Nature*, **429**, 58-61.
Sanloup C, Jambon A, Gillet P 1999 A simple chondritic model of mars. *Phys. Earth Planet. Int.* **112**, 43—54
Sanloup C, Guyot F, Gillet P, Fei Y 2002 Physical properties of liquid fe alloys at high pressure and their bearings on the nature of metallic planetary cores. *J. Geophys. Res.*, **107**, doi: 10.1029/2001JB000808
Saumon D, Chabrier G 1989 Fluid hydrogen at high density~: the plasma phase transition, *Phys. Rev. Letters*, **62**, 2397-2400
Saumon D, Hubbard W B, Chabrier G, van Horn H M 1992 The role of the molecular-metallic transition of hydrogen in the evolution of jupiter, saturn, and brown dwarfs, *Astrophysical Journal*, **391**, 827-31
Schmider F-X, Mosser B, Fossat E 1991 A possible detection of jovian global oscillations, *Astron. Astroph*, **248**, 281-91
Schmider F-X, Gay J, Jacob C, Fossat E, Valtier J-C, Mosser B, Mekarnia D, Guillot T, Provost J 2003 SYMPA: a dedicated instrument and a network for seismology of giant planets, *Astrophysics and Space Science*, **284**, 449-52
Scholz C H 1990 The mechanism of earthquakes and faulting, *Cambridge University Press*, Cambridge.
Shapiro N M, Campillo M 2004 Emergence of broadband rayleigh waves from correlations of the ambient seismic noise, *Geophys Res. Lett.*, **31**, CiteID L07614, 10.1029/2004GL019491.
Shapiro N M, Campillo M, Michel, Rittzwoller MH, Michael H 2005 High-resolution surface-wave tomography from ambient seismic noise, *Science*, **307**, 1615-18
Shearer P 1999 *Introduction to seismology*, Cambridge University Press, pp. 272
Shoemaker EM, Wolfe R F, Shoemaker C S 1990 Asteroid and comet flux in the neighborhood of earth, *Geological Society of America*, Special Paper 247
Smith D E, Zuber M T, Torrence M H, Dunn P J 2003 Estimating the k2 tidal gravity love number of mars, american geophysical union, Fall Meeting 2003, abstract #P31A-05

Sohl F, Spohn T 1997 The interior structure of mars: implications from SNC meteorids. *J. Geophys. Res*. **102**, 1613-36

Sohl F, Schubert G, Spohn T 2005 Geophysical constraints on the composition and structure of the martian interior, *J. Geophys. Res*., **110**, doi: 10.1029/2005JE002520

Solomon S, Bullock M, Grinspoon D 1999 Climate change as a regulator of tectonics on venus, *Science*, **286**, 87 – 90

Spohn T, Konrad W, Breuer D, Ziethe R 2001a The Longevity of Lunar Volcanism: Implications of Thermal Evolution Calculations with 2D and 3D Mantle Convection Models. *Icarus*, **149**, 54-65

Spohn T, Acuña M H, Breuer D, Golombek M, Greeley R, Halliday A, Hauber E, Jaumann R, Sohl F 2001b Geophysical constraints on the evolution of mars, *Space Science Reviews*, **96**, 231-62

Steeples D W, Schmeissner C, Macy B 1997 Recording wind microstructure with a seismograph, *Geophys. Res. Lett*., **24**, 2375-7

Stevenson D J 2001 Mars' core and magnetism. *Nature*, **412**, 214—19.

Stofan ER, Saunders R S, Senske D, Nock K, Tralli D 1993. Venus interior structure mission (VISM): establishing a seismic network on venus. *Lunar Planet. Inst., Worksh. Adv. Technol. Planet. Instr.,* Part 1, pp. 23--24, (SEE N93-28764 11-91), Lunar Planet. Inst. Houston, Texas.

Suda N Nawa K, Y Fukao Y 1998 Incessant excitation of the earth's free oscillations, *Science*, **279**, 2089-91.

Surkov Y 1990 *Exploration of terrestrial planets from spacecraft*, **390** p, page 372-373, Ellis Horwood, New York

Sutton G H, Latham G V 1964 Analysis of a feedback controlled seismometer , *J. Geophys. Res.*, **69**, 3865- 82

Sutton GH, Steinbacher R 1967 Surveyor seismograph experiment, *J. Geophys. Res.,***72**, 841-844.

Tanimoto T, Um J, Nishida K, Kabayashi N 1998 Earth's continuous oscillations observed on seismically quiet days, *Geophys. Res. Let.*,**25**, 10, 1553-56

Tanimoto T 1999 Excitation of normal modes by atmospheric turbulence: source of long period seismic noise, *Geophys. J. Int.*, **136**, 395-402.

Tanimoto T 2001 Continuous free oscillations: atmosphere-solid earth coupling, *Annual Rev. of Earth and Planet. Sciences*, **29**, 563-84

Tanimoto T 2005 The oceanic excitation hypothesis for the continuous oscillations of the earth, *Geophys. J. Int*., **160**, 276–288, doi: 10.1111/j.1365-246X.2004.02484.x.

Taylor S R 1982 Planetary Science: A Lunar perspective. Lunar and Planetary Institute, Houston

Tibi R, Wiens D A 2005 Detailled structure and sharpness of upper mantle discontinuities in the tonga subduction zone from regional broadband arrays, *J. of Geophys. Res*. **110**, B6, doi :10.1029/2004JB003433

Tobias R L 1978 The lunar surface gravimeter and the search for gravitational radiation, Ph.D. Thesis Maryland Univ., College Park.

Toksöz M N 1974 Geophysical data and the interior of the moon, *Annu. Rev. Earth Planet. Sci.,* **2**, 151

Toksöz M N, Goins N R, Cheng C H 1977 Moonquakes: mechanisms and relations to tidal stresses, *Science*, **196**, 979-81

Tolstoy M, Vernon F L, Orcutt J A, F K Wyatt 2002 The breathing of the seafloor: tidal correlations of seismicity on axial volcano, *Geology*, **30**, 503- 6

US Standard atmosphere 1976 Committee on the extension to the standard atmosphere, U.S. Goverment printing office, Washington D.C.

Van Hoolst T, Dehant V, Roosbeek F, Lognonné P 2003 Tidally induced surface displacements, external potential variations, and gravity variations on mars, *Icarus*,, **161**, 281-96

Van Thienen P, Rivoldini A, van Hoolst T, Lognonné P 2006 A top-dow origin for Martian mantle plumes, *Icarus*, **185**, 197-201

Verhoeven O, Rivoldini A, Vacher P, Mocquet A, Choblet G, Menvielle M, Dehant V, Van Hoolst T, Sleewaegen J., Barriot J-P, Lognonné P 2005 Planetary interiors structure inferred from electromagnetic, geodetic and seismic network science I: Forward problem an the case of Mars, *J. Geophys. Res*., **110**, doi: 10.1029/2004JE002271

Vinnik L, Chenet H, Gagnepain-Beyneix J, Lognonné P 2001 First seismic receiver functions on the moon, *Geophys. Res. Lett*, **28**, 3031-34

Von Rebeur-Paschwitz E 1889 The earthquake of tokyo, April 18, 1889, *Nature*, **40**, 294-295.

Vorontsov S V, Zharkov V N, Lubimov V M 1976 The free oscillations of jupiter and saturn, *Icarus*, **27**, 109-18

Vorontsov S V, Zharkov V N 1981 Natural oscillations of the giant planets~: influence of rotation and ellipticity. *Astron. Zh*, **58**, 1101-1114, (also in *Sov. Astron*., **25**, 627-634, 1982).

Waenke H, Baddenhausen H, Blum K, Cendales M, Dreibus G, Hofmeister H, Kruse H, Jagoutz E, Palme C, Spettel B 1977 On the chemistry of lunar samples and achondrites - Primary matter in the lunar highlands: A re-evaluation. Lunar Science Conference, 8th, 2, 2191-13, 1977.

Walker J D, Huebner W F 2004 Seismological investigation of asteroid and comet interiors, pages 234:265, in Belton, M.J.S., Yeomans, D.K., Morgan, T.H. (editors), Mitigation of Hazardous Impacts due to Asteroids and Comets, Cambridge University Press, ISBN: 0521827647

Walter C M, Marley M S, Hunten D M, Sprague AL, Wells W K, Dayal A, Hoffmann W F, Sykes Mark V, Deutsch L K, Fazio G G, Hora J L 1996 A search for seismic waves from the impact of the SL/9 R Fragment, *Icarus*, **121**, 341-50

Walterscheid R L, Brinkman D G, Schubert G 2000 Wave disturbances from the comet SL-9 impacts into jupiter's atmosphere, *Icarus,* **145**, 140-46

Watkins J S, Kovach R L 1972 Apollo 14 active seismic experiment, *Science*, **175**, 1244-45.

Weaver P F, Yuen P C, Prolss G W, Furumoto A S 1970 Acoustic coupling in the ionosphere from seismic waves of the earthquake at kurile islands on august 11, 1969. *Nature*, **226**, 1239-41.

Webb S C 2007 "The Earth's Hum" is Driven by ocean waves over the continental shelves, *Nature*, in press.

Weber J 1971 Gravitational radiation experiments, in relativity and gravitation, based on the proceedings of an international seminar on relativity and gravitation, Edited by Charles G. Kuper and Asher Peres. New York: Gordon and Breach, p.309.

Wieczorek M. A Bradley M, Jolliff L, Khan A, Pritchard M E, Weiss B P, Williams J G , Hood L L , Righter K, Neal C R , Shearer C K , McCallum I S, Tompkins S, Hawke B R, Peterson C, Gillis C J , Bussey B 2006. The Constitution and Structure of the Lunar Interior, *Rev. in Mineralogy & Geochemistry*, **60**, 221-364.

Wieczorek M A, R J Phillips 1998 Potential anomalies on a sphere: applications to the thickness of the lunar crust, *J. Geophys. Res.*, **103,** 1715-24.

Widmer R, Zürn W 1992 Bichromatic excitation of long-period rayleigh and air waves by the mount pinatubo and el chichon volcanic eruptions, *Geophys. Res. Lett.*, **19**, 765-68.

Williams JG, Boggs D H, Yoder C F, Ratcliff J T, Todd J, Dickey J O 2001 Lunar rotational dissipation in solid body and molten core, *J. Geophys. Res.,* **106**, 27933-68.

Woodhouse J H, Dziewonski A M 1984 Mapping of the upper-mantle: three dimensional modeling of earth structure by inversion of seismic waveforms, *J. Geophys. Res*., **89**, 5953-86

Yoder C F, Konopliv A S, Yuan D N, Standish E M, Folkner W M 2003 Fluid core size of mars from detection of the solar tide. *Science* **300**, 299**–**303.

Yuen P C, Weaver P F, Suzuki R K, Furumoto A S 1969 Continuous traveling coupling between seismic waves and the ionosphere evident in may 1968 japan earthquake data, *J. Geophys. Res*., **74**, 2256-64

Zharkov V N, Gudkova T V 1997 On the dissipative factor of martian interiors. *Planet. Space Sci.*, **45**, 401—7.

Zharkov V N, Gudkova T V 2000 Interior structure models, Fe/Si ratio and parameters of figure for mars. *Phys. Earth Planet. Int.*, **117**, 407—20.

Zharkov V N, Gudkova T V 2005 Construction of martian interior model, *Solar System Research*, **39**, 343-373, doi: 10.1007/s11208-005-0049-7.

Zuber M T, Solomon S C, Phillips R C, Smith D E, Tyler G L, Aharonson O, Balmino G, Banerdt G WB, Head J W, Johnson C L, Lemoine F G, McGovern P J, Neumann GA, Rowlands DD, Zhong S 2000 Internal structure and early thermal evolution of mars from mars global surveyor topography and gravity, *Science*, **287**, 1788-93.

Zuber MT 2001 The crust and mantle of mars, *Nature*, **412**, 220-7

Zürn W, Widmer R 1996 World wide observation of bichromatic long-period rayleigh-waves excited during the june 15, 1991 eruption of Mt. pinatubo. In : C. Newhall, R Punongbayan (Ed.), Fire and Mud, Eruptions of Mount Pinatubo, Philippines, Philippin Institute of Volcanology and Seismology, Quezo City and University of Washington Press, 615-24